Advanced Modeling Framework for the Simulation of Greenhouse Climate and the Integration of Sustainable Energy Solutions

by

Queralt ALTES BUCH

Submitted to the Department of Aerospace and Mechanical Engineering
in fulfillment of the requirements for the degree of

DOCTOR OF PHILOSOPHY

at the

UNIVERSITY OF LIEGE

August 8, 2024

Supervisor:
Prof. Vincent LEMORT, University of Liège

President of the jury:
Prof. Pierre DEWALLEF, University of Liège

Examination committee:
Prof. Philippe ANDRE, University of Liège
Prof. Hyun Kwon SUH, Sejong University
Assoc. Prof. Cyril TOUBLANC, ONIRIS Nantes, GEPEA
Assoc. Researcher Patrick SCHALBART, Mines Paris

Acknowledgements

I would like to express my gratitude to Prof. Vincent Lemort for providing me the opportunity to embark on this journey, as well as to Prof. Pierre Dewallef, Prof. Philippe Andre, Prof. Hyun Kwon Suh, Associate Prof. Cyril Toublanc, and Associate Researcher Patrick Schalbart for offering me the chance to successfully conclude it. I would also like to thank Eric Delhez, Dean of the Faculty of School of Engineering. Additionally, I want to thank all my collaborators for their valuable input on my work over these years, in particular, Asst. Prof. Sylvain Quoilin and Tanguy Robert.

I wish to thank Prof. Hyun Kwon Suh, who approached me to participate in the Autonomous Greenhouses Challenge (2nd Edition) with his team Digilog. As we achieved a second place in the Hackathon competition, this incredible opportunity allowed me to broaden my network, have fun, and demonstrate the practical application of my work and the knowledge I had acquired until that moment. Thanks to all Digilog team members for the interesting discussions and for being wonderful, welcoming people.

I would also like to express my gratitude to the Modelica Conference for honoring my work with the first prize in the Library Award at the 13th International Modelica Conference. I believe I speak for many PhD candidates when I say that the journey we pursue is a long and challenging one. Such recognition from the international scientific community reassured me that I was on the right track, which boosted my energy levels to continue my research even in moments of uncertainty.

I warmly thank Camila, Leonardo, and Roberto, my office mates, who made those years easy and filled the office with laughter. A special thanks goes to Javier and Sergio, who joined the laughter-club and made my days brighter. Additionally, I want to express my gratitude to the rest of my colleagues in B49, particularly: Andy, Andres, (Petit) Bernard, Bertrand, Emeline, Marcel, Richard, Rémi, Sam, and Thibaut.

I wish to thank my current colleagues in Engie, Alex, Eric, Tanguy, and especially my manager Christelle, whose understanding and openness to flexibility allowed me to conclude this thesis.

I would like to express my gratitude to my dearest friends Andrea, Camila, Javier, and Pep, who made me feel at home despite being in a foreign country, who were there for me when I needed them, and whith whom I spent the greatest time all these years. As this era concludes, I am confident that our friendship will endure. An additional thanks to wonderful people I met in Liege during this journey: Cristina, Daniele, David, Melisa, Miguel and Nikola.

Last but not least, I want to extend a very special thanks to my family for their unwavering support. To my beloved Angelina and Cristina, and specially, to my mom Gloria, my dad Santi, and my brother Nil. Thanks for always being there for me. This achievement is also yours.

Per a la meva família.

Abstract

Advanced Modeling Framework for the Simulation of Greenhouse Climate and the Integration of Sustainable Energy Solutions

by Queralt ALTES BUCH

This research underscores the compelling necessity for sustainable practices within the greenhouse horticulture sector, propelled by the sector's inherent energy intensity in countries such as the Netherlands. Within the European context, marked by ambitious energy transition goals, the imperative to shift from conventional energy sources to low-carbon alternatives is pronounced. Greenhouses, historically reliant on gas-fired units, emerge as promising candidates for the integration of renewable energy sources. Successful implementations of geothermal projects, biofuel, and residual heat recovery applications exemplify the sector's potential. Concurrently, of equal significance is the investigation into energy efficiency measures aimed to decarbonize existing gas-fired systems, which continue to dominate the energy supply in greenhouses.

To assess the viability of these measures, the necessity for a simulation tool becomes evident. However, the effective execution of these studies faces hinderances due to the absence of suitable tools in the market. Even in instances where individuals are willing to invest in access to one of the few existing proprietary tools, such tools lack the modularity required for the integration of greenhouses with alternative HVAC, generation or storage systems. This dissertation is devoted to the development of a versatile modeling framework valid for different greenhouse climates and designs. The proposed framework stands as a pioneering contribution, furnishing a user-friendly, open-source platform for simulating and optimizing greenhouse climate, crop yield, and intricate energy flows between the greenhouse and its generation and storage units. Its parametric and object-oriented approach provides unmatched flexibility for simulating integrated systems.

Subsequently, three case studies are presented to effectively illustrate how users can derive benefits from employing this modeling framework to address the current research questions. Noteworthy, global findings include the potential benefits of delaying thermal screen deployment and the significant operational cost reductions achievable through the integration of heat pumps in conventional combined heat and power (CHP) systems coupled with thermal energy storage, or through a hybrid electrical-heat-driven control of the CHP unit.

Finally, the developed modeling framework is employed to examine the viability of innovative low-carbon energy sources for greenhouses. In particular, the utilization of thermal energy storage in shallow alluvial aquifers is suggested as a sustainable solution for meeting the energy requirements of greenhouses. Despite initial energy imbalances, the findings underscore the viability of a sustainable system in Atlantic climate with precise calibration of the greenhouse climate controller.

Contents

List of Abbreviations

AI	Artificial Intelligence
ATES	Aquifer Thermal Energy Storage
CHP	Combined Heat and Power
COP	Coefficient of Performance
DM	Dry Matter
EDC	Electrical-Driven Control
EER	Energy Efficiency Ratio
EU	European Union
FAO	Food and Agriculture Organization of the United Nations
FIR	Far Infrared Radiation
HDC	Heat-Driven Control
HPS	High Pressure Sodium
HVAC	Heating Ventilation and Air Conditioning
LAI	Leaf Area Index
LED	Light Emitting Diode
MDC	Mixed-Driven Control
NIR	Near Infrared Radiation
PAR	Photosynthetically Active Radiation
PI	Proportional Integer
PV	Photovoltaics
RES	Renewable energy sources
RH	Relative Humidity
SLA	Specific Leaf Area
SME	Small and Medium Enterprise
TES	Thermal Energy Storage
TMY	Typical Meteorological Year
TYM	Tomato Yield Model
UAA	Utilized Agricultural Area
UV	Ultra Violet

Chapter 1

Introduction

1.1 Setting the Stage

A greenhouse is a usually permanent, climate-controlled structure designed for cultivating crops under optimal conditions, regardless of the season. These structures vary from plastic sheet structures with minimal energy requirements to equipped glass structures that may consume substantial amounts of energy. Indeed, the incorporation of Heating, Ventilation, and Air Conditioning (HVAC) systems in greenhouses offers several advantages. Heating greenhouses facilitates off-season crop production, extending cultivation beyond the crop's native region. Furthermore, highly equipped greenhouses boost productivity by enabling precise climate control under optimal growing conditions, positioning them as a viable solution to ensure food supply, which is one of the biggest challenges of human kind in the twenty-first century [1].

The increasing horticulture market demand in the EU presents opportunities for the greenhouse sector, though demand varies geographically. While some areas in South Eastern Europe still fall below the World Health Organization's recommended daily intake of 400 g per capita of fruits and vegetables [2], rising living standards contribute to an increased demand for high-quality horticulture products. Additionally, there is a general market demand for products outside the summer period, which necessitates the use of highly equipped greenhouses.

According to the Food and Agriculture Organization of the United Nations (FAO), the EU has 405 000 hectares of greenhouses, encompassing both plastic and glass structures [2]. Eurostat reports that glass-covered greenhouses dedicated to vegetables, fruits, flowers, ornamental plants, and permanent crops cover 123 220 hectares in the EU-27 [3].

Driven by market demand and international competition, countries like the Netherlands have invested significantly in developing their greenhouse sector. As of now, greenhouse horticultural businesses in the Netherlands cover 9 395 hectares, with 53% dedicated to vegetables, and the rest allocated to potted and bedding plants, cut flowers, and fruits. In 2022, these greenhouses contributed €7.3 billion to the

Dutch gross domestic product, equivalent to 1% of the country's total economy. Approximately 85% of this contribution comes from exports of greenhouse horticulture products, valued at €9.2 billion annually. This positions greenhouse horticulture as the third-largest export hub in the Netherlands, following the Port of Rotterdam and Schipol Airport [4].

Over the past years, Dutch resources have been invested in increasing innovation, knowledge, and tools to optimize crop production. Objectives include achieving higher values per unit of product and meeting the growing market demand outside the summer period through the use of supplemental lighting. The technological advancements of recent decades have spurred faster growth, particularly in the development of high-tech greenhouses that have substantially improved crop yields. A few years ago, a tomato yield of 100 tonnes per hectare was considered favorable. In contemporary high-tech greenhouses, the same yield easily reaches 600 tonnes per hectare [2]. However, this enhanced productivity comes at a cost, given that the control of temperature, humidity, light, carbon dioxide, and water can be highly energy-intensive. The intensification of production in greenhouses is fundamentally an economically driven process, resulting in an increased energy requirement for crops per square meter of greenhouse.

The recent intensification of greenhouse horticulture has shaped the Dutch greenhouse sector, marked by elevated production rates and value. However, this progress is also accompanied by high costs per square meter of greenhouse. Indeed, despite decreasing by 10% from 2000 to 2014, between 2015 and 2018, the average energy consumption per square meter of greenhouse (adjusted for temperature variations to prevent outdoor temperature effects in year-on-year comparisons) witnessed a 7% increase [5]. In regions where energy-intensive greenhouses are widely employed, it is not unexpected that these structures constitute the most substantial energy consumers within the entire agricultural sector [6]. Specifically, in the Netherlands, greenhouse horticulture accounted for a substantial 79% share of the agricultural final energy consumption in 2013[1], amounting to 109.2 pentajoules [7].

Regrettably, detailed energy consumption data for greenhouses in the broader European context remains insufficiently documented [8]. Nonetheless, given that greenhouses represent one of the most energy-intensive components within the agricultural sector in regions where energy-intensive greenhouses are prevalent, it becomes feasible to utilize the sector's overall consumption data (available from Eurostat) as an indicative measure for assessing greenhouse consumption patterns. Indeed, the share of total final energy consumption by the agricultural sector not only provides insight into the intensity of greenhouses' role within a country but also facilitates cross-country comparisons. The most recent data highlights that in the Netherlands, the agricultural and forestry sector comprised a notable 9.2% share of the country's total final energy consumption in 2021, surpassing other Member States, with the

[1] Latest CBS data. Dataset discontinued from 2013 onwards.

second-highest share significantly lower at 5%, and the EU average registering at 3% [9]. Furthermore, when assessing the final energy consumption by the Dutch agriculture and forestry sector in units relative to the area (to eliminate the country size factor), the figures for 2021 reached 2191 kilograms of oil equivalent per hectare of utilized agricultural area (UAA)[2], markedly exceeding the EU-27 average of 176 kilograms of oil equivalent per hectare of UAA [10]. These findings are elucidated by the extensive production of vegetables, fruits, and plants within greenhouses in the Netherlands.

1.1.1 Energy Supply in Greenhouse Horticulture: From Fossil Fuel Dominance to the Evolving Role of CHP Plants

In 2021, the Dutch greenhouse horticulture sector consumed a total of 117 pentajoules. The majority of this energy was sourced from fossil fuels, specifically 3.672 billion cubic meters, with natural gas accounting for the predominant share at 3.671 billion cubic meters. Despite this significant reliance on natural gas, greenhouses sought external sources for an additional 2.23 pentajoules of heat and 2.86 TWh of electricity from the grid. The sector also witnessed electricity sales totaling 6.76 TWh. Furthermore, renewable energy generation contributed 13.98 pentajoules to the overall energy portfolio, with a portion of it being partially procured from third parties [5].

The significant prevalence of natural gas in the sector's energy consumption is expected, given the 15-year dominance of natural gas-fired combined heat and power (CHP) technology in meeting the energy demands of greenhouses. CHPs gained popularity due to their ability to efficiently provide heat, electricity, and carbon dioxide, aligning with the multifaceted needs of greenhouse cultivation. The intensification of greenhouse practices, leading to increased electricity usage for supplementary lighting and carbon dioxide application for enhanced photosynthesis, prompted the transition from natural gas boilers to CHPs. Additionally, CHPs make more carbon dioxide per unit of heat compared to boilers, as almost half of the natural gas is used to produce electricity. This shift resulted in CHPs contributing to 60% of Dutch greenhouse horticulture acreage in 2021, with an installed capacity of 2.65 GWe and electricity production of 10.4 TWh. In 2022, they accounted for 11% of the total electricity generation in the Netherlands [4].

The majority of CHP units supplying energy to greenhouses are self-owned by horticulture companies, affording them the flexibility to operate according to their specific requirements [5]. Typically, CHP operations are concentrated during daylight hours, driven by three primary factors. Firstly, the utilization of thermal energy storage enables a temporal shift between heat production and consumption. Secondly,

[2]The utilised agricultural area (UAA) is the total area taken up by arable land, permanent grassland, permanent crops and kitchen gardens used by the holding, regardless of the type of tenure or of whether it is used as a part of common land.

the demand for carbon dioxide aligns with daylight hours, coinciding with crop photosynthesis. Additionally, the hourly fluctuations in power market prices influence economic considerations. Producing electricity during daylight is more financially viable, even with limited supplemental lighting consumption, as the excess production can be sold at positive spark spreads. Conversely, purchasing electricity during nighttime hours, when supplemental lighting is commonly used, is more economical due to negative spark spreads.

The operation of CHP units is also influenced by levies but primarily dictated by energy market dynamics. Significant market shifts can consequently impact CHP behavior, as exemplified by events in 2021, detailed in the subsequent section.

Noteworthy, in the context of smart energy systems designed to accommodate fluctuating renewable power production, the evolving role of CHP plants is of paramount importance. Nevertheless, as outlined by [11], their anticipated role is subject to transformation. Considering the long-term perspective, CHP units reliant on fossil fuels should undergo a transformation that may include shifting to synthetic fuels, providing grid services, or adopting alternative technologies such as heat pumps and/or harnessing waste heat from diverse sources [12]. The envisioned strategies foresee a partial phase-out of CHP, redirecting its primary operation towards the electricity market rather than the heat market. This strategic shift aims to capitalize on the flexibility of CHP as a means to achieve a more decarbonized energy system [13].

1.1.2 Navigating the Impact of Surging Energy Prices: Strategies and Challenges in the Greenhouse Horticulture Sector

In 2021, energy prices surged due to a combination of factors: first, the post-corona demand recovery, and second, emerging geopolitical tensions. These tensions disproportionately affected certain natural gas markets, such as TTF in the Netherlands or THE in Germany, due to their dependence on gas pipeline supplies from Russia and Eastern Europe. The increase in prices did not go unnoticed in the greenhouse sector. In 2021, net energy costs in the Dutch greenhouse sector rose by 25% year-on-year, reaching an unprecedented average of 8.5 euros per square meter. Given that energy consumption costs currently constitute over 50% of total production costs, greenhouse growers faced unprecedented economic challenges. Although the energy crisis only commenced in the last quarter of 2021, its impact on greenhouse practices became apparent.

Since 2010, with a growing focus on greenhouse production intensification using supplementary lighting, the electricity produced by CHPs was predominantly self-consumed (see Section 1.1.1). However, due to the surge in energy prices in 2021, this trend shifted. Greenhouse growers opted to limit the use of supplemental lighting, resulting in a decrease in the purchase of electricity from third parties and an

increase in electricity sales to the market, supported by positive clean spark spreads. In 2021, the electricity consumption of greenhouses exhibited a 7% year-on-year decrease, amounting to a 15% reduction compared to 2019, totaling 6.6 TWh. Consequently, there was a corresponding 10% year-on-year decline in electricity purchases to 2.9 TWh, while electricity sales witnessed a 6% increase, reaching 6.8 TWh [5].

Additionally, the reduced use of lighting had to be partially compensated with heat, as greenhouse lamps substantially contribute to heating through their radiation losses. Consequently, the heat-to-electricity consumption ratio shifted from 74%-26% in 2019 to 80%-20% in 2021 [5]. The lower input of lighting due to high energy costs led to lower production volumes in the last quarter of 2021 [5], impacting the harvest of 2022, as the crop growth cycle began in 2021.

In such a volatile energy market, formulating business strategies for optimal outcomes becomes a complex task. The ambiguity regarding the persistence of highly volatile energy prices prompted prudent gas procurement and modifications to the cultivation plan for 2022-2023. These adjustments encompassed reduced lighting, delayed planting, and leaving certain sections unused. Notably, in 2023, the cultivated volumes of tomatoes were again lower, yet lower energy costs in 2023 compared to 2022 led to an overall income improvement in greenhouse horticulture. Some greenhouse companies with a CHP benefited from higher income from electricity sales, thanks to positive spark spreads.

Nevertheless, while some companies had financial gains from increased income through electricity sales amid favorable spark spreads, not all companies benefited from this advantage. The uneven distribution of the crisis's impact was particularly pronounced among growers, affecting those cultivating products with essential lighting needs and smaller growers without a CHP unit more significantly.

1.1.3 Carbon Dioxide Emission Dynamics and Future Targets in Dutch Greenhouse Horticulture

Estimating global carbon dioxide emissions from greenhouse horticulture production proves challenging, as these emissions are influenced not only by the utilization of on-site generation units but also by external procurement of heat and electricity, the emissions of which are accounted for in their respective sectors. Additionally, factors such as the sale of non self-consumed electrical production to the market contribute to the complexity of this assessment. Despite these challenges, monitoring emissions in this sector is crucial for tracking historical trends and meeting regulatory targets established to accelerate the energy transition.

In the Netherlands, both the Dutch greenhouse horticulture sector and the government have undertaken efforts to monitor the sector's carbon dioxide emissions in recent years. Aligned with the European objective of reducing carbon dioxide emissions by 20% in 2020 compared to 1990, the Dutch greenhouse horticulture sector

aimed for a carbon dioxide target of 6.2 Mton in 2020. Although this target was met, the sector's carbon dioxide emissions in 2021 reached 6.5 Mton, representing a year-on-year increase of 5.6% and surpassing the 2021 target of 6.0 Mton. It is essential to contextualize year-on-year absolute value comparisons, considering factors that vary annually, such as outdoor temperatures and greenhouse area. After temperature correction, eliminating the influence of outdoor temperature, carbon dioxide emissions per square meter experienced a modest 2% decrease in 2021. Notably, emissions per square meter of greenhouse have exhibited a downward trend since 1990, but this trend appears to have plateaued around 45.4 kilograms per square meter annually since 2019 [5].

For the year 2030, the Dutch government has mandated the agriculture and land use sectors to achieve an additional reduction of 3.5 Mton in greenhouse gas emissions. This stringent target is essential to meet the government's overarching goal of a 49% reduction for the Netherlands and represents a crucial step toward the 2050 objective. The specified emissions reduction allocated to greenhouse horticulture ranges from 1.8 to 2.9 Mton. The Climate Agreement [14] outlines key measures to accomplish this target, including greenhouse intensification, integration of geothermal energy, utilization of residual heat, and adoption of sustainable electricity and carbon capture and supply.

It is acknowledged that certain emission factors are influenced by external variables beyond the control of greenhouse companies, such as colder outdoor temperatures, expanded greenhouse areas driven by heightened product demand, or increased electricity sales due to elevated prices in the electricity market (see Section 1.1.2). However, greenhouse growers can exert influence over several factors, including the proportion of renewable sources, energy consumption per square meter, and the extent of electricity or heat procurement from external entities (with emissions accounted for in their respective sectors). To accelerate the energy transition, it is imperative for greenhouse companies to actively address these factors and contribute to reducing emissions in the sector.

1.1.4 Advancements and Transformations in Renewable Energy Integration and Sustainable Practices within the Greenhouse Horticulture Sector

Renewable energy sources (RES) commenced their integration into the greenhouse horticulture sector in the year 2000. The adoption of RES was driven, on one hand, by sustainability considerations, originating from either growers themselves or customer requirements, coupled with its enhanced long-term economic viability. On the other hand, the motivation arose from the perceived risks associated with dependence on natural gas, a vulnerability that has been accentuated by recent geopolitical tensions (see Section 1.1.2). However, the intricate nature and economic risks inherent in renewable projects posed challenges for greenhouse companies, resulting in

a gradual penetration of RES from 2000 to 2010. During this period, the proportion of energy derived from renewable sources in the total energy balance increased from less than 1% in 2000 to 1.9% in 2010. From 2015 onward, the trajectory shifted. Enhanced collaboration between greenhouse companies and external entities in renewable energy initiatives contributed to a substantial uptick in the utilization of renewable sources. While the penetration of RES commenced at a measured pace, the share of energy from renewable sources in the total energy balance experienced rapid growth in recent years, reaching 4.9% in 2015 and surging to 11.9% in 2021 [5].

In the current landscape of the Netherlands, 92% of the renewable energy consumed in the greenhouse sector constitutes heat, with only 8% attributed to electricity. Geothermal energy holds the highest share, accounting for 45% of the total renewable energy supply, 14% of which is sourced from third parties. In 2019, there were approximately 17 ongoing projects at horticulture businesses utilizing geothermal energy, with an objective to reach a total of at least 52 projects by 2030 [14]. By 2023, the number of geothermal sources connected to greenhouses had increased to 20. A projection for 2040 anticipates a total of 65 projects that will fulfill half of the heat demand for greenhouses [4]. The development of geothermal projects has been made possible through vital financial support from the Dutch government, for intance via the SDE++ scheme.

Geothermal is followed closely by biofuel at 41% of the current total renewable share, 24% of which is sourced from third parties. Another burgeoning application is the recovery of solar heat through aquifer wells, currently constituting 6%, particularly applicable to crop productions requiring cooling.

Simultaneously to these existing projects, the introduction of innovative and efficient heat supply sources, including large-scale heat pumps and the recovery of excess heat from diverse sources, is underway [13]. Specifically, residual heat is emerging as a significant energy source for greenhouse growers, projected to meet one-fifth of the heat demand in greenhouse horticulture by 2040 [4]. Additionally, sustainably generated electricity, biomass, hydrogen, and green gas dedicated to boilers and CHPs are expected to collectively fulfill an additional one-fifth of the heat demand by 2040. This transformative phase acts as a counterbalance to the phased-out capacities of traditional CHP units and boilers, signifying a comprehensive shift in the energy source landscape within the evolving energy framework.

In the current context of integrated smart energy systems, certain projects already integrate multiple renewable sources, and the derived heat serves purposes beyond greenhouse cultivation. One such initiative is the Warmtesysteem Westland (Westland Heating System), which systematically connects existing and new geothermal energy sources and local heating sources in a heat distribution network. This network is further linked to residual heating systems from the Port of Rotterdam and the built environment in Westland and Midden Delfland. The initiative involves

various stakeholders, including greenhouse horticultural businesses, the municipality of Westland, Warmtebedrijf Westland, the Port of Rotterdam Authority, and Gasunie. Operated as a market system, the project aims to optimize the use of geothermal heat and heat generated by the port to provide a reliable and affordable low-carbon heating supply for the entire region. The heating network encompasses a substantial area, supporting greenhouse horticulture businesses, and is anticipated to heat a significant portion of the 2 385 hectares of greenhouses in Westland, along with over 500 000 households [15]. This integrated approach is expected to result in a noteworthy reduction of carbon emissions, exceeding 1 Mton per year [14].

As previously mentioned, electricity currently constitutes 8% of the overall renewable energy supplied to greenhouses. It is primarily sourced from third-party renewable providers and partially derived from internal generation [5]. The internal production of electricity through solar photovoltaic (PV) systems is steadily increasing, albeit within defined limits. The constraints stem from the incapacity to utilize the greenhouse cover as a structural support for PV panels, given the imperative need for light in fostering crop growth. Furthermore, the concentration of electricity demand during winter or nighttime, when sunlight is diminished or entirely absent, adds to the limitations.

It is crucial to emphasize that growers must maintain the ability to acquire or produce sufficient pure carbon dioxide. With the anticipated phasing out of traditional CHPs in the future, entrepreneurs should have the capability to procure carbon dioxide externally. Before the mid-1990s, the only viable alternative was the purchase of liquid carbon dioxide, transported by tanker. However, the processes of compressing, liquefying, and transporting are not only costly but also energy-intensive. Furthermore, road transport poses significant drawbacks.

A more viable solution involves capturing carbon dioxide at industrial sources for repurposing as a nutrient in the greenhouse horticulture sector. An exemplar of such a system is OCAP in the Netherlands: from a pipeline provided by the government, OCAP established a distribution network and erected a compressor station. Initial operations commenced in 2005, with one industrial source. Over the years, OCAP has successfully identified two industrial-level sources. Presently, OCAP supplies hundreds of kilotons of carbon dioxide annually to over 600 greenhouse growers. Despite having two sources, the security of supply is not entirely robust. Continuous endeavors are thus underway to enhance the supply by incorporating carbon dioxide from additional sources.

1.1.5 Perspectives of the Greenhouse Horticulture Sector

In the current context, the greenhouse sector stands out as a substantial energy consumer with a growing demand primarily driven by fossil fuels and subject to the fluctuations of energy markets. Concurrently, the evolving landscape of EU climate

policies imposes progressively stringent environmental regulations, underscoring an urgent imperative for the sustainability and decarbonization of the sector. However, this imperative necessitates a delicate balance to ensure the sector's competitiveness.

In Europe, over 90% of greenhouse growers operate as small and medium enterprises (SMEs) [16]. These SME growers confront unprecedented economic challenges stemming from the recent energy crisis, along with rising labor and transportation costs, and increasingly stringent EU climate regulations. As they contend with decreasing competitiveness vis-à-vis markets outside the EU, characterized by lower labor costs and lax environmental regulations, a critical imperative emerges. To sustain the competitiveness of European greenhouse growers in the regional market, a substantial reduction in total production costs is imperative. Given that energy consumption costs currently contribute over 50% to the total production costs, it becomes evident that the competitiveness of growers hinges on diminishing the costs associated with energy consumption.

Thus, the greenhouse sector must transition towards sustainable production, characterized by lower carbon dioxide emissions and reduced energy costs. The essence of this dual commitment is in lign with the Dutch Climate Agreement [14], which encapsulates the key objective for greenhouse horticulture as "On the road to **sustainable**, **economically attractive**, and **climate-neutral** production". A range of measures can be employed to achieve these goals. Optimizing energy resources emerges as a key strategy to improve the energy efficiency of greenhouses, potentially reducing energy consumption and enhancing the sector's competitiveness while minimizing environmental impact. Concurrently, the integration of RES can play a substantial role in sector-wide decarbonization, offering a solution to mitigate vulnerability to energy market volatility. However, which energy efficiency measure can yield the most significant improvement? What is the impact on crop yield from these energy saving measures? Which renewable source is best suited to meet the greenhouse demand? Are greenhouses suitable candidates for demand side management applications? Can the integration of greenhouses in urban agricultural sites through district heating networks rend these systems more efficient? To assess the potential impact of these measures, the necessity of a simulation tool becomes imperative.

1.2 Thesis Structure and Contributions

The primary objective of this study is to contribute to the acceleration of the energy transition within the greenhouse horticulture sector. Central to this endeavor are investigations into the sector's decarbonization and the enhancement of greenhouse energy efficiency to reduce energy costs, as outlined in Section 1.1.5. However, the effective execution of these studies is hindered by the absence of suitable tools in the market. Even in instances where individuals are willing to invest in access to one

of the few existing proprietary tools, such tools lack the modularity required for the integration of greenhouses with alternative HVAC, generation or storage systems. It is, therefore, imperative to make such a tool readily available for the scientific community. This accessibility will empower other researchers, as well as greenhouse growers, to engage with it, allowing them to focus their efforts directly on generating new studies. If, on each occasion, the implementation of available methodologies is necessitated for investigating research questions, the pace of the transition is inevitably impeded. We posit that the availability of this tool holds substantial potential in hastening the energy transition.

In pursuit of this objective, this dissertation is devoted to the development of a versatile and user-friendly modeling framework with the capacity to simulate greenhouse climate across different designs and climates, as well as the complex interactions between greenhouse systems and thermal and electrical energy systems. This dissertation represents a compilation of distinct contributions to the fields of greenhouse horticulture and energy systems. Each contribution addresses a specific facet of this overarching theme, focusing on aspects such as modeling, case study simulation, or the integration of the developed modeling framework with other systems to explore the viability of low-carbon supply sources. Consequently, the document is structured into three parts, each comprising several chapters corresponding to the individual contributions, as outlined in Figure 1.1.

Part I

Part I of this manuscript is dedicated to modeling. It commences with **Chapter 2**, which presents a literature review on greenhouse climate models. The review critically examines the current state-of-the-art publications of models and software for greenhouse climate simulation. Key findings regarding the gaps in the literature and available software for greenhouse climate simulation can be summarized as follows:

- A few *proprietary software* for greenhouse climate simulation are available in the market, but they do not release source code.
- A limited number of *validated methods* for greenhouse climate simulation are found in the literature. Of the latter, most are validated for a specific type of greenhouse design or climate, limiting their usability.
- *Simulation tools* with source code based on these methods are rarely accessible, with only three recent exceptions, as outlined in a recent review [17]: [18], [19], with the third being the present work. These simulation tools lack a graphical user interface to facilitate model usage (e.g., [18] based in Matlab and [19] in XML scripts).
- The few available tools (proprietary software or from the literature) exhibit limited modularity:

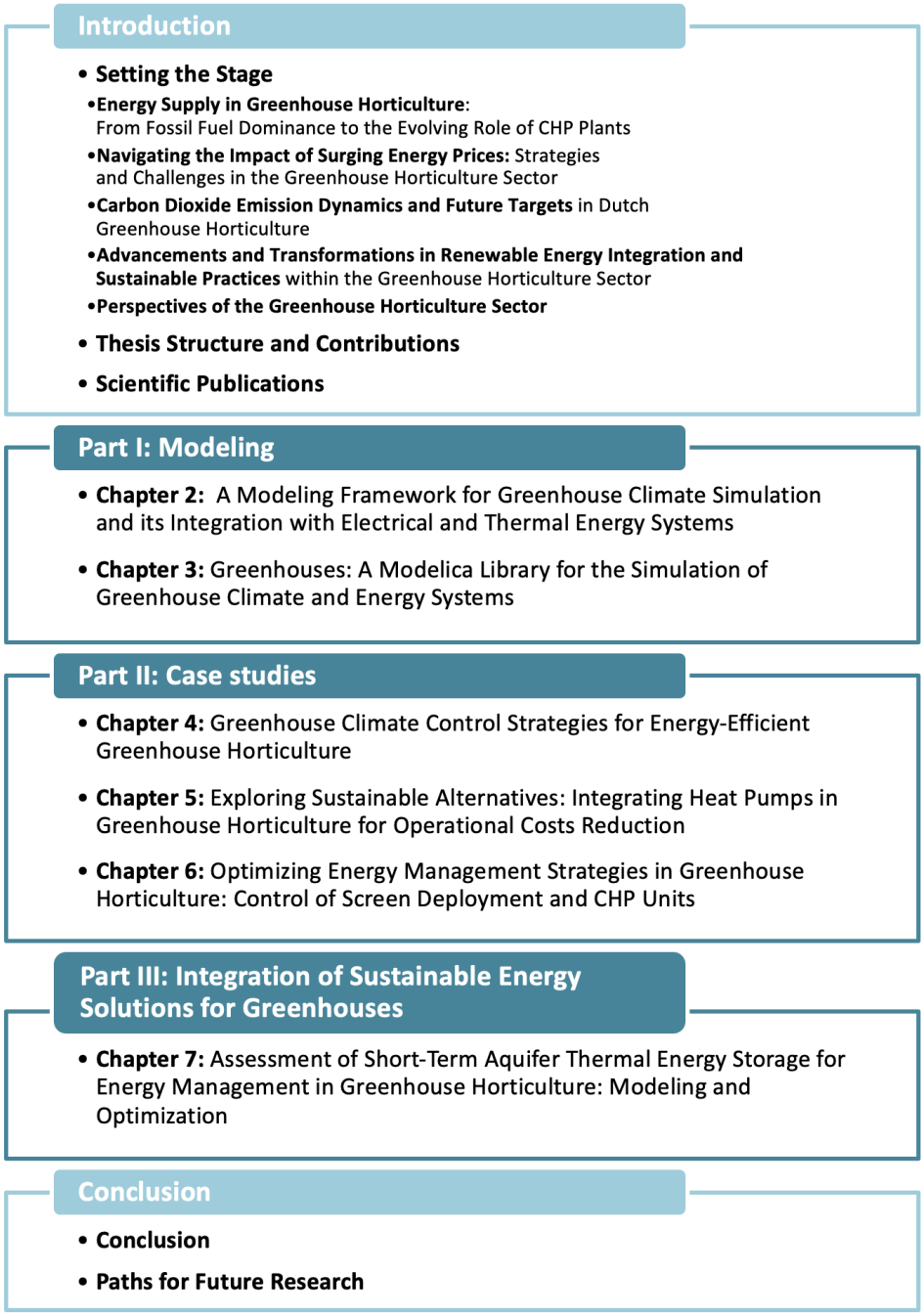

FIGURE 1.1: Thesis structure

- They exclusively simulate greenhouse climate, neglecting their generation units.
- While some integrate CHP simulation, other types of generation units are overlooked.
- Modularity within conventional greenhouse components is restricted (e.g., inability to simulate multiple screens, or to change the technical characteristics of the screen).
- Users are unable to introduce additional developments, such as modeling different generation or heat distribution systems and coupling them with the greenhouse to assess their potential for the energy transition.
- Modularity concerning greenhouse design is limited, rendering them incapable of simulating non-conventional greenhouses (e.g., those with concrete walls or double glazing).

The comprehensive examination of greenhouse climate models in the literature facilitated the judicious selection of the most suitable methodologies for each model developed within this thesis. The detailed exposition of the implemented methodologies is provided in Chapter 2. These methodologies encompass a range, beginning with the depiction of the greenhouse climate through energy and mass balances inherent to a greenhouse. This includes an intricate account of all pertinent sensible heat and mass flows, enabling a comprehensive description of the climate.

Furthermore, the methodologies extend to crop yield models that describe the photosynthesis process of the crop, providing a quantifiable measure for crop production under specific climatic conditions. Quantifying the impact of climate on crop production is crucial for assessing the feasibility of novel strategies or energy solutions. This will not only aid in dismissing energy-saving measures that negatively affect crop production but may also assist in identifying energy-saving solutions that offer significant reductions in energy costs with only marginal impacts on production.

Moreover, as the primary objective of this thesis is to enable the simulation of greenhouses in conjunction with thermal systems other than CHP to address the current research questions (cf. Section 1.1.5), Chapter 2 includes the methodologies of various heat generation models, heat distribution models, and heat storage models that have been implemented.

Finally, within Chapter 2, an exhaustive literature review on greenhouse climate control is presented. Climate control focuses on two main aspects: firstly, the definition of climate set-points, and secondly, the control of greenhouse appliances to respect the set-points. The identified methods from the literature review were subsequently

employed in the development of control strategies. These strategies, in turn, facilitated the simulation of the aforementioned models to emulate real-world actions, thereby generating realistic results.

All the models implemented in this work are summarized in Tables 1.1, 1.2 and 1.3. These tables provide an overview of the four main model blocks (greenhouse climate, crop yield, thermal generation, distribution and storage, and climate control) along with their respective sub-models. Each table entry includes the primary reference for each model, the year of the reference, and a brief description of the model type and its validation status. There is no global validation of the entire model because each block is based on previously validated models from the literature. Consequently, this thesis has not focused on validating these individual blocks; however, Chapter 4 is dedicated to ensuring that the integrated model produces physical results consistent with those of the foundational models.

Knowledge of common practices has been acquired throughout the course of this thesis. This has been achieved through information published in the literature and discussions with other researchers in the field, including those from the Gembloux campus of the University of Liege, the Geel campus of KU Leuven, Thomas More, Warmtekracht Ondersteunings Maatschappij, Wageningen University & Research, A-net, Hankyong National University, Seoul National University, Samsung Electronics, EZFarm, FARM8, Spacewalk, and ioCrops.

TABLE 1.1: Summary of models used in this thesis (Part I)

Model	Sub-model	Reference	Year	Type
Greenhouse climate model		[21]	2011	Physical model based on sensible energy, moisture and CO_2 balances. **Validated** for temperate marine climate (Netherlands), Mediterranian climate (Sicily, Italy) and semi-arid climate (Texas)
	Free convective heat exchange coefficients (can-air, air-flr, air-scr, scr-top, air-cov, top-cov, pip-air)	[22]	1996	Physical model based on Nusselt-Rayleigh (Nu-Ra) relation
	Forced convective heat exchange coefficients (cov-out, pip-air)	[23]	1983	Experimentally-derived model
	Conductive heat exchange coefficients	[22]	1996	Physical model based on thermal conductivity
	Ventilation exchange coefficient through the screen	[24]	1989	Experimentally-derived model studying the temperature-driven flow
	Ventilation heat exchange coefficient through the screen gap	[25]	1998	Physical model based on Navier-Stokes equations
	Ventilation heat exchange coefficient through windows (air-out)	[26]	1993	Physical model
	Latent heat flows	[21]	2011	Physical model based on heat of vaporization of water
	Long-wave raditaion exchange coefficients	[22]	1996	Physical model based on the Stefan-Boltzmann equation
	Short-wave radiation model (also applicable to supplementary lighting)	[21] - [27]	2011	Physical model based on trasmission, reflection and absorption factors. The canopy part is modeled with exponential decomposition of light with the LAI
	Moisture flow from evaporation or consendation on surfaces	[22]	1996	Physical model based on a linear correlation between the moisture exchange coefficient and the convective heat exchange coefficient

TABLE 1.2: Summary of models used in this thesis (Part II)

Model	Sub-model	Reference	Year	Type
Greenhouse climate model (continuation)				
	Moisture flow from ventilation (air-top, air-out)	[22]	1996	Physical model based on vapor pressure and temperature difference
	Canopy transpiration	[27]	1987	Experimentally-derived model
	CO_2 flow absorbed by the canopy	[28]	2011	Physical model. **Validated** for mild and extreme temperatures with varying light and CO_2 conditions
Crop yield model (tomato crop)		[28]	2011	Physical model based on carbohydrate mass balances taking into account photosynthesis in the presence of a buffer, including the growth rates and growth and maintenance respirations. **Validated** for mild and extreme temperatures with varying light and CO_2 conditions
Climate control strategies				
	Temperature and CO_2 set-point definition	[64]-[84]	2003, 2022	Based on **validated** models & common practice
	Supplementary lighting operation	[84]	2022	Based on common practice
	Windows aperture	[84]	2022	Based on common practice
	Thermal screen deployment set-point	[84]	2022	Based on **validated** models & common practice
	Thermal screen deployment strategy	[84]	2022	Based on **validated** models & common practice
	Thermal screen opening for humidity gap	[84]	2022	Based on **validated** models & common practice

TABLE 1.3: Summary of models used in this thesis (Part III)

Model	Sub-model	Reference	Year	Type
Heat distribution				
	Discretized flow	[29]	2014	Physical model with enthalpy as a state variable
	Heating pipes by means of discretized flow	[79]	2019	Physical model based on a finite volume approach with several cells interconnected by nodes
	Heating and cooling coils	[30]	1990	Physical model based on single zone epsilon-NTU. **Validated** experimentally
Heat generation				
	Combined heat and power (CHP) (only full-load operation)	[31]	2018	Performance-based model based on the secondary law and Carnot efficiencies
	Heat pump (only full-load operation)	[31]	2018	Performance-based model based on the COP of Carnot and the secondary law efficiency
	Water-to-water heap pump (part- and full-load operation)	[32]	2022	Polynomial-based performance model fitted with manufacturing data
Heat storage				
	Stratified tank with internal heat exchanger	[31]	2018	Physical model based on a nodal model with energy and mass conservation principles and assuming thermodynamic equilibrium at all times inside the control volume
Aquifer thermal energy storare (ATES)		[89]-[90]-[91]	2010	**Validated**

In **Chapter 3** of Part I, the implementation of the methods outlined in Chapter 2 in the Dymola language is meticulously detailed. This implementation is subsequently released as the **Greenhouses Modelica Library** in an open-source capacity. The primary objective is to showcase the library's capabilities to potential users. Accordingly, this chapter provides a high-level overview of the methodology (without delving into specifics) and offers a user-centric description of each model, outlining parameters, default values, and required exogenous inputs. The graphical interface and structure of the library are presented, and ready-to-simulate models (termed *Examples* in the library) are introduced to the user.

Furthermore, users are directed to an existing online documentation of the Library for comprehensive guidance. This documentation includes a setup guide for new users, facilitating their initial engagement, and a step-by-step guide for simulating predefined examples within the library.

Finally, Chapter 3 succinctly summarizes certain numerical aspects of the modeling process in the Dymola language. It specifically addresses the enhancement of computational efficiency by circumventing the generation of state events during integration. The complexity of the final model largely depends on the selected discretization scheme for the piping and for the ground. However, for a typical complete greenhouse example model (e.g. the model *Greenhouse1* in the *Examples* package), the system of equations comprises 4222 unknowns, among which 197 are differentiated variables. After the symbolic manipulation, the size of the non-linear systems of equations is 236 for the initialization problem and 3 for the integration. The typical solving time is 48 minutes for a one-year simulation with a 3 GHz I7 processor.

Part II

As a reminder, the developed tool is designed to facilitate the addressing of research questions aimed at accelerating the energy transition in greenhouse horticulture. As outlined in Section 1.1.5, this involves exploring energy efficiency measures, the impact of greenhouse climate control and the control of generation units on operational costs, as well as studying alternative solutions for energy supply. To illustrate how can the developed modeling framework be employed to assess novel solutions, **Part II** presents three case studies, each addressing a specific research question.

Firstly, **Chapter 4** tackles the following question:

How can climate control strategies in technologically equipped greenhouses be optimized to enhance energy efficiency, i.e. maximize crop production while minimizing energy consumption?

This chapter aims to *i)* illustrate the use of the library, particularly emphasizing the influence of greenhouse control strategies on total energy consumption; *ii)* showcase the physical characteristics of the developed modeling framework through a case study, presenting a detailed analysis of results values and profiles. To that end,

the models are coupled and run for a simulation time period equivalent to a growing cycle for tomato crops in mild-climate conditions. Results, including thermal consumption of the greenhouse and crop harvest rate, are presented. Control variables and indoor climate variables and flows are illustrated, with obtained results aligning with existing literature, ensuring the model's physical behavior and the effectiveness of proposed control strategies.

Subsequently, **Chapter 5** demonstrates the use of the proposed modeling framework by addressing the following questions:

How can current greenhouse systems, composed of a CHP unit coupled with TES, be modified to enhance sustainability?

Specifically, is the integration of heat pumps in these systems a sustainable alternative that can potentially reduce overall system costs, and what are the implications and benefits of such integration?

In the context of the Netherlands, as discussed in Section 1.1.1, CHP has been the predominant energy supply for greenhouses over the past 15 years, with a current installed capacity of 2.65 GWe. In 2021, out of the total 10.4 TWh of electricity generated by the greenhouse sector, only 3.7 TWh were used for self-consumption[3]. Notably, the remaining 6.8 TWh, constituting 65% of the total generation, were sold to the market. Consequently, over half of the electricity produced by CHP units in the sector is directed to market sales. In the absence of subsidies, the electricity sale is remunerated at a price close to the wholesale price. This chapter proposes the addition of a heat pump as a strategic measure to enhance electrical self-consumption.

This approach aims to address the economic advantages enjoyed by prosumers in maximizing their level of self-consumption, particularly in the context of the notable difference between retail and wholesale electricity prices [20]. Additionally, it is expected to decrease the operational hours of the CHP, thereby contributing to a reduction in emissions. The proposed addition of a heat pump, coupled with thermal energy storage, aims to enhance the system's economic efficiency by minimizing electricity sold back to the grid while covering the greenhouse heating needs. The optimized control strategy ensures crop production is sustained.

Recent events have demonstrated a surge in electricity prices in the power market, promoting the sale of electricity rather than prioritizing self-consumption. Nevertheless, it is noteworthy that the utility of this paper remains intact, as its primary objective was to showcase the model's capabilities.

Finally, **Chapter 6** presents the concluding case study within this thesis, which aims at addressing the following question:

[3]It is important to note that the sector's overall electricity consumption amounted to 6.6 TWh, with 2.9 TWh being acquired from third-party sources.

What are the optimal energy management strategies for enhancing energy efficiency in greenhouse horticulture, with a specific focus on screen deployment control and the operation of CHP units, and what are the potential benefits associated with these optimizations?

This chapter demonstrates the capabilities of the modeling framework in achieving energy savings and operational cost reduction through a specific case study. To this end, the case study is simulated under six different control strategies, associated with two sensitivity studies. The first study evaluates the impact on energy savings resulting from the control of components within the greenhouse, specifically the thermal screen. The second study assesses the impact on both energy savings and operational costs through the control of units external to the greenhouse, specifically a CHP unit coupled to TES.

The case study is tailored to a real system in the Netherlands, with its characteristics documented in the literature. Consequently, results from these simulations are anticipated to align with real-world scenarios. This case study underscores the substantial influence that tuning the climate controller or controlling heat generation units can have on operational costs. Additionally, it emphasizes the considerable dependency of these costs on energy market prices.

Part III

Ultimately, in **Part III** the developed modeling framework has been employed to examine the viability of innovative low-carbon energy sources for meeting the energy requirements of greenhouses. In particular, these research questions have been addressed:

What sustainable energy solutions are viable for greenhouses, and how can the developed modeling framework contribute to exploring these integrated systems?

Specifically, what is the energy recovery potential of greenhouses with thermal storage in shallow alluvial aquifers in Atlantic climates, and what are the advantages and implications of such integration?

Currently, the utilization of thermal energy storage in alluvial aquifers is in its nascent stages of development and lacks well-established foundations. In the context of the Netherlands, aquifer thermal energy storage (ATES) accounts for only 6% of the existing RES generation. The concept involves air-conditioning greenhouses during the summer, allowing the storage of excess energy in an underground seasonal buffer. This stored energy can then be utilized for heating in the winter, facilitated by a heat pump. The evaluation of the benefits derived from employing ATES to meet energy demands in greenhouse applications necessitated the modeling of specific systems. To address this, new models were developed and integrated into the Greenhouses Library, notably a water-to-water heat pump model and heating and

cooling coil models. The aquifer, modeled in a separate software, is represented by a deterministic 3D groundwater flow and heat transport numerical model. The detailed methodology is expounded upon in **Chapter** 7.

The models are sized to a specific case study based on a 100 m thick aquifer in the Cretaceous chalk located in Wallonia (Belgium) and are simulated over a two-year period. Due to the nature of the models, the experimental protocol is iterative and consists of 4 simulations. The first year is exclusively dedicated to storage, simulating the establishment of cold and warm wells. In the second year, the thermal energy stored in the aquifer is recovered according to the greenhouse's requirements, utilizing the cold well for air-conditioning and the warm well for heating. Results, deliberated in Chapter 7, demonstrate that shallow alluvial aquifers can be highly beneficial, offering a sustainable solution for heating and cooling greenhouses.

1.3 Scientific Publications

In the context of this doctoral thesis, an array of research activities has been conducted. The ensuing **peer-reviewed** publications, wherein I assume the role of the **principal author**, encapsulate the fundamental contributions of this thesis to the scientific discourse:

- **Q. Altes-Buch**, S. Quoilin, and V. Lemort. "Modeling and control of CHP generation for greenhouse cultivation including thermal energy storage." In *Proceedings of ECOS 2018 - The 31st International Conference on Efficiency, Cost, Optimization, Simulation and environmental impact of energy systems*, 13. 2018.
  - Solely my contribution:
    - idea on the article's research question (i.e. maximizing level of self-consumption to de-carbonize current systems);
    - literature review on greenhouse climate & thermal systems models, selection of models & implementation in Modelica;
    - idea & design of case study (i.e. coupling of a heat-pump in the classic Dutch greenhouse-CHP-TES system), implementation in Modelica, including control system;
    - sizing, simulation, analysis & selection of most important results;
    - full article scripting;
    - application of changes from peer-reviewed process & scripting of rebuttal letter.
  - Quoilin's & Lemort's contribution: Review of article before submission & review of my modifications after peer-review process.

- **Q. Altes-Buch** and V. Lemort. "Modeling framework for the simulation and control of greenhouse climate." In *Proceedings of the 10th International Conference on System Simulation in Buildings*, 20. 2018.
  - Solely my contribution:
    - idea on the article's research question (i.e. increase energy efficiency of a system by means of adequate climate control strategies);
    - literature review on greenhouse climate control strategies;
    - selection of models & implementation in Modelica;
    - design of case study & idea on proposed control strategies, implementation in Modelica;
    - simulation, analysis & selection of most important results;
    - full article scripting;
    - application of changes from peer-reviewed process & scripting of rebuttal letter.
  - Lemort's contribution: Review of article before submission & review of my modifications after peer-review process.
- **Q. Altes-Buch**, S. Quoilin, and V. Lemort. "Greenhouses: A Modelica Library for the Simulation of Greenhouse Climate and Energy Systems." In *Proceedings of the 13th International Modelica Conference*. 2019. doi:10.3384/ecp19157533 **Winner of the first prize of the Modelica Library Award in 2019.**
  - Solely my contribution:
    - idea on the article;
    - literature review on greenhouse climate, thermal systems & climate control models;
    - research on common Modelica practices and conventions with the objective to create a structured library that uses universal fluids and ports so that it can be used together with other libraries;
    - implementation in Modelica, including decision on library structure (i.e. split between models & sub-models, level of hierearchy between models, modeling of new universal ports), numerical decisions (i.e. transformation of conditional equations to sigmoid functions), documentation of all variables, parameters and model descriptions in each model of the library, graphical interface of each model etc.;
    - versioning of the code in Git-hub with open-access including basic documentation on the *Readme*;

    * development of an online user guide that is highly useful for users as it centralizes both the description of the entire set-up process and includes description of the models and their equations in detail;
    * full article scripting;
    * application of changes from peer-reviewed process & scripting of rebuttal letter.
  - Quoilin's & Lemort's contribution: Review of article before submission & review of my modifications after peer-review process.

- **Q. Altes-Buch**, S. Quoilin, and V. Lemort. "A modeling framework for the integration of electrical and thermal energy systems in greenhouses." *Building Simulation*, 15: 779–797. 2022. doi:10.1007/s12273-021-0851-2
  - Solely my contribution:
    * idea on the article's research question (i.e. quantify the increase in energy efficiency of classic Dutch CHP-TES systems by optimizing the control of the generation unit or the thermal screen);
    * extended literature review on greenhouse climate control strategies, research on the sector's practices on operating the generation and TES units;
    * idea & design of case study (sized to real system with public data found in the literature) & proposed control strategies;
    * implementation of the control strategies in Modelica (i.e. PID & state graphs);
    * simulation, analysis & selection of most important results;
    * full article scripting;
    * application of changes from peer-reviewed process & scripting of rebuttal letter.
  - Quoilin's & Lemort's contribution: Review of article before submission & review of my modifications after peer-review process.

- **Q. Altes-Buch**, T. Robert, S. Quoilin, and V. Lemort. "Assessment of short-term aquifer thermal energy storage for energy management in greenhouse horticulture: modeling and optimization." In *Proceedings of the 7th International High Performance Buildings Conference*, 2022.
  - Solely my contribution:
    * idea on the article's research question (i.e. assess the viability of ATES for greenhouses in Cretaceous chalk);

    - literature review on sustainable solutions (from established practices to early stages of development) for greenhouses in Dutch climate, review on energy recovery potential of greenhouses;
    - idea & design of case study part excluding ATES: greenhouse, pipes, coils, heat pump;
    - implementation of case study in Modelica, development of control strategies for the system operation;
    - sizing & simulations on the greenhouse side, analysis & selection of most important results;
    - full article scripting (except for the description of ATES model - see Robert's contributions);
    - application of changes from peer-reviewed process & scripting of rebuttal letter.
  - Solely Robert's contribution:
    - literature review on ATES models;
    - implementation of ATES model;
    - proposal of a location for the case study size and sizing of ATES wells;
    - simulation of ATES with the greenhouse inputs;
    - scripting the description of the ATES model in the article;
  - Robert's, Quoilin's & Lemort's contribution: Review of article before submission & review of my modifications after peer-review process.

Furthermore, the research pursuits conducted within the framework of this thesis have yielded an additional publication, not encompassed within this manuscript, wherein I hold a co-authorship:

- T. Resimont, **Q. Altes-Buch**, K. Sartor, and P. Dewallef. "Economic and environmental comparison of a centralized and a decentralized heating production for a district heating network implementation." In *10th International Conference on System Simulation in Buildings*, 2018.
  - Solely my contribution: Provide a sized greenhouse model adapted to be connected to the district heating.

It should be noted that, in order to respect the integrity of the original publications, the articles have been reproduced exactly as published, including any minor typographical errors. As a result, some notations may have changed during the course of this work. For example, Chapter 4 and 5 use $\dot{T}$ instead of the dT/dt notation used in the rest of the manuscript. Readers are encouraged to refer to the nomenclature

section at the end of the chapters for clarification. We apologize for any inconvenience this may cause, but we have prioritized preserving the original articles in their published form.

Part I

Modeling

Chapter 2

A Modeling Framework for Greenhouse Climate Simulation and its Integration with Electrical and Thermal Energy Systems

This chapter is a reprint of the modeling part in *Q. Altes-Buch, S. Quoilin, and V. Lemort. "A modeling framework for the integration of electrical and thermal energy systems in greenhouses." Building Simulation, 15: 779–797. 2022. doi:10.1007/s12273-021-0851-2*

Summary

This paper presents a comprehensive examination encompassing a literature review, an overview of current state-of-the-art, and the mathematical formulation of the various models developed within the context of this thesis. These models span across diverse domains, including the greenhouse climate, crop yield, heat generation, heat distribution, heat storage, and greenhouse climate control.

Contributions

The primary contribution of this article is the integration of validated models from diverse fields: the greenhouse model (building simulation), a crop yield model (biology), thermal systems models (thermodynamics), and greenhouse climate control (control). The objective is to develop a unified simulation platform, as detailed in Section 1.2.

The second contribution of this article is the improvement of the greenhouse model, which originally utilized an isothermal hypothesis for heat transfer from the heating pipes within the greenhouse. To improve model accuracy, a more detailed approach has been implemented, wherein the water flow through the pipes is represented by a discretized model that segments the pipes into multiple cells.

The third contribution of this article is the innovative method for computing temperature and CO_2 set-points. This work combines the set-point computation method from [64] for daylight periods, with an optimization of the set-point during nighttime based on the literature review of temperature effects on crop growth. The computation of the set-point for nighttime depends on the previous daylight hours and considers an average temperature and a maximum spread between the maximum and minimum temperatures over 24 hours. This model, employed in the Autonomous Greenhouses Challenge (2nd Edition)[1], demonstrated significant improvements in tomato growth and reductions in energy consumption compared to traditional set-point definitions, greatly contributing to our success in achieving second position.

The last contribution of this article is the open-source release of the code for all models, including the default values for all model parameters, to facilitate reproducibility. This article thus presents the inaugural release of a modeling framework that enables the dynamic simulation of greenhouses connected to thermal and electrical systems.

Reading tips

This chapter exclusively focuses on reproducing the modeling segment of the article, and therefore presents an abridged rendition of the conclusions. Notably, the conclusions related to the case study results are intentionally omitted here and will be revisited in Chapter 6.

[1] Wageningen University & Research (WUR) and Tencent attracted 21 teams with more than 200 participants and 26 nationalities to participate in the 2nd edition of the Autonomous Greenhouses Challenge. The goal of the Hackathon was to optimize net profit of a virtual tomato crop grown in a virtual greenhouse. For that tomato yield and product quality, thus income, had to be maximized on one side, while the use of resources such as energy, CO_2 and water, thus costs, had to be minimized on the other side. The teams themselves determine the ideal set points for temperature, amount of light, CO_2 concentration and a number of cultivation-related parameters, such as plant and stem density. The optimization had to be done using models of WUR of a virtual greenhouse and tomato crop using artificial intelligence algorithms.

I participated to the challenge with team Digilog and used my model to optimize the set-point definition, greatly contributing in achieving a second place in the Hackaton competition.

2.1 Introduction

In the European context, the agriculture sector accounted for 3.2% of the EU-27 final energy consumption in 2018 [33]. A large share of this consumption originated from the greenhouse horticulture sector due to its high heating and electricity requirements. For instance, in a country like the Netherlands, greenhouses accounted for 79% of the total energy consumed by agriculture in 2013, even though they represented only 0.5% of the total utilized agricultural area [34].

The improvement of energy efficiency in greenhouses has been the subject of a substantial literature. Over the past years, developments were primarily focused on energy saving solutions in order to decrease the energy requirements. However, energy supply in greenhouses still mostly relies on gas-fired units that inevitably contribute to CO_2 emissions. In the context of the energy transition, it is important to identify how renewable energy sources (RES) can be utilized to supply the energy needs of greenhouses. Additionally, it is important to investigate the potential services that the remaining gas-fired units such as combined heat and power (CHP) can provide to the grid to facilitate the penetration of RES. Furthermore, as a multi-energy consumer requiring heating, electricity and CO_2, greenhouses can provide good opportunities for flexibility across several energy sectors.

Applications of greenhouses integrated with low-carbon sources have been successfully implemented in many countries. For instance, in 2019, the Netherlands counted with 17 existing and 35 under-development geothermal projects to heat greenhouses [14]. In parallel, the recovery of residual heat from industries is also being developed. An example is the under-construction heat network that uses the residual heat generated in the port of Rotterdam alone to heat a significant part of the 2 385-ha of greenhouses in Westland (and over 500 000 households) [15]. Although weather-dependent, applications with solar energy coupled to thermal energy storage (TES) are also being investigated and implemented. Some examples are the recent SOLHO off-grid unit [35], which serves 100% of the heating and electricity demand of a greenhouse in the South of France, and the biogas, solar and ground energy heating unit in Elazig, Turkey [36].

As previously mentioned, in order to help the integration of RES, the potential services provided by greenhouses to the grid should be investigated. CHP units in the horticulture sector have the ability to ramp-up to full capacity in less than one hour [37]. When coupled to TES, they can readily provide ancillary services or decentralised storage capacity for load balancing [38]. In a country such as the Netherlands, the CHP capacity dedicated to the agriculture and horticulture sectors was 3 000 MW_{el} (for a national peak load of 18 000 MW_{el}) and represented 63.7% of the CHP installations in 2012 [39]. In 2016, these units accounted for 7.8% of the national electrical production [40].

A platform capable of simulating the greenhouse climate and the complex energy exchanges between greenhouses and their energy generation units is necessary to evaluate the potential contribution to the energy transition. A recent review listed 30 available models for greenhouse climate simulation [41]. However, the existing models are incomplete in several aspects. First, although most of these models offer a small number of customized parameters, little flexibility is given on the greenhouse design. In fact, the models are calibrated for one type of greenhouse and do not allow selecting the modeled energy systems within the greenhouse. In addition, although the mathematical formulation of some of the models is openly presented, their implementation remains closed source. Examples range from the well-known KASPRO model [42], to recent models such as [43]. In a similar way, commercial climate simulation tools (e.g. CASTA, Hortinergy) are proprietary software that do not openly release code. Only recently a climate simulation model implemented in Matlab was released open-source [18], but does not include a user interface and has limited modularity. Finally, none of the reviewed existing models include the dynamic modeling of the energy supply and storage systems, which are required when evaluating the energy flexibility potential of greenhouses. The main goal of this work is to fill these gaps by:

- Providing an open-source modeling framework capable of simulating and optimizing the greenhouse climate, the crop yield and the complex energy flows relative to the energy systems coupled to the greenhouse.
- Offering a wide range of models that allow the configuration of completely customized systems by means of a user-friendly interface.
- Facilitating studies focused on the evaluation of various energy sources for heating and/or cooling the greenhouse by providing a greenhouse model parametrized to the typical Venlo-type design that allows the connection to different generation systems.
- Illustrating the capabilities of the modeling framework for energy saving and operational cost reduction through a particular case study simulated under six different control strategies.

To that end, the developed framework primarily consists in the following models:

- A greenhouse climate model completely user-definable that was validated for a range of climates and greenhouse designs.
- A broad range of energy systems models, namely heating distribution (water-to-air and air-to-air), generation (CHP units, heat pumps, heating coils), storage, cooling (chiller, cooling coils), ventilation (natural and mechanical) and lighting (high pressure sodium).
- A crop yield model that accounts for the impact of indoor climate and hence energy saving solutions on productivity levels.

- A number of rule-based control strategies, both for the climate and the integrated system.

All the models parameters are user-definable. If no change is introduced by the user, typical values are assumed. The framework is written in the Modelica language and the proposed simulations are run within the Dymola software. The object-oriented nature of this language facilitates the simulation of completely customized systems. Users can build simulations by intuitively inter-connecting the available models in a 'physical' manner in the diagram interface [44]. In addition, two models based on the Venlo-type greenhouse design are parametrized with typical values and are made available for simulation.

The developed modeling framework can be used for multiple purposes. For instance, to evaluate the potential of the aforementioned low-carbon energy sources (e.g. heat pumps, geothermal energy, heat recovery, solar energy etc.) as well as to define the optimal energy generation capacities in specific case studies. In addition, it can be used to optimally integrate the CHP or heat pump units with the electricity markets to provide flexibility. Finally, it can be used to analyze energy saving solutions for greenhouses as well as the sizing of their HVAC systems. Although the number of modeled energy systems remains limited, the full compatibility (connector-wise) of the framework allows the connection to other Modelica libraries (e.g. Buildings [45], IDEAS [46], ThermoCycle [29], ThermoPower [47], etc.). These include a wide range of models such as district heating networks, solar cycles, dwellings or other HVAC systems. The modeling framework was successfully used in a previous work [48] to simulate an urban agricultural site. The obtained results showed that a district heating network connecting a residential building stock can increase its efficiency by adding a greenhouse to the network. In 2019, the modeling framework was also used in the Autonomous Greenhouses International Challenge [49] to train an artificial intelligence (AI) algorithm controlling a greenhouse remotely, which opens an interesting and yet unexplored field of research.

The following sections elaborate on state-of-the-art greenhouse climate simulation models and provide the theoretical background used for the developed framework.

2.2 Methods

2.2.1 Greenhouse climate model

Most of the reported greenhouse climate models in the literature (e.g. [22], [23], [50]–[52]) are defined for a specific location and for a specific greenhouse structure and outdoor climate. In this work, a more generic greenhouse climate model [21] combining, among others, the work of [23] and [22] has been implemented. The heat transfer model has however been improved with respect to these models, in which an isothermal hypothesis is used for the heat transfer from the heating pipes.

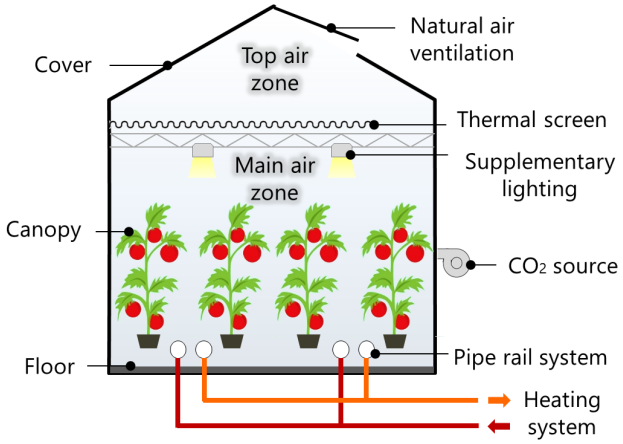

FIGURE 2.1: Example of a greenhouse and its components

A more detailed approach in which the water flowing through the pipes is modeled by means of a discretized model that divides the pipes into several cells is preferred for the sake of model accuracy.

The greenhouse climate model describes the indoor climate of a greenhouse resulting from a greenhouse design, outdoor climate and a specific control. In greenhouses, the indoor climate is characterized by the temperature, the humidity and the CO_2 concentration in the air. The climate is influenced by all the elements in the greenhouse and the energy flows between them. These elements, shown in Figure 2.1, are mainly the air, the canopy, the envelope (i.e. the cover and the floor), the heating pipes and the thermal screen. For instance, the canopy temperature has an impact on its photosynthesis and transpiration, which decrease the CO_2 concentration and increase the moisture content of the air. The temperature of the envelope influences the vapor pressure of water of the air, which is decreased by condensation at the cover and at the thermal screen. The thermal screen is an horizontally movable membrane used to reduce the far-infrared radiative losses to the cover and to the sky. When the screen is deployed, the air of the greenhouse is divided in two zones, i.e. below and above the screen. These zones, entitled *main* and *top* zones, are modeled separately and their respective climate is assumed to be homogeneous.

The description of the implemented greenhouse climate model is organized as follows. Subsections 2.2.1, 2.2.1 and 2.2.1 respectively describe the sensible energy, moisture and CO_2 balances in the climate model. Subsections 2.2.1, 2.2.1 and 2.2.1 respectively describe the energy, moisture and CO_2 flows between the greenhouse components.

Sensible energy balance

The first state variable describing the greenhouse climate is the dry-bulb air temperature. This temperature is computed by applying a sensible energy balance on each

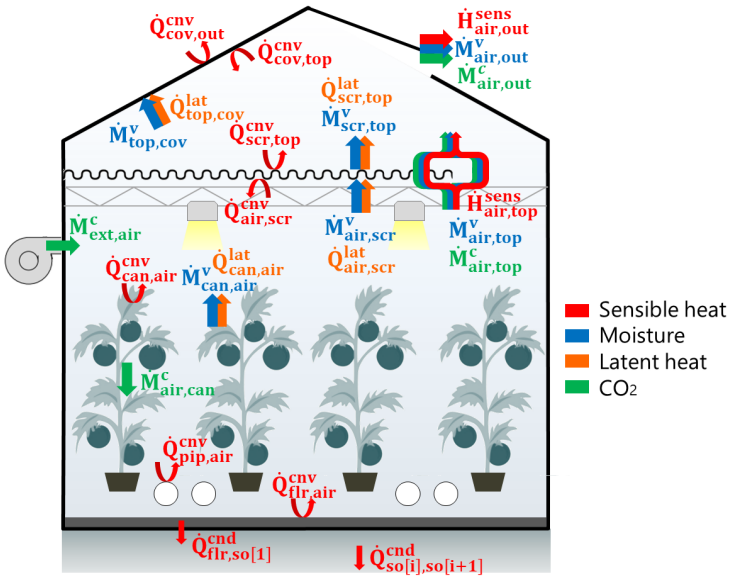

FIGURE 2.2: Schematic representation of the greenhouse climate model flows related to sensible heat, moisture transfer, latent heat and CO_2 transfer

component. The general form of this balance is defined by Equation (2.1):

$$\rho \, c_p \, V \, \frac{dT}{dt} = \sum \dot{Q} + \sum \dot{H}^{sens} \tag{2.1}$$

where $\dot{Q}$ includes the convection ($\dot{Q}^{cnv}$) and conduction flows ($\dot{Q}^{cnd}$), and $\dot{H}^{sens}$ includes the sensible heat related to a mass transfer. When Equation (2.1) applies to a surface, $\dot{H}^{sens}$ is null and $\dot{Q}$ also includes the long-wave radiation flows ($\dot{Q}^{rad}$), the absorption of short-wave radiation ($\dot{Q}^{swr}$) and the latent heat flows from evaporation or condensation ($\dot{Q}^{lat}$). These flows are graphically represented in Figure 2.2 and 2.3.

The energy balance on the main air zone is described by Equation (2.2). The temperature of the air is increased primarily by the heating system, but also by the short-wave radiation absorbed by the greenhouse components and later exchanged through convection to the air. Additionally, because of the screen material porosity, sensible energy and moisture are exchanged between both zones. The air is further cooled down by natural ventilation through the vents as well as by infiltrations or exfiltrations through the greenhouse envelope.

$$\begin{aligned} \rho_{air} \, c_{p,air} \, V_{air} \, \frac{dT_{air}}{dt} = \dot{Q}^{swr}_{sun,\,air} + \dot{Q}^{swr}_{ilu,\,air} + \dot{Q}^{cnv}_{pip,\,air} \\ + \dot{Q}^{cnv}_{can,\,air} - \dot{Q}^{cnv}_{air,\,flr} - \dot{Q}^{cnv}_{air,\,cov} \\ - \dot{Q}^{cnv}_{air,\,scr} - \dot{H}^{sens}_{air,\,top} - \dot{H}^{sens}_{air,\,out} \end{aligned} \tag{2.2}$$

The energy balance on the cover is described by Equation (2.3). The temperature of the cover depends on the convective heat flows with the indoor and outdoor air.

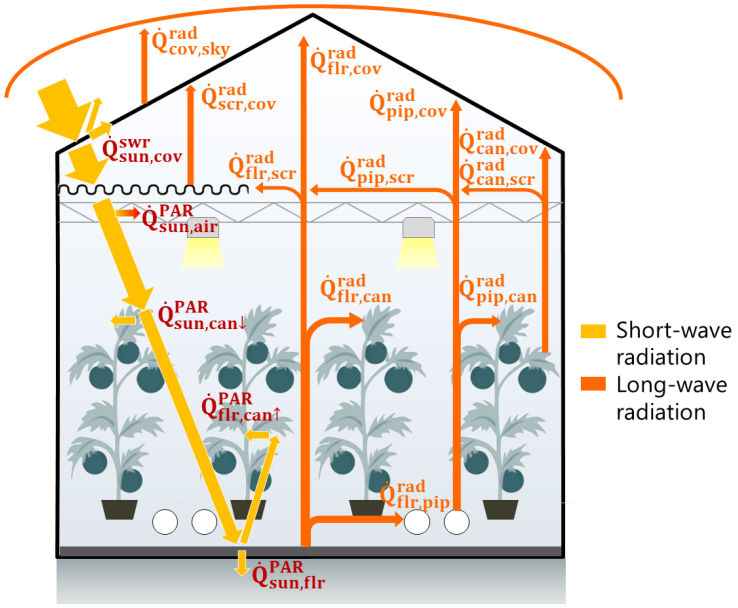

FIGURE 2.3: Schematic representation of the greenhouse climate model flows related to long-wave radiation and the absorption of short-wave photosynthetically active radiation (PAR)

Depending on the water vapor pressure difference with respect to the air, condensation at the inner side of the cover may occur. The convective and latent flows are modeled between the cover and the main air zone if the greenhouse has no thermal screen or in case the screen is open. However, when the screen is deployed, they are included in the energy balance of the top air zone. Long-wave radiation is modeled between the cover and all the greenhouse components, as well as the sky. The model also includes the absorbed incident solar radiation. Therefore, the energy balance on the cover is described by:

$$\begin{aligned} \rho_{cov}\, c_{cov}\, V_{cov}\, \frac{dT_{cov}}{dt} &= \dot{Q}^{swr}_{sun,\,cov} + \dot{Q}^{cnv}_{top,\,cov} + \dot{Q}^{lat}_{top,\,cov} \\ &+ \dot{Q}^{cnv}_{air,\,cov} + \dot{Q}^{lat}_{air,\,cov} + \dot{Q}^{rad}_{pip,\,cov} + \dot{Q}^{rad}_{can,\,cov} \\ &+ \dot{Q}^{rad}_{flr,\,cov} + \dot{Q}^{rad}_{scr,\,cov} - \dot{Q}^{cnv}_{cov,\,out} - \dot{Q}^{rad}_{cov,\,sky} \end{aligned} \tag{2.3}$$

The energy balance on the canopy is defined by Equation (2.4), where the heat capacity per unit of leaf area is a constant estimated by [27]. The magnitude of the energy exchanged by the canopy depends on the size of its leaves, which is increased by crop growth and decreased by leaf pruning. The leaf area index (LAI), defined as the leaf area per unit of ground area, is a variable used to quantify this. The short-wave

radiation absorbed by the canopy depends on its absorption coefficients, which differ according to the spectrum of the incident radiation.

$$\begin{aligned} c_{leaf}\, LAI\, \frac{dT_{can}}{dt} = \dot{Q}^{swr}_{sun,\,can} + \dot{Q}^{swr}_{ilu,\,can} + \dot{Q}^{rad}_{pip,\,can} \\ -\dot{Q}^{cnv}_{can,\,air} - \dot{Q}^{lat}_{can,\,air} - \dot{Q}^{rad}_{can,\,cov} \\ -\dot{Q}^{rad}_{can,\,flr} - \dot{Q}^{rad}_{can,\,scr} \end{aligned} \tag{2.4}$$

The energy balance on the floor is defined by Equation (2.5). The floor temperature is increased by the absorbed short-wave radiation from the sun and from supplementary lighting. Moreover, it is influenced by long-wave radiation flows, convection with the air and conduction through the ground.

$$\begin{aligned} \rho_{flr}\, c_{flr}\, V_{flr}\, \frac{dT_{flr}}{dt} = \dot{Q}^{swr}_{sun,\,flr} + \dot{Q}^{swr}_{ilu,\,flr} + \dot{Q}^{rad}_{pip,\,flr} \\ +\dot{Q}^{rad}_{can,\,flr} + \dot{Q}^{cnv}_{air,\,flr} - \dot{Q}^{cnv}_{flr,\,cov} \\ -\dot{Q}^{cnv}_{flr,\,scr} - \dot{Q}^{cnd}_{flr,\,so[1]} \end{aligned} \tag{2.5}$$

To account for the high thermal capacity of the floor, conduction through the ground is modeled by means of a nodal model. The ground is divided into several layers, whose thickness increases with the depth. The temperature of the ground layer 'i' is described by the energy balance of Equation (2.6). The temperature of the deepest layer is a boundary condition. The model is written in a general form so that the ground can be made of a single material (e.g. soil) or a combination of materials (e.g. concrete layers on top of soil).

$$\rho_{so[i]}\, c_{so[i]}\, V_{so[i]}\, \frac{dT_{so[i]}}{dt} = \dot{Q}^{cnd}_{so[i-1]so[i]} - \dot{Q}^{cnd}_{so[i]so[i+1]} \tag{2.6}$$

The energy balance on the screen is described by Equation (2.7). Although the radiative, convective and latent heat flows are modeled for both sides of the screen, the latter is assumed to be at a single temperature. This assumption is justified by the fact that its thickness (commonly lower than 1 mm) implies a very low heat capacity. Since the screen is mostly deployed at night (i.e. when there is no sunlight), the absorbed heat from short-wave radiation is neglected. It should be noted that the flows related to the screen are function of the screen position, i.e. they are null if the screen is completely open.

$$\begin{aligned} \rho_{scr}\, c_{scr}\, V_{scr}\, \frac{dT_{scr}}{dt} = \dot{Q}^{rad}_{pip,\,scr} + \dot{Q}^{rad}_{can,\,scr} \\ +\dot{Q}^{rad}_{flr,\,scr} + \dot{Q}^{cnv}_{air,\,scr} + \dot{Q}^{lat}_{air,\,scr} \\ -\dot{Q}^{cnv}_{scr,\,top} - \dot{Q}^{lat}_{scr,\,top} - \dot{Q}^{rad}_{scr,\,cov} \end{aligned} \tag{2.7}$$

As previously stated, when the screen is deployed, the indoor air is divided in two zones. In that case, the model computes an energy balance in each air zone. Thus, the flows that take place above the screen are no longer considered in Equation (2.2) but in the top air balance. This energy balance is described by Equation (2.8).

$$\rho_{top}\, c_{p,top}\, V_{top}\, \frac{dT_{top}}{dt} = \dot{Q}^{cnv}_{scr,\,top} + \dot{H}^{sens}_{air,\,top} - \dot{Q}^{cnv}_{top,\,cov} - \dot{H}^{sens}_{top,\,out} \tag{2.8}$$

Moisture balance

The second characteristic describing the greenhouse climate is the moisture content of the air, which is increased by the transpiration of the canopy and decreased by the ventilation and by the condensation on the cover and on the screen. In the model, the main state variable is the water vapor pressure of the air, which is computed by applying a moisture mass balance on the main and top air zones (Equations (2.9) and (2.10), respectively).

$$M_v\, \frac{V_{air}}{R\,T}\, \frac{dP^v_{air}}{dt} = \dot{M}^v_{can,\,air} - \dot{M}^v_{air,\,cov} - \dot{M}^v_{air,\,scr} - \dot{M}^v_{air,\,top} - \dot{M}^v_{air,\,out} \tag{2.9}$$

$$M_v\, \frac{V_{top}}{R\,T}\, \frac{dP^v_{top}}{dt} = \dot{M}^v_{air,\,top} + \dot{M}^v_{scr,\,top} - \dot{M}^v_{top,\,cov} - \dot{M}^v_{top,\,out} \tag{2.10}$$

To compute the flows related to condensation and evaporation, the water vapor pressure of the surfaces (i.e. the canopy, the cover and the screen) is defined as the saturated vapor pressure at the surface temperature. As suggested by [22], the mass transfer capacity of the air is assumed to be independent of its temperature (i.e. $T = 291$ K in Equation (2.9) and (2.10)).

CO_2 balance

The third state variable describing the greenhouse climate is the CO_2 mass concentration of the air, which is determined by means of a CO_2 mass balance. The CO_2 concentration of the indoor air is decreased by ventilation and the CO_2 consumption of the canopy. At the same time, it can be increased by the CO_2 supply from an external source. The CO_2 mass concentration of the main and top air zones is described by Equations (2.11) and (2.12), respectively.

$$V_{air}\, \frac{d\gamma^c_{air}}{dt} = \dot{M}^c_{ext,air} - \dot{M}^c_{air,\,can} - \dot{M}^c_{air,\,top} - \dot{M}^c_{air,\,out} \tag{2.11}$$

$$V_{top}\, \frac{d\gamma^c_{top}}{dt} = \dot{M}^c_{air,\,top} - \dot{M}^c_{top,\,out} \tag{2.12}$$

Sensible energy flows

Since all the components are uniformly distributed, all model flows (energy, moisture, CO_2) are described per square meter of greenhouse floor.

Convection The convective heat flow on a surface is function of the heat exchange coefficient (U_{ij}) and is described by:

$$\dot{q}_{ij}^{cnv} = U_{ij} \left(T_i - T_j\right) \tag{2.13}$$

The calculation method for the heat exchange coefficient depends on the type of convection. Most of the convective processes in greenhouses are governed by free convection. Nonetheless, some are considered to be forced. In free convection, the Nusselt number (Nu) describing the convective exchange can be defined as a function of the Rayleigh number (Ra) [24]. By means of the Nu-Ra relation, [22] described the heat exchange coefficients for free convection processes. In forced convection, the heat exchange coefficients are derived from experimental results. This is the case of the outer side of the greenhouse cover, where convection is driven by wind speed. The heat exchange on the heating pipes can also be considered to be hindered if the pipes are situated close to the floor and are surrounded by leaves. Therefore, their heat transfer coefficient is modeled differently than for pipes in free air. These two forced convection processes were fitted by [23] using experimental data. All the heat transfer coefficients are presented in Table 2.1.

Conduction The only conductive flow considered in greenhouse modeling is the conduction through the soil. The ground under the greenhouse floor represents a significant thermal capacity with a poor thermal conductivity. In order to describe the temperature gradient, the soil is modeled in several layers. The heat flow between the layers is described by Equation (2.13), using the conduction heat exchange coefficient from Table 2.1.

Ventilation In the greenhouse, air exchange is mainly driven by natural ventilation between the indoors and outdoors as well as between the main and top air zones. Their convective flows are modeled by an air exchange rate between two volumes i and j, as described by:

$$\dot{h}_{ij}^{sens} = \rho_{air}\, c_{p,air}\, \dot{v}_{ij} \left(T_i - T_j\right) \tag{2.14}$$

As shown in Figure 2.2, the ventilation flow between the main and top air zones is a combination of two air flows: i) through the screen fabric pores and ii) through a gap when the screen is not fully deployed. The former was derived from experimental data obtained by studying the temperature-driven flow through fully deployed screens ($u_{scr} = 1$) [24]. The latter, which dominates the exchange, was theoretically modeled by [25] using the Navier-Stokes equation. Combining both air flow rates,

TABLE 2.1: Heat exchange coefficients for convective and conductive heat transfer

Heat exchange coefficients U_{ij} [W m^{-2} K^{-1}]
Free convection
$U_{can,\,air} = 2 \cdot LAI \cdot U_{leaf,air}$
$U_{air,\,flr} = \begin{cases} 1.7\,(T_{flr} - T_{air})^{0.33}, & \text{if } T_{flr} > T_{air} \\ 1.3\,(T_{air} - T_{flr})^{0.25}, & \text{otherwise} \end{cases}$
$U_{air,\,scr} = u_{scr}\,1.7\,\lvert T_{air} - T_{scr}\rvert^{0.33}$
$U_{scr,\,top} = u_{scr}\,1.7\,\lvert T_{scr} - T_{top}\rvert^{0.33}$
$U_{air,\,cov} = (1 - u_{scr})\,1.7\,(T_{air} - T_{cov})^{0.33} cos\,\varphi^{-0.66}$
$U_{top,\,cov} = u_{scr}\,1.7\,(T_{air} - T_{cov})^{0.33} cos\,\varphi^{-0.66}$
$U_{pip,\,air} = 1.28\,\pi\,d_{pip}^{0.75}\,l_{pip}\,\lvert T_{pip} - T_{air}\rvert^{0.25}$
Hindered convection
$U_{pip,\,air} = 1.99\,\pi\,d_{pip}\,l_{pip}\,\lvert T_{pip} - T_{air}\rvert^{0.32}$
Forced convection
$U_{cov,\,out} = \begin{cases} (2.8 + 1.2\,v_w)\dfrac{1}{cos\,\varphi}, & \text{if } v_w < 4\ [\text{m s}^{-1}] \\ 2.5\,v_w^{0.8}\dfrac{1}{cos\,\varphi}, & \text{otherwise} \end{cases}$
Conduction
$U_{so[i-1]so[i]} = \dfrac{2}{\dfrac{e_{so[i-1]}}{\lambda_{so[i-1]}} + \dfrac{e_{so[i]}}{\lambda_{so[i]}}}$

the total ventilation rate between the main and top zones is described by:

$$\begin{aligned} \dot{v}_{air,\,top} &= u_{scr}\, K_{scr}\, |T_{air} - T_{top}|^{0.66} \\ &+ \frac{1 - u_{scr}}{\overline{\rho}} \sqrt{0.5\, \overline{\rho}\, W\, g\, (1 - u_{scr}) |\rho_{air} - \rho_{top}|} \end{aligned} \tag{2.15}$$

where $\overline{\rho}$ is the mean value between the main and top air zones density.

The air flow rate to the outside air through the roof windows mainly depends on the windows opening (u_{ven}), but also on the wind pressure coefficient and the coefficient of energy discharge caused by friction at the windows [26]:

$$\dot{v}_{air,\,out} = \frac{u_{ven}\, A_{ven}\, K_d}{2\, A_{flr}} \sqrt{g\, \frac{h_{ven}}{2}\, \frac{T_{air} - T_{out}}{\overline{T}} + K_w\, v_w^2} \tag{2.16}$$

The total ventilation rate of the greenhouse is influenced by the leakage rate through the greenhouse structure, which is linearly dependent on wind speed and is a function of the leakage coefficient of the greenhouse. The latter has a constant value, characteristic of the structure. The leakage rate is described by:

$$\dot{v}_{leak} = \begin{cases} 0.25\, K_{leak}, & \text{if } v_w < 0.25 \\ v_w\, K_{leak}, & \text{otherwise} \end{cases} \tag{2.17}$$

Long-wave radiation Long-wave radiation is modeled between all greenhouse components and between the cover and the sky. The Stefan-Boltzmann equation is written:

$$\dot{q}_{ij}^{rad} = A_i\, \varepsilon_i\, \varepsilon_j\, F_{ij}\, \sigma\, (T_i^4 - T_j^4) \tag{2.18}$$

The emission coefficients are characteristic of the surfaces and the view factors of the greenhouse elements are described in [22].[2]

Latent heat flows The latent heat from condensation or evaporation flows is function of the moisture mass flow rate associated to its process, as described by:

$$\dot{q}_{ij}^{lat} = \Delta h_{fg}\, \dot{m}_{ij}^{v} \tag{2.19}$$

where the heat of vaporization of water (Δh_{fg}) is computed at 21 °C.

Short-wave radiation Short-wave radiation in a greenhouse originates from the sun or from supplementary lighting. Although the contribution of supplementary lighting is small during summer, in winter it can double the solar input through a

[2]The definition of the Stefan-Boltzmann equation and the computation of the view factors per greenhouse elements is elaborated in Annex A

day and thus, have an important impact on crop growth. The solar radiation incident on a greenhouse can be split in three spectral parts: ultra violet (UV, from 0.3 to 0.4 μm), visible light (from 0.4 to 0.7 μm) and near infrared light (NIR, from 0.7 to 3 μm). The visible light has an interest for biological growth and is referred as photosynthetically active radiation (PAR). The portion of UV and PAR of the global radiation is 6-10% and 45-60%, respectively [53]. However, for plant growth it is common to assign 50% to PAR (η^{PAR}), neglect the UV and assign the other 50% to NIR (η^{NIR}) [22]. As proposed by [21], the solar model of this work is simplified by making no distinction between diffuse and direct solar radiation and by assuming that the transmission coefficient of the greenhouse cover does not depend on the solar angle.

The heat flow from the solar radiation absorbed by the cover is described by:

$$\dot{q}^{swr}_{sun,cov} = \alpha_{cov}\, I^G \tag{2.20}$$

The radiation that is not reflected or absorbed by the cover is transmitted into the greenhouse. Since the absorption coefficients of the canopy and floor differ according to the spectrum, their absorbed heat flow is computed separately for PAR and NIR. The transmitted PAR, i.e. the PAR above the canopy, can be defined by:

$$I^{PAR}_{\tau} = (1 - \eta^G_{air})\, \tau^{PAR}_{cov}\, \eta^{PAR}\, I^G \tag{2.21}$$

where η^G_{air} is the ratio of the radiation that is absorbed by the greenhouse elements and is later released to the air.

The deployment of the thermal screen may reduce the amount of transmitted light. Thus, τ^{PAR}_{cov} is a lumped value of the greenhouse cover and the movable thermal screen transmission coefficients.

Part of the transmitted radiation is absorbed by the canopy and the floor. As shown in Figure 2.3, the PAR absorbed by the canopy is a combination of the PAR directly absorbed by the canopy and the PAR reflected by the greenhouse floor and then absorbed by the canopy:

$$\dot{q}^{PAR}_{sun,can} = \dot{q}^{PAR}_{sun,\,can\downarrow} + \dot{q}^{PAR}_{flr,\,can\uparrow} \tag{2.22}$$

In a homogeneous crop, the absorbed radiation is described by an exponential decomposition of light with the LAI [54]:

$$\dot{q}^{PAR}_{sun,\,can\downarrow} = I^{PAR}_{\tau}\,(1 - \rho^{PAR}_{can})\left(1 - e^{-LAI \cdot K^{PAR}}\right) \tag{2.23}$$

$$\dot{q}^{PAR}_{flr,\,can\uparrow} = I^{PAR}_{\tau}\, e^{-LAI \cdot K^{PAR}}\, \rho^{PAR}_{flr}(1 - \rho^{PAR}_{can})\left(1 - e^{-LAI \cdot K^{PAR}}\right) \tag{2.24}$$

The heat flow of PAR absorbed by the floor is described by:

$$\dot{q}^{PAR}_{sun,flr} = I^{PAR}_{\tau} \left(1 - \rho^{PAR}_{flr}\right) \left(1 - e^{-LAI \cdot K^{PAR}}\right) \tag{2.25}$$

Since the PAR reflection coefficient of the canopy and floor is low, the restant PAR reflected back into the greenhouse is neglected. On the contrary, a non-negligible share of NIR is reflected by the canopy and floor. This share, which is again scattered, increases the NIR absorbed by the canopy and the floor. In the model, the absorbtions are lumped into a single coefficient (α^{NIR}_{can} and α^{NIR}_{flr}), which is computed as proposed by [21]. The absorbed heat flow from NIR for the canopy and floor are described by:

$$\dot{q}^{NIR}_{sun,can} = \alpha^{NIR}_{can} \left(1 - \eta^{G}_{air}\right) \eta^{NIR} I^{G} \tag{2.26}$$

$$\dot{q}^{NIR}_{sun,flr} = \alpha^{NIR}_{flr} \left(1 - \eta^{G}_{air}\right) \eta^{NIR} I^{G} \tag{2.27}$$

Part of transmitted radiation not absorbed by the canopy or the floor is assumed to be absorbed by the greenhouse structural elements and later released to the greenhouse air. This heat flow is described by:

$$\dot{q}^{swr}_{sun,air} = \eta^{G}_{air} I^{G} \left(\tau^{PAR}_{cov} \eta^{PAR} + \left(\alpha^{NIR}_{can} + \alpha^{NIR}_{flr}\right) \eta^{NIR}\right) \tag{2.28}$$

The heat absorption flows from the short-wave radiation coming from supplementary lighting are computed in a similar manner. For PAR, they are computed with Equations (2.22)-(2.25) by replacing I^{PAR}_{τ} by the PAR emitted by supplementary lighting. For NIR, they are computed with Equations (2.26)-(2.27), with recalculated absorption coefficients. It should be noted that only part of the electric consumption of the supplementary lighting is converted to short-wave radiation. In addition, the fraction of PAR and NIR of the emitted radiation depends on the type of lighting. For instance, high intensity discharge lamps e.g. high pressure sodium (HPS) lamps convert 17% of the electrical power to NIR and 25% to PAR [55]. The remaining 58% is released to the greenhouse air in the form of heat.

Moisture flows

Condensation and evaporation Condensation on a surface is governed by processes at the boundary layer of the surface, whose moisture transport mechanism is similar to the one of heat transfer. This similarity implies a correlation between the heat and moisture transfer coefficients. For instance, the moisture exchange coefficient for condensation or evaporation is linearly related to the convective heat

exchange coefficient on that surface [22]. The moisture flow of condensation or evaporation on a surface is described by:

$$\dot{m}^v_{ij} = \begin{cases} \xi\, U_{ij}(P^v_i - P^v_j), & \text{if } P^v_i > P^v_j \\ 0, & \text{otherwise} \end{cases} \tag{2.29}$$

where $\xi = 6.4 \cdot 10^{-9}$ and U_{ij} is obtained from Table 2.1. i and j correspond to the air and the surface for condensation, and vice versa for evaporation.

Condensation is modeled on the inner side of the cover and the lower side of the screen. As previously stated, air and moisture are exchanged through the screen fabric. The model assumes that the screen is capable of transporting water from its lower side to its upper side. Storage of water in the screen is neglected. Therefore, evaporation from the upper side is only possible when condensation takes place at the lower side. This implies that the rate of evaporation is lower or equal to the rate of condensation. In other words, the model assumes that the condensate is either evaporated at the upper side of the screen or dripped from the screen. To take this into account, the evaporation mass flow rate is computed with a modified version of Equation (2.29):

$$\dot{m}^v_{ij} = \begin{cases} \min\left(\xi\, U_{ij},\ \xi\, U_{air,i}\dfrac{P^v_{air} - P^v_i}{P^v_i - P^v_j}\right)(P^v_i - P^v_j), & \text{if } P^v_i > P^v_j \\ 0, & \text{otherwise} \end{cases} \tag{2.30}$$

where i and j correspond to the screen and the top air zone, respectively.

Ventilation The moisture flow exchanged in a ventilation process (i.e. main-top, indoor-outdoor) is related to its air flow rate (Equations (2.15)-(2.16)) and is described by:

$$\dot{m}^v_{ij} = \frac{M_{H2O}\,\dot{v}_{ij}}{R}\left(\frac{P^v_i}{T_i} - \frac{P^v_j}{T_j}\right) \tag{2.31}$$

Canopy transpiration The transpiration flow from the canopy originates from a phase interface somewhere inside the cavities of a leaf. The resistance to vapor transport from the canopy leaves to the greenhouse air is made of an internal resistance (r_s) and a boundary layer resistance (r_b) [27]. The internal resistance, and hence the canopy transpiration, is function of the short-wave radiation, the temperature, the CO_2 concentration and the water vapor pressure in the air. The canopy transpiration can be defined as:

$$\dot{m}^v_{can,\,air} = \frac{2\,\rho_{air}\,c_{p,air}\,LAI}{\Delta h_{fg}\,\gamma\,(r_b + r_s)}\,(P^v_{can} - P^v_{air}) \tag{2.32}$$

CO_2 flows

Ventilation Similar to moisture transfer, the CO_2 flow accompanying a natural ventilation flow is function of its air flow rate (Equations (2.15)-(2.16)) and is described by:

$$\dot{m}^c_{ij} = \dot{v}_{ij} \left(\gamma^c_i - \gamma^c_j\right) \tag{2.33}$$

Photosynthesis The CO_2 flow absorbed by the canopy depends on its photosynthesis rate and respiration processes. It is computed in the crop yield model in the next section.

2.2.2 Crop yield model

Several inputs used in the computation of the greenhouse climate (e.g. the LAI, the CO_2 flow absorbed by the canopy) are characteristics of the crop and must be quantified by a dynamic crop growth model. In addition, crop growth models allow to compare the yield and hence, the profitability (e.g. savings in energy) from different control strategies. For those reasons, a dynamic crop yield model is implemented.

Crop growth is related to the carbohydrate intake by the fruits, leaves and stems. The crop's carbohydrate input, which comes from photosynthesis, passes through a buffer before being distributed. As every storage system, the buffer has a maximum capacity above which no inflow (i.e. photosynthesis) is possible, and a lower limit below which no outflow (i.e. distribution) is allowed. The in- and out-flows depend on the state of charge of the buffer and thereby, may not be simultaneous. For instance, although the photosynthesis flow is only positive during daylight, the carbohydrates distribution may continue at nighttime if the state of charge allows it.

Models for tomato crops accounting for the dynamics of the carbohydrate buffer are available in the current literature (e.g. [56]–[60]). In this work, a relatively recent yield model developed and validated for a variety of temperatures [28] is implemented. The model structure is shown in Figure 2.4. Given that yield models differ between crops, the model implemented in this work is only valid for tomato crop, but can easily be adapted for other varieties.

The availability of carbohydrates in the buffer is described by a mass balance that takes into account the inflow from photosynthesis, the outflow to the leaves, the fruits and the stems (and roots), and the growth respiration of the plant:

$$\begin{aligned}\frac{dm^{ch}_{buf}}{dt} = \dot{m}^{ch}_{air,buf} - \dot{m}^{ch}_{buf,fru} - \dot{m}^{ch}_{buf,leaf} \\ - \dot{m}^{ch}_{buf,stem} - \dot{m}^{ch}_{buf,air}\end{aligned} \tag{2.34}$$

The photosynthesis flow is function of the canopy temperature, the CO_2 concentration of the greenhouse air and the PAR absorbed by the canopy. Their values are

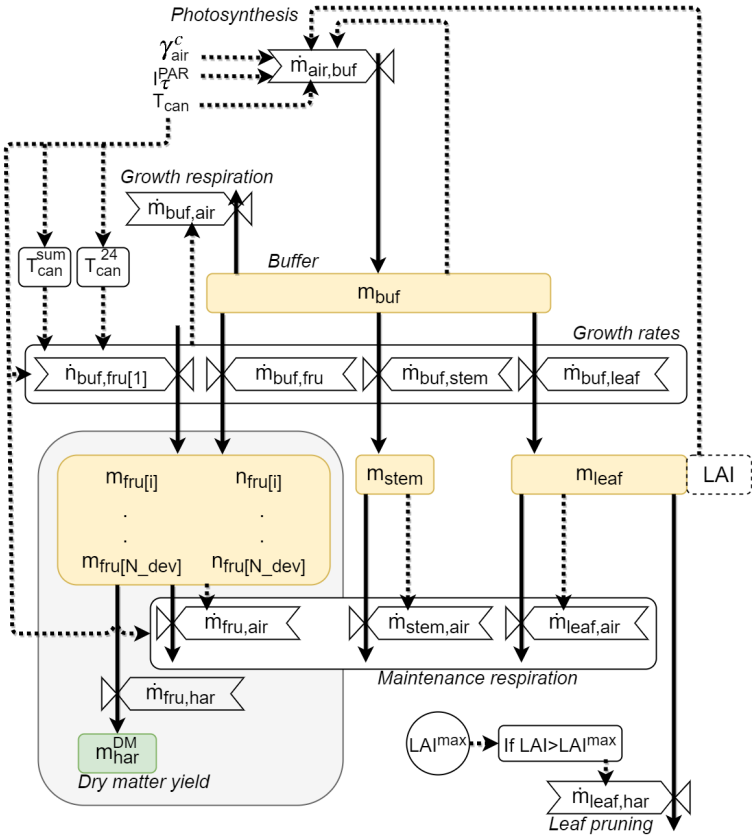

FIGURE 2.4: Schematic representation of the tomato yield model. All mass flows and variables are carbohydrate unless stated otherwise. Arrows define mass flows (solid lines) and information flows (dotted lines). Adapted from [28].

retrieved from the greenhouse climate simulation model, in which the two former ones are state variables and the latter one is function of the global irradiation. The distribution flows to the crop parts are function of the buffer state of charge, the growth rate coefficient of each part, two temperature dependent growth inhibition functions (i.e. one for instantaneous and the other for 24-h mean temperature) and the development stage of the plant.

The fruit growth period, defined as the time between fruit set and fruit harvest, is modeled using the "fixed boxcar train" method [61]. To that end, several successive development stages are distinguished. The carbohydrate flow from one stage to the next follows a development rate given by the method. At the generative stage of the plant, the carbohydrates are stored in a fruit development stage. For a stage i, the stored carbohydrates are described by a mass balance:

$$\begin{aligned} \frac{dm^{ch}_{fru[i]}}{dt} &= \dot{m}^{ch}_{buf,\,fru[i]} + \dot{m}^{ch}_{fru[i-1],\,fru[i]} \\ &-\dot{m}^{ch}_{fru[i],\,fru[i+1]} - \dot{m}^{ch}_{fru[i],\,air}, \quad i = 1, 2...N_{dev} \end{aligned} \tag{2.35}$$

where N_{dev} is the total number of fruit development stages. For the first stage ($i = 0$),

$\dot{m}^{ch}_{fru[i-1],\,fru[i]}$ is zero. For the last stage ($i = N_{dev}$), $\dot{m}^{ch}_{fru[i],\,fru[i+1]}$ equals to the harvest $\dot{m}^{ch}_{fru,\,har}$, main output of the model. $\dot{m}^{ch}_{fru[i],\,air}$ is the maintenance fruit respiration of the stage i.

Analogous to the carbohydrate flows between stages, the number of fruits from one stage to the next is defined by a development rate given in the method. Its evolution at fruit development stage i is described by:

$$\frac{dn_{fru[i]}}{dt} = \dot{n}_{fru[i-1],\,fru[i]} - \dot{n}_{fru[i],\,fru[i+1]},\ i = 1, 2...N_{dev} \tag{2.36}$$

The amount of carbohydrates stored in the leaves is increased by the distribution from the buffer and decreased by the leaf maintenance respiration and leaf pruning. Its evolution is defined by a mass balance on the leaves, as described by:

$$\frac{dm^{ch}_{leaf}}{dt} = \dot{m}^{ch}_{buf,\,leaf} - \dot{m}^{ch}_{leaf,\,air} - \dot{m}^{ch}_{leaf,\,har} \tag{2.37}$$

The LAI is a semi-state variable of the model that can be determined by the specific leaf area (SLA) and the carbohydrates stored in the leaves:

$$LAI = SLA \cdot m^{ch}_{leaf} \tag{2.38}$$

The evolution of the carbohydrates stored in the stems and roots is influenced by the distribution from the buffer and the maintenance respiration, as described by:

$$\frac{dm^{ch}_{stem}}{dt} = \dot{m}^{ch}_{buf,\,stem} - \dot{m}^{ch}_{stem,\,air} \tag{2.39}$$

The harvested tomato dry matter (DM) is assumed to evolve with a continuous harvest rate. Therefore, the accumulated DM equals to the carbohydrate outflow from the last fruit development stage converted to DM by a conversion factor, as described by:

$$\frac{dm^{DM}_{har}}{dt} = \xi_{ch \to DM} \cdot \dot{m}^{ch}_{fru,\,har} \tag{2.40}$$

The development stage of the plant is described by the canopy temperature sum (Equation (2.41)), which allows describing the transition from vegetative to generative stage. Its value is zero when the generative stage starts.

$$\frac{dT^{sum}_{can}}{dt} = \tau^{-1} \cdot T_{can} \tag{2.41}$$

Finally, the 24 hour mean canopy temperature, used in one growth inhibition function, is determined by a 1st order approach:

$$\frac{dT_{can}^{24}}{dt} = \tau^{-1} \cdot (T_{can} - T_{can}^{24}) \tag{2.42}$$

For Equations (2.41) and (2.42), τ is 86400 s.

2.2.3 HVAC and storage models

This section describes a selection of implemented models for heat distribution, generation and storage.

Heating distribution system

The most common heating distribution system in greenhouses is the so-called pipe rail system, which consists of several parallel pipe loops along the crop rows, and is also used as rails for transporting the harvest. An example is shown in Figure 2.1. Given their rail function, they are plain non-finned pipes and are placed some centimeters above the ground (i.e. below the canopy). To cope with their low heat transfer coefficient, they commonly work at high temperature (between 50°C and 90°C). As shown in Figure 2.2 and 2.3, heat is transferred by long-wave radiation to the canopy, the floor and the greenhouse cover, and by hindered convection to the air. Depending on the location and the type of crop, greenhouses may have a smaller secondary low temperature heating circuit placed on top of the canopy.

Because of the importance of temperature-dependent convection and radiation, a constant heat transfer coefficient cannot be assumed along the pipe. A discretized model has therefore been selected. Water flowing through the pipes is modeled using a finite volume approach by means of a discretized model that divides the pipes into several cells, each one connected in series by a node [29]. In each cell, the flow is described with enthalpy as a state variable. The dynamic energy balance and static mass and momentum balances are applied in each cell. The model assumes uniform speed through the cross section as well as constant pressure. Axial thermal energy transfer is neglected. The heat flow is computed by an ideal heat transfer model with constant heat transfer coefficient. The energy balance on the fluid for a cell i is described by:

$$V_i \, \rho_i \, \frac{dh_i}{dt} + \dot{M}(h_{ex,i} - h_{su,i}) = A_i \, \dot{q}_i, \quad i = 1, 2...N_{cell} \tag{2.43}$$

where h_i is the fluid specific enthalpy at cell i, and h_{ex} and h_{su} are the enthalpy at the cell's outlet and inlet nodes, respectively.

Generation unit

This work proposes a generic CHP model that can be used for different CHP technologies. The CHP is modeled by means of a performance-based model that does not consider part-load operation. Given the latter, the gas consumption is assumed to be constant and follows an On-Off regulation. The unit's total efficiency is also assumed to be constant. The electrical and thermal powers are described by:

$$\dot{W} = u_{chp} \cdot \eta_{el} \cdot \dot{Q}_{gas} \tag{2.44}$$

$$\dot{Q} = u_{chp} \cdot (\eta_{tot} - \eta_{el}) \cdot \dot{Q}_{gas} \tag{2.45}$$

where u_{CHP} is a boolean control variable that defines the operational status of the CHP.

The electrical efficiency is function of the nominal second-law efficiency, which is assumed constant, and the Carnot efficiency, which is function of the high and low temperatures of the cycle. Its value is described by:

$$\eta_{el} = \eta_{II,n} \cdot \eta_{Carnot} \tag{2.46}$$

The nominal value of the second-law efficiency is defined by Equation (2.46) at nominal operation conditions (i.e. the nominal electrical efficiency as well as nominal high and low temperatures of the cycle).

Thermal energy storage

Thermal energy storage is modeled by means of a nodal model applied to a stratified tank with an internal heat exchanger. The water tank is modeled using the energy and mass conservation principles and assuming thermodynamic equilibrium at all times inside the control volume. The internal heat exchanger is discretized in the same way as the tank, i.e. each cell of the heat exchanger corresponds to one cell of the tank and exchanges heat with that cell only. The model takes into account ambient heat losses and neglects axial thermal conductivity. The energy balance of the fluid in the heat exchanger is described by Equation (2.43). The energy balance of the fluid in the tank is described by:

$$\frac{V^{tes}}{N_{cell}} \rho_i \frac{dh_i}{dt} + \dot{M}(h_{ex,i} - h_{su,i}) - A_{hx,i}\, \dot{q}_{hx,i} = \frac{A_{amb}}{N_{cell}}\, \dot{q}_{amb}, \quad i = 1, 2...N_{cell} \tag{2.47}$$

where A_{amb} is the total heat exchange area from the tank to the ambient.

2.2.4 Climate control

In order to maximize crop yield, greenhouses have strict requirements on indoor climate control. The climate controller adjusts heating, ventilation and CO_2 supply to attain the desired climate. In this work, several control systems are proposed and implemented.

Climate set-points definition

The determination of temperature and CO_2 set-points is key to maximize photosynthesis and thus the harvest. As measured in [62], different combinations of temperature and CO_2 levels for a given radiation level lead to different photosynthesis rates. Moreover, although a sharp reduction in photosynthesis rate is measured at non-optimal temperatures, similar rates are measured for close-to-optimal temperatures (i.e. optimal temperature ± 3°C). This allows selecting set-points that not only maximize photosynthesis rate but also minimize energy consumption.

The definition of temperature set-points for optimal crop growth and energy use has been the subject of a substantial literature (e.g. [63]–[66]). However, since this work does not focus on climate set-points optimization, the strategy proposed in [64] is adopted and implemented. The strategy consists in selecting the pair of temperature and CO_2 levels at a given radiation level that minimizes energy consumption while maintaining a close-to-maximal crop growth rate. This is achieved by the following process:

i) computing a 2-D table of photosynthesis rates at a given PAR for a range of CO_2 and temperature values,

ii) selecting from the table the pairs of CO_2 and temperature that ensure at least 80% of the photosynthesis rate (the 100% being the maximum value of the 2-D array), and

iii) defining the temperature and CO_2 set-point ($T_{air,SP}$, $\gamma^c_{air,SP}$) as the pair in ii) with the lowest temperature.

In the model, a proportional integer (PI) controller ensures that the air temperature set-point is respected by adjusting the power output of the heating system. A second PI controller ensures that the CO_2 set-point is respected by adjusting the supply from the enrichment system. The CO_2 admission valve is a modulating valve, whose operating range is assumed to go from 0 to 100%. Given that CO_2 is an expensive resource, in high ventilation conditions the set-point is modified so that it decreases proportionally with the increase in the ventilation rate. This is done as defined by Equations (2.48) and (2.49).

$$\gamma^c_{air,SP'} = \eta_{ven} \left(\gamma^c_{air,SP} - \gamma^{c,min}_{air,SP} \right) + \gamma^{c,min}_{air,SP} \tag{2.48}$$

$$\eta_{ven} = \begin{cases} 1 - \dfrac{u_{ven}}{u_{ven}^{max}}, & \text{if } u_{ven} < u_{ven}^{max} \\ 0, & \text{otherwise} \end{cases} \tag{2.49}$$

Supplementary lighting

In this work, the lighting model parameters correspond to HPS lamps, which are the most used commercial type of lamp in horticulture because of their high emission in the PAR spectrum range. The control strategy is based on the following conditions and rules:

- *Time window:* allow lights to be turned On during a time window (t_{start}, t_{end}), e.g. from 5 AM to 10 PM.
- *Threshold:* during the time window, allow lights to be turned On if the level of transmitted short-wave radiation decreases below a threshold ($I_{Off \to On}$) and to be turned Off if it increases above a threshold ($I_{On \to Off}$), with $I_{On \to Off} > I_{Off \to On}$.
- *Proving time:* the level of transmitted radiation must be above or below the threshold for a certain time (t_{prove}) before acting.
- *Maximum accumulation:* turn Off lights or do not allow turning them On if the daily accumulated short-wave radiation exceeds a threshold (I_{acc}^{max}).
- *Minimum time On:* to prevent cycling, which dramatically reduces the lamp lifespan, lights must remain On for a minimum time (t_{On}^{min}) once they are turned On, regardless of other conditions.

Windows

In greenhouse climate control, windows are opened for two different purposes. The first is dehumidification, since excessive humidity can cause fungal diseases or physiological disorders to the canopy [67]. The most common technique for dehumidification is natural ventilation with the outside air, which requires heating to maintain the indoor temperature at the set-point. Although this technique is energy consuming and thus expensive, dehumidifying systems based on refrigerant cycles, e.g. heat pumps, have not yet proved to be economically feasible [55]. The second purpose is cooling the indoor air in case of excessive temperature, since this has a negative impact on the harvest rate. For instance, in [28], the harvest rate at daytime temperatures of 40°C was only 54.5% of that at 25°C. In addition, temperatures above 25°C can penalize fruit quality e.g. size and color [55].

In the model, a PI controller selects the opening of the windows depending on the purpose:

- *Air sanitation:* when humidity exceeds a threshold (RH_{ven}), set by the user (commonly 85%).

- *Air cooling:* when air temperature exceeds a threshold (T_{ven}), which can be variable in function of for instance outside temperature.

Thermal screen

As previously mentioned, the thermal screen is an horizontally movable membrane used to limit the far-infrared radiative losses to the cover and to the sky. When deployed, these losses can be reduced by 38% to 60% [68]. This capability is defined by the screen material, which is mainly selected according to the climate of the region where the greenhouse is located. The selected material also implies a certain short-wave transmission coefficient, whose value can vary from 88% to 15%.

Deployment set-point Since the screen reduces considerably the transmitted light, the most conventional method to operate the screen is to open it at sunrise, to benefit from the available sunlight, and to draw it at sunset, when heating demand becomes significant.

A possibility to further reduce energy consumption is to deploy the screen before sunset and to delay the opening until after sunrise. However, this method implies a loss of crop production caused by a reduction on the available light. Determining the optimal tradeoff between energy saving and production loss in terms of deployment and opening times has been the object of several studies (e.g. [64], [68]). It is however a complex task, subject to multiple uncertainty sources are requiring multiple assumptions.

A simpler approach is to define the deployment of the screen in function of the sole outside irradiation. This is justified by the fact that the photosynthetic activity of the plant achieves its maximal potential about one hour after sunrise and diminishes just before sunset [69].

In this work, a hybrid approach has been selected, where the deployment of the screen is defined by an outside temperature-dependent radiation criterion. This method promotes energy savings in cold, cloudy days and avoids overheating in warm mornings, which is an improvement compared to the radiation-only dependent approach.

Deployment strategy In order not to generate cold air flows on top of the canopy, the screen is removed progressively until reaching a certain gap size, from which it can be fully removed. For instance, in mild conditions, a screen is typically removed progressively at around 1% per minute (with an interval pause of 3 minutes) followed by a full removal after 30%. The duration of this process can be adapted to the outside weather. For instance, in Dutch-conditions this process can last about 45 min to 60 min in cold days and 30 min in mild days [69]. The same applies for the screen deployment.

In the model, the duration of the process (t_{open}) and the gap size from which the screen can be removed completely ($u_{scr,open}$) are defined as adjustable parameters. In order to avoid the computational overhead linked to *events* during the simulation [70], the removal/deployment processes are not performed step-wise but continuously.

Humidity gap It is common during night-time to perform small temporary openings of the vents to decrease the relative humidity in the main air zone. As for the *deployment strategy*, to maintain a sufficient computational efficiency, the humidity gap is not controlled step-wise (as proposed in [71]) but continuously. This is done by means of a PI controller, which compares the actual humidity value to a set-point (RH_{gap}). The control signal ranges between no gap to a maximum gap value set by the user.

In a similar way, a small opening may be required because of temperature excess. This opening is also controlled by a PI controller, whose set-point (T_{gap}) is set some degrees above the indoor air set-point.

2.3 Conclusions

The presented modeling framework is dedicated to the energy management and system integration of greenhouses. It gathers in a single library relevant models accounting for crop yield, greenhouse climate simulation, heat and power generation units and greenhouse control systems. The framework is released as open-source, thus ensuring a proper reproducibility and reusability of this work [72] (Download from: https://github.com/queraltab/Greenhouses-Library).

The parametric, object-oriented approach offers a high degree of flexibility to the user. The model can easily be adapted to meet different greenhouse designs by parametrizing the existing components (e.g. floor material, type of cover, capacities of the HVAC systems, etc.) or even to add other components (e.g. the addition of secondary heating circuits, side vents, shading screens, cooling, forced ventilation, etc.). Although not presented in this manuscript, models for the above mentioned components are included in the library. The modeling framework can thus be used for a wide range of greenhouse designs and climates.

In conclusion, the presented open-source modeling framework can be used for a wide range of possibilities that can contribute to the necessary energy transition. Apart from optimizing the control strategies to drive productivity while reducing energy use, it can also evaluate the potential use of renewable energy sources (e.g. solar, geothermal), the use of energy-related emissions (e.g. waste-heat or CO_2 emissions) or even the impact in the power grid by using existing CHP units for ancillary services.

Nomenclature

Physic constants

γ	Psychrometric constant	Pa K^{-1}
σ	Stefan-Boltzmann constant	W m^{-2} K^{-4}
g	Gravitational constant	m s^{-2}
R	Molar gas constant	J mol^{-1} K^{-1}

Subscripts

τ	Transmitted
acc	Accumulated
air	Greenhouse main air zone
amb	Ambient air
b	Boundary
buf	Carbohydrate buffer
can	Canopy
$Carnot$	Carnot Cycle
$cell$	Cells of a discretization model
chp	Combined heat and power
cov	Cover
d	Discharge
dev	Development stage
el	Electrical
ex	Exhaust node
ext	External source of CO_2
flr	Floor
$fru[i]$	Crop fruits at the i^{th} development stage

gas	Fuel gas
har	Harvest
hx	Heat exchanger
II	Second-law
ilu	Supplementary lighting
in	Within boundaries
$leaf$	Crop leaves
$leak$	Leakage
n	Nominal
oh	Overheating
out	Outside air
pip	Heating pipes
s	Stomata
scr	Thermal screen
sky	Sky
$so[i]$	The i^{th} soil layer
SP	Set-point
$stem$	Crop stems and roots
su	Supply node
sun	Sun
th	Thermal
thr	Threshold
top	Greenhouse top air zone
tot	Total
uh	Underheating
ven	Ventilation
w	Wind

Upperscripts

24	24-hour mean
buy	Energy bought

c	CO_2
ch	Carbohydrate
chp	CHP unit
cnd	Conduction
cnv	Convection
DM	Dry matter
G	Global radiation
gh	Greenhouse
lat	Latent
max	Maximum value
min	Minimum value
NIR	Near infrared radiation
PAR	Photosynthetically active radiation
rad	Long-wave infrared raditaion
$sell$	Energy sold
$sens$	Sensible heat
sum	Sumation
swr	Short-wave radiation
tes	Thermal storage tank
v	Vapor

Remaining Symbols

α	Absorption coefficient	-
Δh_{fg}	Latent heat of evaporation of water	J kg^{-1}
$\dot{H}$	Heat flow associated to a mass transfer	W
$\dot{h}$	Heat flow averaged per square meter of greenhouse floor	W m^{-2}
$\dot{M}$	Mass flow rate	kg s^{-1}, mg s^{-1}
$\dot{m}$	Mass flow rate averaged per square meter of greenhouse floor	kg s^{-1} m^{-2}, mg s^{-1} m^{-2}
$\dot{n}$	Number of fruits flow rate averaged per square meter of greenhouse floor	fruits m^{-2} s^{-1}

$\dot{Q}$	Heat flow	W
$\dot{q}$	Heat flow averaged per square meter of greenhouse floor	$W\,m^{-2}$
$\dot{v}$	Air flow rate averaged per square meter of greenhouse floor	$m^3\,s^{-1}\,m^{-2}$
$\dot{W}$	Electrical power	W
η	Efficiency, ratio	-
γ	Mass concentration	$mg\,m^{-3}$
λ	Thermal conductivity	$W\,m^{-1}\,K^{-1}$
π	Energy price	$€\,MWh^{-1}$
ρ	Density, reflection coefficient	$kg\,m^{-3}$, -
τ	Transmission coefficient, time constant	-, s
ε	FIR emission coefficient	-
φ	Roof slope	deg
ξ	Conversion factor	
A	Area	m^2
B	Benefit	€
C	Cost	€
c_p	Specific heat capacity	$J\,kg^{-1}\,K^{-1}$
d	Diameter	m
E	Integrated energy	MWh
e	Thickness	m
F	View factor	-
h	Vertical dimension, enthalpy	m, $J\,kg^{-1}$
I	Solar irradiation	$W\,m^{-2}$
K	Coefficient	-
l	Length per square meter of greenhouse flooe	$m\,m^{-2}$
LAI	Leaf area index	$m^2\,\{leaf\}\,m^{-2}\,\{flr\}$
M	Molar mass	$kg\,mol^{-1}$
m	Mass averaged per square meter of greenhouse floor	$mg\,m^{-2}$
N	Total number	-
n	Number of fruits averaged per square meter of greenhouse floor	$fruits\,m^{-2}$

P	Power input	W
P^v	Vapor pressure of water	Pa
r	Resistance	$\mathrm{s\,m^{-1}}$
RH	Relative humidity	-
SLA	Specific leaf area index	$\mathrm{m^2\,\{leaf\}\,mg^{-1}}$
T	Temperature	K
t	Time	s
U	Heat exchange coefficient	$\mathrm{W\,m^{-2}\,K^{-1}}$
u	Control variable	-
V	Volume	$\mathrm{m^3}$
v	Speed	$\mathrm{m\,s^{-1}}$
W	Width of fully deployed screen	m

Chapter 3

Greenhouses: A Modelica Library for the Simulation of Greenhouse Climate and Energy Systems

This chapter is a reprint of *Q. Altes-Buch, S. Quoilin, and V. Lemort. "Greenhouses: A Modelica Library for the Simulation of Greenhouse Climate and Energy Systems." In Proceedings of the 13th International Modelica Conference. 2019. doi:10.3384/ecp19157533*

Winner of the first prize of the Modelica Library Award in 2019.

Summary

This chapter marks the release of Greenhouses, an open-source Modelica Library encompassing the models detailed in Chapter 2. It delineates the library's graphical interface and structure, aiming to familiarize users with its applicability. The methodology underpinning each model is presented at a high level, with a focus on user-centric descriptions encompassing parameters, exogenous inputs, etc.

Additionally, this chapter provides a concise overview of certain numerical aspects related to the implementation, primarily geared towards enhancing computational efficiency. Conclusively, it directs users to the available online documentation of the Library, featuring a user guide for beginners and a how-to guide for simulating preconfigured examples within the library.

Contributions

The primary contribution of this work is the release of a modeling framework for simulating greenhouse climate and thermal systems, provided as a Modelica language-based library: the Greenhouses Library. This enables researchers in related fields to utilize the library directly, thereby saving the considerable time required to implement such a complex model and allowing them to focus on investigating energy solutions involving greenhouses.

This article is written with a user-oriented approach to facilitate this process. The online documentation and user guide are significant contributions, providing researchers and other users with an attractive interface to access information about the models and enabling them to quickly commence their studies.

An additional contribution of this article is the focus on computational efficiency and robustness of the models. Consequently, this article proposes two solutions to address these aspects. First, because of the important time constants involved in some parts of the model (e.g. the vapor content of the air within the greenhouse), most equations are initialized in steady-state. While this adds some complexity to the initialization problem (in this Chapter's example, a system of 236 non-linear equations), it avoids long and unnecessary transients at the beginning of the simulation. Second, as previously seen in Chapter 2, some equations of the model include conditional statements (in the form of Equation (2.17), (2.29), (2.30), (2.49)) which, during integration, generate state events and thus decrease the computational efficiency of the model. To enhance computational efficiency, these conditional statements have been replaced by a differentiable switch function.

Reading tips

The sub-sections within Section 3.2 and Section 3.4.2 revisit aspects discussed in Chapter 2. Despite the reader's prior engagement with that chapter, these sections retain value by providing user-oriented descriptions of the models without delving extensively into the underlying methodology.

Furthermore, Section 3.2.5 presents two heat pump models, with a detailed exposition of their methodology reserved for subsequent sections of the manuscript (cf. Chapter 5 and 7).

3.1 Introduction

Greenhouses present the peculiarity of requiring heating, electricity and CO_2. As an energy consumer, they contribute to the depletion of non-renewable energy sources and to global warming through energy-related emissions (e.g. CO_2 emissions from fossil fuel combustion gases). Their energy sources should therefore provide the combined demands in a competitive but also sustainable way. Up to now, the use of combined heat and power (CHP) is proposed as an efficient technology for that purpose: the CHP thermal generation is used for heating purposes, the electricity covers the consumption of the appliances and the CO_2 from the exhaust gases can be recovered to activate photosynthesis. In most cases, there is an excess electricity generation that is fed back to the grid. CHP units in greenhouse horticulture are highly flexible, with the ability to go to full load in less than one hour [37]. Therefore, when coupled to thermal storage, CHP units can be valuable for the power system by providing services such as load balancing, ancillary services or decentralised storage capacity [38]. For example, in a country like the Netherlands, the CHP units dedicated to greenhouse horticulture produced 7.8% of the national production in 2016 [40]. Greenhouses can also be coupled to district heatings, in which case activities such as heat recovery from the industry are made possible.

To evaluate the potential of such activities, the complex energy flows within greenhouses must be understood, which also requires ad hoc greenhouse climate models. In addition, a platform for dynamic simulation of the thermal flows interacting between greenhouses and external thermal systems (e.g. district heating networks, generation units, thermal storage) is required. In the current literature, a small number of models are openly available for grenhouse climate simulation and crop growth. Although researchers openly present model structures and simulation scenarios, an open-source simulation platform is still lacking. In fact, the most common climate simulation softwares (e.g. CASTA, KASPRO, VirtualGreenhouse) are not open-access and are not able to handle the integration of greenhouses with external thermal systems. The Greenhouses Modelica library aims at filling this gap by providing an open-source modeling framework capable of simulating greenhouse climate as well as its complex interactions with thermal systems. To that end, the library proposes models covering the following aspects:

- Greenhouse climate, to compute the energy consumption of a greenhouse given its specific design, outdoor conditions and a specific control.
- Thermal systems, with models ranging from heat distribution systems in greenhouses to generation and thermal storage units.
- Crop yield, to account for crop requirements as well as crop behavior (e.g. transpiration and photosynthesis), which influence the indoor climate and thus, the greenhouse energy consumption.

Climate control systems (heating, ventilation, CO_2 enrichment and supplementary lighting) are also included in the library. Furthermore, several numerical methods are developed and implemented in order to enhance the robustness and the simulation speed of the models during initialization and integration.

The library is simple to implement and intuitive to use. The required information for a new user to get started is provided in this paper. Moreover, an additional documentation including a user guide with the required steps to run the models and extended documentation of the library content is available online (cf. Section 3.5 for more details).

The library shows potential for both research and industry applications. On the one hand, it can be useful for greenhouse operators when it comes to optimizing the control of the actuators or the sizing of the HVAC appliances. On the other hand, it can be used for purposes such as optimizing the integration of CHPs in the electricity markets.

3.2 The Greenhouses Modelica library

The Greenhouses Modelica library aims at providing a robust framework to simulate greenhouse climate and its integration with energy systems. The goal is to provide an integrated and fully open-source solution ranging from the computation of energy flows in a greenhouse, to the simulation of complex systems with their control strategy. The Modelica language is thus well adapted to the formulation of this problem, mainly because of its acausal characteristic language that allows interconnecting the models in a 'physical' way [44]. The key features of the library are the following:

- Designed for system level simulations.
- Full compatibility (connector-wise) with the Modelica Standard Library and libraries such as ThermoCycle, ThermoPower or Buildings.
- Various numerical robustness strategies implemented in the components and accessible through Boolean parameters.
- High readability of the models (limited levels of hierarchical modeling).

The components provided in the library are designed to be as generic as possible. For example, the detailed geometry records of the greenhouse structure are not compulsory. Instead, only the floor area, the mean greenhouse height and the roof tilt are required. In all the models, default values relative to the most commonly used greenhouse structure (e.g. the Venlo greenhouse) are proposed for all the parameters.

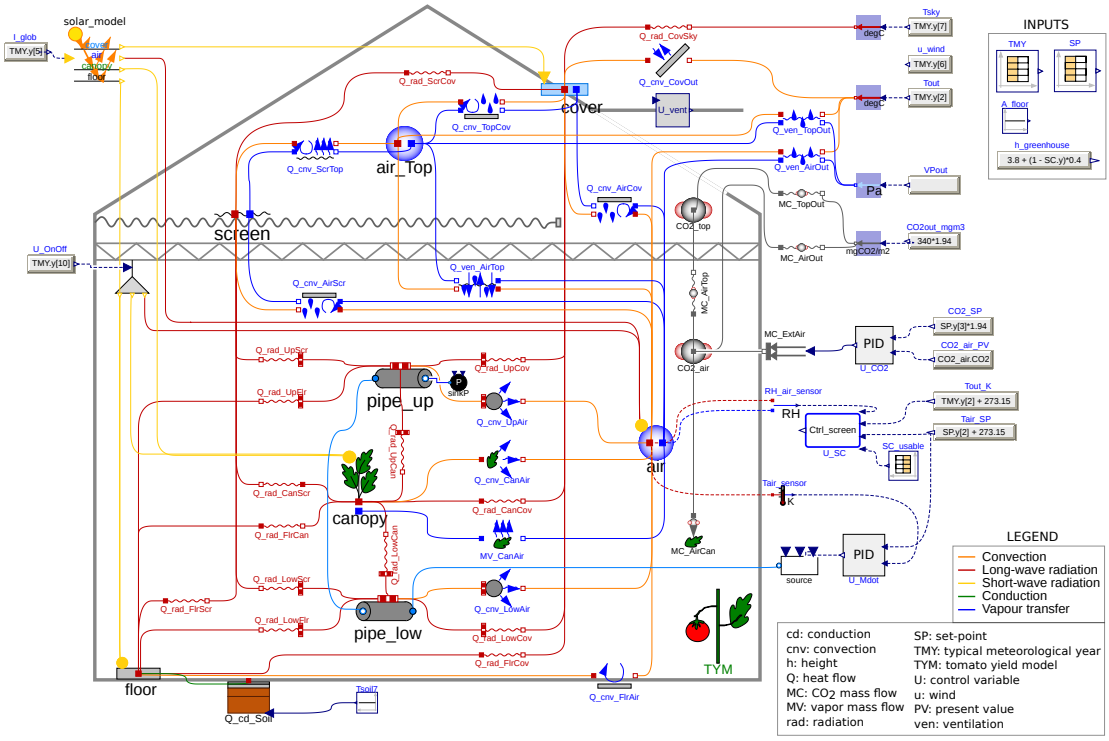

FIGURE 3.1: Graphical interface of the greenhouse climate simulation model (*Greenhouse1* in the *Examples* package)

3.2.1 Modeling of greenhouse climate

Greenhouse climate models have been the object of a substantial literature. While many models have been developed [22], [23], [50]–[52], most of them can only be used for a single location and for a specific greenhouse structure and climate. Recently, a more generic greenhouse climate model combining the work of Bot [23] and De Zwart [22] was developed. For the purpose of this work, this model, which was developed by Vanthoor, Stanghellini, Henten, *et al.* [21] and validated for a range of climates and greenhouse designs, has been implemented.

The model describes the indoor climate of a greenhouse resulting from the greenhouse design, the outdoor climate and a specific climate control. The indoor climate is characterized by the air temperature, water vapor pressure (to account for the air relative humidity) and CO_2 concentration. Besides, the variables with an indirect influence on the climate are also modeled. These are mainly the characteristics relative to the canopy and the envelope (i.e. the cover, the floor and the thermal screen). In order to compute the indoor climate, the modeling approach consists in applying the energy conservation principles on each greenhouse component and the mass balance on the air. To that end, all the existent energy and mass flows must be modeled. A detailed description of the latter can be found in Altes-Buch and Lemort [73]. Using the encapsulation capabilities of the Modelica language, the balances and flows are defined in independent models that should be inter-connected to build the

greenhouse system. The Modelica language offers a high degree of flexibility to the user because:

(i) the greenhouse structure and energy systems are not predefined, i.e. the model can easily be adapted to match different types of greenhouses

(ii) the models are parametrizable i.e. the user can define the materials and system sizes.

The main models of the library are described in the following sections. For a full description of the equations of the models, please consult the online documentation of the library in https://greenhouses-library.readthedocs.io. An example of greenhouse model is shown in Figure 3.1. As it can be distinguished, the greenhouse modeled in this example consists of a two-level heating circuit, roof windows (no side vents), natural ventilation (no forced ventilation) and a movable thermal screen. It should be noted that, when the screen is drawn, the air of the greenhouse is divided in two zones, i.e. below and above the screen. These zones are modeled separately and their respective climate is assumed to be homogeneous.

Surfaces

This section describes the modeling approach used to model the cover, the floor, the canopy and the thermal screen. The energy balance on these surfaces is defined by Equation (3.1):

$$\rho c V \frac{dT}{dt} = \sum \dot{Q} + \sum \dot{Q}_L + P_{Sun} + P_{Light} \tag{3.1}$$

which takes into account the following exchanges:

- Sensible heat flows ($\dot{Q}$), including convection with the indoor or outdoor air, long-wave radiation between all surfaces or to the sky, and conduction through the soil.
- Latent heat flows ($\dot{Q}_L$), such as the heat exchanged by condensation on the inner side of the cover, condensation or evaporation on the screen, or evaporation on the leaves. These flows can be treated as forced flows, since they are determined by the moisture mass flow rate caused by condensation or evaporation ($\dot{M}_v$) and the heat of evaporation (Δh_{fg}):

$$\dot{Q}_{L,12} = \Delta h_{fg} \cdot \dot{M}_{v,12} \tag{3.2}$$

- Short-wave radiation inputs, such as the absorbed radiation from the sun (P_{Sun}) and/or supplementary lighting (P_{Light}).

The water vapor pressure at a surface is defined as the saturated vapor pressure at the surface temperature. No mass balance is applied on the modeled surfaces.

Cover

The cover is the only surface exchanging with both the inside and outside air. The model (*cover* in Figure 3.1) can be parametrized for any type of glazing (single-glass, double-glass, polycarbonate, etc.). For single glazing, since glass thickness is commonly small (4 mm), conduction is neglected. Depending on the vapor pressure difference, condensation may take place at the inner side of the cover. Evaporation of moisture from the cover to the air is neglected since the condensate is commonly drained.

Canopy

The magnitude of the energy exchanged by the canopy depends on the size of the leaves, which is increased with crop growth and decreased by leaf pruining. To take this into account, the leaf area index (LAI), defined as the leaf area per unit of ground area, is used. The LAI is computed in the crop yield model and input in the canopy model (*canopy* in Figure 3.1). The heat capacity per unit of leaf area is the main parameter. The canopy temperature has an impact on its photosynthesis and transpiration, which decrease the CO_2 concentration and increase the moisture content of the air, respectively.

Floor

The floor model (*floor* in Figure 3.1) can be parametrized for a range of floor materials (e.g. soil, concrete). Conduction through the soil is modeled by a nodal model, dividing it into several layers. The temperature of the deepest layer is a boundary condition. Vapor transfer is not modeled.

Thermal screen

The thermal screen (waved line in Figure 3.1) is a membrane used to reduce the energy requirement to heat the greenhouse. When drawn, thermal losses to the outside are reduced by 38 to 60%, depending on the nature of its material [68]. The screen model (*screen* in Figure 3.1) can easily be parametrized to cover the wide variety of commercial screens nowadays used by horticulture growers. The screen thickness, commonly less than 1 mm, implies a very low heat capacity. Since the screen is mostly drawn at night (i.e. when there is no sunlight), the absorbed heat from short-wave radiation is neglected.

Given the porous nature of the screen, air and moisture are exchanged through its fabric. The present model assumes that the thermal screen is capable of transporting water from the lower side to the upper side. The storage of moisture in the screen is

however neglected. This implies that the vapor that condenses at the screen is either evaporated at the upper side or drips from the screen. The rate of evaporation is therefore lower or equal to the rate of condensation.

Air

The energy balance on the indoor air (*air* in Figure 3.1) is defined by Equation (3.3):

$$\rho c_p V \frac{dT}{dt} = \sum \dot{Q} + P_{Sun} + P_{Light} \tag{3.3}$$

which takes into account the following exchanges:

- Sensible heat flows ($\dot{Q}$), including convection at surfaces and ventilation flows (natural, forced or leakage) with the outside air.
- Forced heat inputs, including the short-wave radiation from the sun (P_{Sun}) or supplementary lighting (P_{Light}), which are first absorbed by the greenhouse construction elements and later released to the air.

The moisture content of the air is increased by the transpiration of the canopy and decreased by ventilation and by condensation on the cover and the screen. In the model, it is characterized by the water vapor pressure of the air (P_v), which is determined by the vapor mass balance defined in Equation (3.4):

$$M_H \frac{V}{RT} \frac{dP_v}{dt} = \sum \dot{M}_v \tag{3.4}$$

where M_H is the molar mass of vapor and $\dot{M}_v$ is the vapor mass flow rate.

The CO_2 concentration of the greenhouse air, being independent from the heat and vapor exchanges, is computed in a separate model (*CO2_air* in Figure 3.1). Its value is decreased by ventilation processes and by the CO_2 consumption of the canopy, and increased by the CO_2 supply from an external source controlled by the climate controller. The CO_2 mass concentration (γ_{CO2} [mg{CO2} m^{-3}{air}]) of the air is determined in the CO_2 mass balance, defined in Equation (3.5).

$$V \frac{d\gamma_{CO2}}{dt} = \sum \dot{M}_c \tag{3.5}$$

where $\dot{M}_c$ is the CO_2 mass flow rate.

The top air zone has a very low heat capacity and is only modeled when the screen is drawn (i.e. mostly at night, to mitigate losses in the lack of sunlight). For this reason, its heat and vapor balances are computed in a simplified version of the air model (*air_Top* in Figure 3.1), in which the heat input from short-wave radiation (P_{Sun} in Equation (3.3)) is neglected. The CO_2 balance (*CO2_top* in Figure 3.1) is done in the same manner as for the main zone.

Heating pipes

The fluid in the heating pipes from the greenhouse heating ciruit is modeled by means of the discretized model for incompressible flow described in Section 3.2.4. Heat is transferred by long-wave radiation to the canopy, floor and cover, and by convection to the air. Since the thermal resistance from the outer pipe surface to the air is about 100 times greater than the thermal resistance from the inner surface to the outer one [22], the temperature of the pipe surface can be assumed equal to the water temperature.

Greenhouse heating circuits are commonly made of several parallel heating loops. The main parameters of the model (*pipe_low* in Figure 3.1) are the pipe diameter, the installed length per unit of ground area per loop, and the number of parallel loops. The nominal mass flow rate and the number of nodes in which each loop is discretized are also parameters of the model.

3.2.2 Modeling of heat flows

Several models are proposed for computing the different types of heat transfer. It should be noted that convection and long-wave radiation are modeled separately.

Free convection at surfaces

The upward or downward heat exchange by free convection from an horizontal or inclined surface is modeled. The heat exchange coefficients are modeled based on the Nuselt-Rayleigh (Nu-Ra) relation [24]. The model can be used for convection at the cover (upward flow, inclined surface), the floor (upward/downward flow, horizontal surface) or the screen (upward flow, horizontal surface). The bi-direction nature of the convective flow on the floor is due to the fact that the latter can be warmer or colder than the air above it. The different natures of the flows lead to different Nu-Ra relations for each surface. Therefore, the user should indicate (by means of the Boolean parameters) which surface is being modeled.

Depending on the status of the thermal screen, the heat flow to the cover can originate either from the top or the main air zone, and the heat flow to the screen can have a different magnitude. Therefore, when the model is used for the cover or the screen, the screen closure (control variable in the global system) is a required input.

Free convection at the leaves

The heat exchange coefficient on the leaves of tomato crop was derived experimentally by Stanghellini [27]. Because of the lack of required input data to compute it, in the present model it is however simplified to a constant value. This coefficient is expressed per unit of leaf area. In order to compute the global heat exchange coefficient, the LAI is thus a required input.

Free convection at heating pipes

The magnitude of convective heat from the heating pipes to the air depends on the pipe position, which implies a free exchange (i.e. pipes in free air) or a hindered exchange (i.e. pipes situated close to the canopy and near the floor). The free exchange is modeled based on the Nu-Ra relation. The hindered exchange, considered to be forced, is modeled by experimental correlations derived by Bot [23]. The user should indicate which exchange should be modeled by means of a Boolean parameter. The diameter of the pipes and the installed pipe length per unit of ground area are also required parameters.

Forced convection with the outside air

The convection at the outer side of the greenhouse cover is modeled according to the experimental work of Bot [23], who characterised the heat exchange coefficient at this saw-tooth surface as a function of the wind speed. The wind speed is an exogenous input of the model. The main parameter is the cover tilt.

Natural ventilation

The heat transfer between the inside and outside air due to natural ventilation is computed as a function of the air exchange rate. This rate, derived by Boulard and Baille [26], depends mainly on two factors. The first one is the window opening, a required input which is set by the climate controller. The second one is the window characteristics (e.g. the wind pressure coefficient and the coefficient of energy discharge caused by friction at the windows), which in order to simplify the model, are set to constant values relative to standard roof windows.

Depending on the status of the thermal screen, the heat flow can originate either from the top or the main air zones. Therefore, the screen closure (control variable from the climate controller) is also a required input.

This model also takes into account the leakage rate through the greenhouse structure, which is dependent on the wind speed (exogenous input of the model) and the leakage coefficient of the greenhouse (parameter of the model, characteristic of its structure).

Forced ventilation

The heat flow from forced ventilation is computed as a function of the air exchange rate between two air volumes, which depends on the capacity of the ventilation system (parameter of the model) and the position of the control valve (required input set by the climate controller).

Ventilation through the screen

Analogously to the other ventilation models, the heat transfer caused by air exchange between the main and top air zones is computed as a function of the air exchange rate, which is the sum of the air rates caused by two mechanisms. The first one is the air exchange through the openings in the fabric of the screen, which is temperature driven and was derived experimentally by Balemans [24]. The second one is the exchange through the gap when the screen is opened, which is caused by density difference and was theoretically modeled by Miguel [25] using the Navier-Stokes equation. The main required input is the screen closure (control variable from the climate controller).

Long-wave radiation

The long-wave infrared radiation flows are modeled for each exchange between all the surfaces in the greenhouse (red lines in Figure 3.1). These flows are modeled by the Stefan-Boltzmann equation. The emission coefficients, characteristic of the surfaces, are parameters of the model for which a standard value is proposed in the documentation of the model. The view factor of each surface is computed according to De Zwart [22] in its component model and is an input of the model.

Short-wave radiation

Short-wave radiation in a greenhouse can be originated from the sun or from supplementary lighting.

Solar model

The main input is the solar radiation incident in a greenhouse, which can be split in three spectral parts: ultra violet (UV, from 0.3 to 0.4 μm), visible light (from 0.4 to 0.7 μm) and near infrared light (NIR, from 0.7 to 3 μm). The visible light has an interest for biological growth and is referred as photosynthetically active radiation (PAR) in greenhouse modeling. The fraction of UV and PAR in the global radiation is 6-10% and 45-60%, respectively [53]. However, for plant growth it is common to assign 50% to PAR, neglect the UV and assign the other 50% to NIR [22]. Besides the spectral division, the solar radiation can be divided in direct and diffuse radiation. The solar model of this work is simplified by making no distinction between diffuse and direct solar radiation and by assuming that the transmission coefficient of the greenhouse cover does not depend on the solar angle. It should be remarked that the optical properties of the greenhouse elements differ for PAR and NIR.

On the cover, the incident radiation from the sun is partially reflected, absorbed and transmitted inside the greenhouse. The transmitted radiation is absorbed by the construction elements, the canopy or the floor. The transmitted PAR to be absorbed by the canopy or the floor is defined by:

$$\dot{q}_{PAR,\tau} = (1 - \eta_{Glob,Air}) \cdot \tau_{Cov,PAR} \cdot \eta_{Glob,PAR} \cdot I_{Glob} \tag{3.6}$$

where $\eta_{Glob,Air}$ is the ratio of the radiation that is absorbed by the greenhouse construction elements, $\tau_{Cov,PAR}$ is the transmission coefficient of the cover and $\eta_{Glob,PAR}$ is the fraction of PAR in the outside global radiation (I_{Glob}). When the thermal screen is closed, $\tau_{Cov,PAR}$ is a lumped transmission coefficient of the greenhouse cover and the movable thermal screen.

For instance, the PAR absorbed by the canopy is the sum of the PAR transmitted by the cover and directly absorbed by the canopy and the PAR reflected by the floor and later absorbed by the canopy. In a homogenous crop, this is described by an exponential decomposition of light with the LAI [54]:

$$\begin{aligned} \dot{q}_{PAR,Can} = \dot{q}_{PAR,\tau}(1 - \rho_{Can,PAR}) \left(1 - e^{-K_{PAR} \cdot LAI}\right) + \\ \dot{q}_{PAR,\tau} \cdot e^{-K_{PAR} \cdot LAI} \cdot \rho_{Flr,PAR}(1 - \rho_{Can,PAR}) \left(1 - e^{-K_{PAR} \cdot LAI}\right) \end{aligned} \tag{3.7}$$

where $\rho_{Can,PAR}$ and $\rho_{Flr,PAR}$ are the reflection coefficients for PAR of the canopy and the floor, and K_{PAR} is the extinction coefficient for PAR of the canopy.

Supplementary lighting

Although the contribution of supplementary lighting is very small during summer, in winter it can double the sun input during a day and thus, have an important impact on crop growth. The illumination model is designed for high intensity discharge lamps (e.g. high pressure sodium (HPS) lamps) and the main parameter is the installed power per unit of ground area. For these lamps, only 17% and 25% of the electrical power is converted into NIR and PAR, respectively. The remaining 58% is released to the greenhouse air [55]. The fraction of radiation absorbed by the greenhouse components is computed similarly than in the solar model.

3.2.3 Modeling of moisture and CO_2 flows

This section presents the modeling approach for the computation of moisture and CO_2 flows.

Condensation and evaporation

The mass exchange coefficients for condensation and evaporation at the screen and the cover are linearly related to their convective heat exchange coefficients by a conversion factor [22]. As previously stated, evaporation from the cover and from the screen's lower side is not modeled. Therefore, the mass flow rates due to condensation are prohibited from being negative. Condensation on the upper side of the screen is prohibited as well. Negative flows are avoided by setting the mass transfer

coefficients to zero when the water vapor pressure difference between the air and the surface is negative.

Mass transfer through ventilation

Mass transfer occurs in ventilation processes, i.e. between the main and top air zones, and between these and the outside air. The moisture and CO_2 flows accompanying an air exchange are function of the air flow rate, which is computed as explained in Sections 3.2.2 and 3.2.2.

Mass transfer at the canopy

The canopy transpiration originates from a phase interface somewhere inside the cavities of a leaf. The resistance to moisture transport from the leaves to the air was derived by Stanghellini [27] as a function of leaf temperature, CO_2 concentration of the air, water vapor pressure difference and absorbed solar irradiation. These variables, computed elsewhere, are inputs of this sub-model. Furthermore, transpiration is also function of the dimension of the leaves. The LAI is therefore an input of the model.

The CO_2 flow from the air absorbed by the canopy depends on the canopy photosynthesis rate and the respiration processes. It is computed in the crop yield model and input in this model.

3.2.4 Modeling of fluid flows

Fluid flows are modeled using the finite volume approach by means of a discretized model for incompressible flow, adapted from Quoilin, Desideri, Wronski, *et al.* [29]. The model distinguishes between two types of variables: cell and node variables. The main features and hypothesis of the model can be summarized by:

- Dynamic energy balance and static mass and momentum balance are applied in each cell
- Upwind or central differences discretization scheme
- Uniform velocity through the cross section and constant pressure
- Axial thermal energy transfer is neglected

The overall flow model can be built by connecting several cells in series. The model is compatible with the *Media* package of the Modelica Standard Library, at the condition that the considered fluid is incompressible.

3.2.5 Modeling of HVAC systems

In the Greenhouses library, several HVAC models are provided in order to enable system-level simulations such as the energy integration of greenhouses with generation and storage units. To that end, performance-based models of CHP units, heat pump and thermal storage units are developed. Although the number of modeled HVAC systems remains limited, the full compatibility (connector-wise) of the Greenhouses library allows the connection with other libraries more specialized in modeling thermal systems (e.g. Buildings, ThermoCycle, ThermoPower, etc.). In all the developed HVAC models, fluid flow is modeled by means of the fluid model described in Section 3.2.4. To illustrate the modeling possibility of the Greenhouses library, two system-level simulations are included in the *Examples* package.

CHP

The CHP model does not consider part-load operation (ON/OFF regulation is assumed). Thus, constant natural gas consumption and total efficiency are assumed. The electrical efficiency is computed assuming a constant second-law efficiency, whose value is obtained using the nominal operating conditions.

Heat pump

For heat pumps, two models are proposed. First, a peformance-based model similar to the CHP model is developed, in which the second-law efficiency is assumed to remain unchanged in part-load operation.

A second more detailed model is also implemented, in which the heat pump performance are predicted at both full- and partial-load operation by three polynomial laws fitted through manufacturing data [74].

Thermal energy storage

The thermal energy storage model is a nodal model of a stratified tank with an internal heat exchanger and ambient heat losses, adapted from Quoilin, Desideri, Wronski, *et al.* [29]. The water tank is modeled using the energy and mass conservation principles and assuming thermodynamic equilibrium at all times inside the control volume. The following hypothesis are applied:

- No heat transfer between the different nodes.
- The internal heat exchanger is discretized in the same way as the tank: each cell of the heat exchanger corresponds to one cell of the tank and exchanges heat with that cell only.
- Incompressible fluid in both the tank and the heat exchanger.
- Axial thermal conductivity is neglected.

3.2.6 Modeling of crop yield

Several inputs used in the computation of the greenhouse climate (e.g. the LAI, the CO_2 flow absorbed by the canopy) are characteristics of the crop and should be quantified by a crop growth model. Moreover, with a crop growth model, the yield and hence, the profitability (e.g. savings in energy) from different control strategies can be compared. For those reasons, a dynamic crop yield model is implemented. Given that yield models differ between crops, the model implemented in this work is only valid for tomato crop.

Crop growth is related to photosynthesis and most of the existent crop yield models directly relate these two variables without considering a carbohydrate buffer. The buffer is a storage system of the crop, whose function is to store the carbohydrates from the photosynthesis (inflow) before they are distributed to the plant organs (outflow). It has a maximum capacity, above which carbohydrates cannot be stored anymore, and a lower limit, below which the carbohydrate outflow stops. Thus, the in- and out-flows depend on the level of carbohydrates in the buffer and thereby, may not be simultaneous. For instance, crop growth may continue after dusk, when photosynthesis has stopped but distribution can still be possible if the buffer content has not yet reached its lower limit. The presence of a carbohydrate buffer is thus important when modeling crop growth, as suggested in Dayan, Keulen, Jones, *et al.* [56], Heuvelink [57], Linker, Seginer, and Buwalda [58], Marcelis, Heuvelink, and Goudriaan [59], and Seginer, Gary, and Tchamitchian [60].

In this work, a recent yield model developed and validated for a variety of temperatures [28] is implemented. The model structure is shown in Figure 3.2. The carbohydrate assimilation is modeled by distinguishing three crop parts: the leaves, the fruits and the stems (and roots). Mass balances are applied on each part and on the buffer. For instance, the mass balance on the buffer is described by:

$$\frac{dC_{Buf}}{dt} = \dot{M}_{C,AirBuf} - \dot{M}_{C,BufFruit} - \dot{M}_{C,BufLeaf} - \dot{M}_{C,BufStem} - \dot{M}_{C,BufAir} \tag{3.8}$$

where C_{Buf} is the availability of carbohydrates in the buffer and $\dot{M}_C$ are the carbohydrate flows, which are computed as a function of fixed parameters related to the tomato crop. The inputs of the model are the instantaneous temperature of the canopy, the CO_2 concentration of the greenhouse air and the PAR absorbed by the canopy. Their values are retrieved from the greenhouse climate simulation model. The main outputs of the model are the LAI, the harvested dry matter, the photosynthesis rate and the respiration rates.

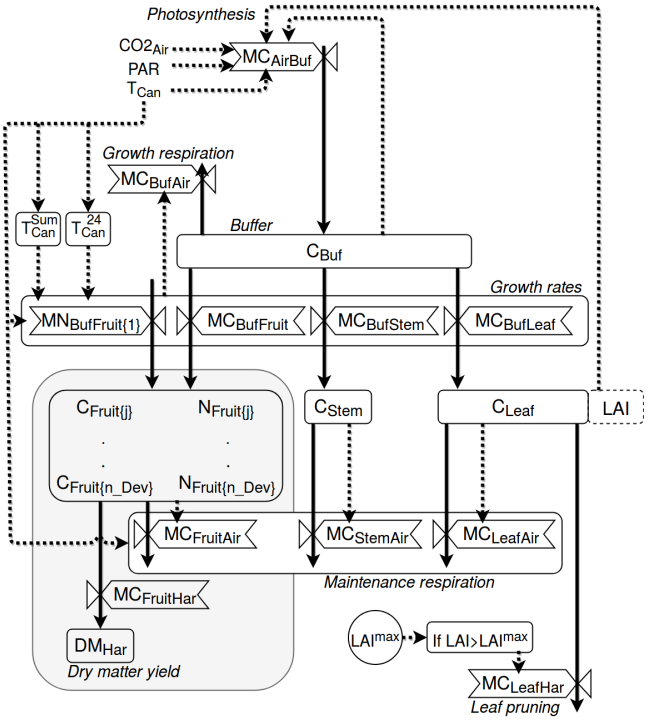

FIGURE 3.2: Schematic representation of the crop yield model. Boxes define state variables (blocks), semi-state variables (dotted blocks) and carbohydrate flows (valves). Arrows define mass flows (solid lines) and information flows (dotted lines). Adapted from Vanthoor, Visser, Stanghellini, *et al.* [28].

3.3 Numerical aspects

The complexity of the final model largely depends on the selected discretization scheme for the piping and for the ground. However, for a typical complete greenhouse example model (e.g. the model *Greenhouse1* in the *Examples* package), the system of equations comprises 4222 unknowns, among which 197 are differentiated variables. After the symbolic manipulation, the size of the non-linear systems of equations is 236 for the initialization problem and 3 for the integration. The typical solving time is 48 minutes for a one-year simulation with a 3 GHz I7 processor.

Because of the important time constants involved in some parts of the model (e.g. the vapor content of the air within the greenhouse), most equations are initialized in steady-state. While this adds some complexity to the initialization problem (in the current example, a system of 236 non-linear equations), it avoids long and unnecessary transients at the beginning of the simulation.

Some equations of the model include conditional statements (in the form of Equation (3.9)) which, during integration, generate state events and therefore decrease the computational efficiency of the model [75].

$$y = \begin{cases} y_1 & \text{if } k > k_s \\ y_2 & \text{otherwise} \end{cases} \tag{3.9}$$

In order to increase the computational efficiency of the model, these conditional statements have been replaced by a differentiable switch function. For the general case where $y_1, y_2 \in \mathbb{R}$, the statement is replaced by:

$$y = y_1 \cdot S_k + y_2 \cdot (1 - S_k) \tag{3.10}$$

where S_k is the value of a differentiable switch function that is determined by the state variable k, which is defined by:

$$S_k = \frac{1}{1 + e^{s_k(k-k_s)}} \tag{3.11}$$

where k_s is the value of k where S_k is 0.5, and s is the slope of the differentiable switch at k_s. The sign of s is set according to if S_k increases ($s < 0$) or decreases ($s > 0$) with an increasing k. For instance, in the case where some crop parameters differ between day and night, k is the global irradiation, k_s is equal to zero, and y_1 and y_2 are the values of the parameter at daytime and nighttime, respectively.

The model also includes conditional statements in which the output value is equal to the indicator function, defined by Equation (3.12).

$$y = \begin{cases} 1 & \text{if } k \in [k_{s1}, k_{s2}] \\ 0 & \text{otherwise} \end{cases} \tag{3.12}$$

These conditional statements are approximated by:

$$y = S_k^1 \cdot S_k^2 \tag{3.13}$$

where S_k^1 and S_k^2 are two differentiable switch functions, which are defined according to Equation (3.11) for k_{s1} and k_{s2} and have opposite slope signs (i.e. the former is negative, the latter is positive).

3.4 Library implementation

3.4.1 Library structure

The Greenhouses library is hierarchically structured into different packages, including:

- *Components*, is the central part of the library. It is organized in three subpackages:
  - *Greenhouse*, contains models from the simple greenhouse components (i.e. all the models described in Section 3.2.1) to already-build greenhouse models ready to use (similar to Figure 3.1);

  - *HVAC*, contains the models for generation and storage units presented in Section 3.2.5;
  - *CropYield*, contains the yield model for tomato crop described in Section 3.2.6.
- *Flows*, contains models of the flows that are encountered in a greenhouse system. It is organized in seven sub-packages that model the heat, moisture and CO_2 mass transfer, as well as fluid flow. These models are described from Section 3.2.2 to 3.2.4.
- *ControlSystems*, organized in two sub-packages, contains control units to control *Climate* (i.e. the thermal screen closure, the operation of supplementary lighting and the window's aperture) and *HVAC* (i.e. the operation of generation units, the storage (dis-)charge) (cf. Section 3.4.2 for more details).
- *Examples*, contains examples that demonstrate the usage of this library. It includes simulations of greenhouses (e.g. Figure 3.1) and two system-scale simulations of a greenhouse connected to a thermal storage, a CHP and a heat pump (e.g. Figure 3.4).
- *Interfaces*, contains all the type of connectors used in the library.
- *Functions*, contains the empirical correlations used to characterize some of the models presents in the library.

Figure 3.3 shows an overview of the library structure.

3.4.2 Control Systems

Greenhouses have high requirements on indoor climate control. The control strategies used in commercial climate controllers differ from manufacturers and are commonly private-access. For this reason, several control strategies for the control of climate systems are developed. The implemented control strategies are based on a literature review on climate requirements and control practices [22], [28], [55], [64], [67]–[69], [71]. In the library, depending on the nature of the strategies, two implementation approaches are distinguished: proportional-integral (PI) and state graph based controllers. The library includes models for the control of:

- *Supplementary lighting*: ON/OFF operation determined by a state graph based controller. The strategy sets up a time window for lighting, during which a lighting set-point condition is applied. To prevent cycling, natural light levels must be below or above the set-point for a proving time, and once turned on, lights must remain on for a minimum time.
- *Natural ventilation*: a PI controller sets the windows' aperture based on air sanitation and air cooling, i.e. the air relative humidity and temperature are not allowed to increase above a certain value.

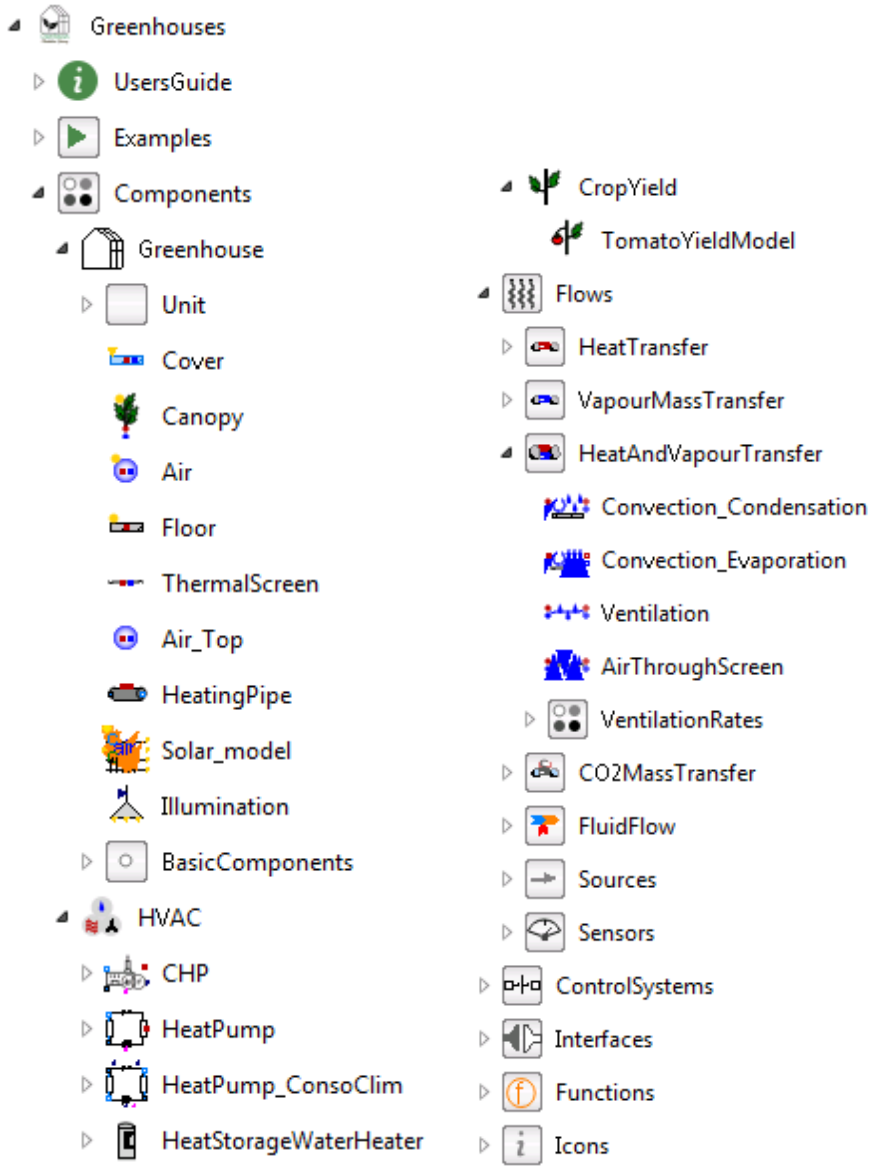

FIGURE 3.3: An overview of the library structure from the Dymola graphical user interface

- *Thermal screen*: the screen's closure is set by a state graph based controller model. The screen deployment is done progressively as a function of the outside irradiation. Depending on the night, a small temporary opening of the screen may be required to regulate humidity or temperature.
- *Heating*: a PI controller adjusts the heating power output by varying the supply mass flow rate of the heating pipes according to the difference between the air temperature set-point and actual value.
- *CO_2 external source*: a PI controller adapts the CO_2 supply rate to attain the set-point. In high ventilation conditions, CO_2 enrichment is commonly reduced due to the high exchange rate to the outside air.

The developed control strategies remain relatively simple compared to some state-of-the-art commercial climate controllers. Users are therefore encouraged to develop their own controls systems adapted to their climate requirements.

3.5 Open-source implementation

Quality of science relies upon basic principle such as reproducibility, transparency or peer-review, which are greatly facilitated by open-source and open-data approaches [72]. For this reason, the presented library is released as open-source (using the permissive Modelica License 2). The required documentation for a new user to use the models is described in this paper. The library can be downloaded from https://github.com/queraltab/Greenhouses-Library.

In addition to this paper, an online documentation of the library is available in https://greenhouses-library.readthedocs.io. Apart from an overview of the library, the online documentation includes a user guide with the required steps for a new user to get started. Furthermore, it includes an extended description of each model of the library, in which the main modeling assumptions and equations are stated. To demonstrate the usage of the library, the example simulations from the *Examples* package are also commented.

3.6 Conclusions

The development of the Greenhouses library is an on-going process aiming at providing a completely open-source tool for the simulation of greenhouse climate and its energy integration with thermal systems or the power system. The library comprises a number of components that can be used to simulate a wide range of greenhouse structures and climates. Moreover, the crop growth model allows determining the yield, and hence, the profitability of different control strategies. The components can finally be used to simulate the coupling of greenhouses with generation units and thermal storage, as proposed by the authors in a previous publication Altes-Buch, Quoilin, and Lemort [31] and illutrated in Figure 3.4. In that work the library was used to optimize the control of a greenhouse connected to a CHP, a heat pump and a storage system in such a way to maximize self-consumption, leading to significant savings (9 % of the total operation cost) compared to the baseline.

The full compatibility (connector-wise) of the library allows the connection with other libraries more specialized in modeling thermal systems, thus increasing the simulation possibilities of the Greenhouses library. The library is released as open-source, ensuring a proper reproducibility and re-usability of this work. Ongoing and future works will mainly focus on the integration of new components and on the validation of the proposed models.

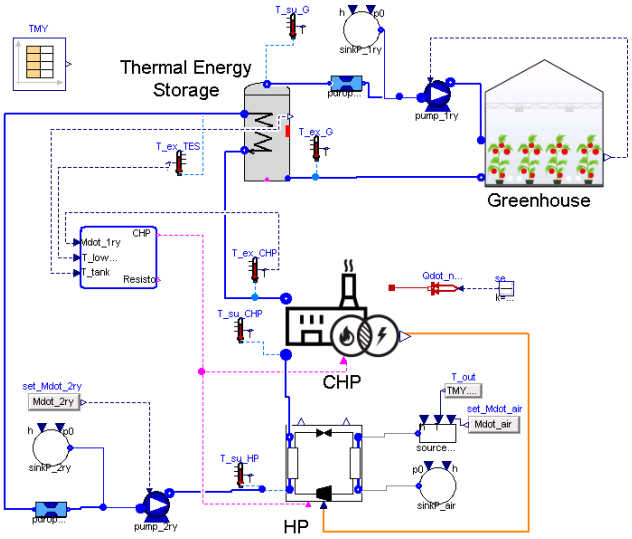

FIGURE 3.4: Diagram of a simulation example

Part II

Case Studies

Chapter 4

Greenhouse Climate Control Strategies for Energy-Efficient Greenhouse Horticulture

This chapter is a reprint of *Q. Altes-Buch and V. Lemort. "Modeling framework for the simulation and control of greenhouse climate." In Proceedings of the 10th International Conference on System Simulation in Buildings, 20. 2018.*

Research Question

How can climate control strategies in technologically equipped greenhouses be optimized to enhance energy efficiency, i.e. maximize crop production while minimizing energy consumption?

Summary

This article illustrates the physical characteristics of the developed modeling framework through a case study that includes a comparison of three climate control strategies. Additionally, the article aims to demonstrate the library's utility, specifically focusing on the impact of greenhouse control strategies on total energy consumption.

To that end, a greenhouse model was built by interconnecting the components from the Greenhouses Library, presented in Chapter 2 and 3. Subsequently, dedicated climate controllers were devised for each strategic approach.

Contributions

The principal contribution of this work is the demonstration of the model developed during the initial years of research for this thesis. This work validates that the greenhouse model reproduces physical results consistent with the validated models from the literature upon which it is based.

Additionally, a minor contribution of this article is the proposal of various strategies for screen usage, illustrating the potential energy savings achievable through different approaches.

Finally, a contribution of this article is the transformation of the control units of the screen from discrete steps (as done in practice) to continuous functions, to avoid the computational overhead linked to *events* during the simulation [70]. This transformation is applied to both the screen removal/deployment processes and the screen's gap for humidity control.

Reading Tips

The methodology, detailed in Section 4.2 (which outlines the primary energy flows within a greenhouse, the crop yield model, and climate control strategies), was reformulated and expanded in a paper published in Building Simulation (cf. Chapter 2). Hence, readers who have already reviewed that chapter may proceed directly to the case study.

It is important to note that the control strategies for windows and thermal screens employed in this case study are simpler compared to those presented in Chapter 2, as this work was initiated during the early stages of this research.

4.1 Introduction

In the European context, energy consumption by agriculture only accounted for 2.7% of final energy consumption in the EU-28 in 2016 [76]. The Netherlands was the country with the highest share, with a 7.4% of its final energy consumption. Although the average energy consumption by agriculture of the EU-28 decreased about 18.6% from 1996 to 2016, it has increased in some countries. The utilized agricultural area (UAA) is used as a common denominator for the comparison of the results across different countries. In fact, the Netherlands was the country with the highest use in energy by agriculture per ha UAA between 1996 and 2016 [77]. This was due to intensive farming. According to the Farm Structure Survey, although greenhouses covered only the 0.5% of the total UAA in the Netherlands in 2013, they represented about 79% of the total energy consumption by agriculture [34].

Agriculture, as an energy consumer, contributes to the depletion of non-renewable energy sources and to global warming, for instance through CO_2 emissions from fossil fuel combustion gases. It is therefore important to study energy-saving options not only for greenhouses but also, in the current context of energy transition, for a higher-scale system with integrated district heating and electrical production. The goal of this work is to implement a model able to simulate the complex flows in a greenhouse to facilitate the future study of energy integration of greenhouses with other energy systems. To that end, this work implements:

- A detailed model of a greenhouse climate, including the modeling of heat, vapor and CO_2 flows, to simulate the indoor climate and energy consumption of a greenhouse given its specific design, outdoor conditions and a specific control. The modeling of heating systems is also included.
- A crop yield model, to account for the needs of the crop and the flows related to plant transpiration and photosynthesis. These flows influence the indoor climate and thus, the energy consumption.
- Climate control system models to regulate heating, ventilation, CO_2 enrichment and supplementary lighting in the greenhouse. A control strategy for the thermal screen is also proposed.

This paper presents a detailed description of the mentioned models. In order to illustrate the capabilities of the modeling framework, the greenhouse, the crop yield and the climate control system models are coupled and run simultaneously for a real case study. Results for the case study are presented and discussed. The models are written in the Modelica language and are run within the Dymola simulation platform. The Modelica language has the asset of being flexible and it allows simulating system integration through the connection with other components such as thermal generators. The models are released as open-source, thus ensuring a proper reproducibility and reusability of this work [72].

4.2 Methods

4.2.1 Greenhouse climate model

A greenhouse climate model is a model that describes the indoor climate of a greenhouse resulting from the greenhouse design, the outdoor climate and a specific control. In greenhouses, the indoor climate is characterized by the temperature, the vapor pressure of water (i.e. the relative humidity) and the CO_2 concentration of the air. Together with the temperature of the heating pipes, the indoor climate constitutes the climate controller feed-back quantities. However, in order to attain the desired climate, the variables with an indirect influence on the climate also need to be modeled. These are mainly the characteristics relative to the canopy and the envelope (i.e. the cover, the floor and the thermal screen). The canopy temperature has an impact on its photosynthesis and transpiration, which decrease the CO_2 concentration and increase the vapor content of the air, respectively. Evaporation or condensation at surfaces may occur depending on the water vapor pressure difference with respect to the air. The temperature of the envelope influences the vapor pressure of water of the air, which is decreased by condensation at the cover and at the thermal screen. The thermal screen is a membrane used to reduce the energy requirement to heat the greenhouse (waved line in Figure 4.1). When drawn, thermal losses to the outside are reduced by 38 to 60%, depending on the nature of its material [68]. Given the porous nature of the screen, air and moisture is exchanged through its fabric. Air exchange with the outside decreases the partial vapor pressure and the CO_2 concentration of the air, which can be increased by supplementary CO_2 supply. The here above mentioned variables are stated in Figure 4.1.

Greenhouse climate models have been the object of a substantial literature. While many models have been developed [22], [23], [50]–[52]), most of them can only be used for a single location and for a specific greenhouse structure and climate. Recently, a more generic greenhouse climate model [78] combining the work of Bot [23] and De Zwart [22] was developed. The model was validated for a range of climates and greenhouse designs. For the purpose of this work, the model [78] has been implemented in the Modelica language, thus enabling system integration through the connection with other components such as thermal generators.

It should be noted that, when the screen is drawn, the air of the greenhouse is divided in two zones, i.e. below and above the screen. The model assumes the climate of each zone to be homogeneous. For the rest of the manuscript, the zones below and above are going to be referred as main and top air zones, respectively. The model includes the energy and mass balances to compute all the mentioned variables. These are energy balances on the main and top air zones, canopy, heating pipes, cover, floor and thermal screen; and mass balances of vapor and CO_2 on the main and top air zones. The vapor pressure of water at a surface is defined by the saturated vapor pressure at its temperature. The entirety of the balances are described in [31] and

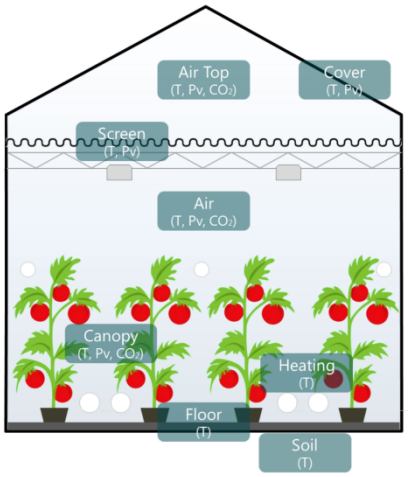

FIGURE 4.1: Graphical representation of the state variables (T: temperature, P_v: vapor pressure of water, CO_2: CO_2 concentration) of the greenhouse climate model.

follow the structure of Equations (4.1)-(4.3). Since no spatial differences in temperature, vapor pressure of water and CO_2 concentration are considered, all the model flows are described per square meter of greenhouse floor. For the main air zone, the temperature, vapor pressure of water and CO_2 concentration are described by:

$$c_{Air}\dot{T}_{Air} = p_{SunAir} + \dot{q}_{cnv,UpAir} + \dot{q}_{cnv,LowAir} + \dot{q}_{cnv,CanAir} - \dot{q}_{cnv,AirFlr} - \dot{q}_{cnv,AirCov} - \dot{q}_{cnv,AirScr} - \dot{q}_{cnv,AirTop} - \dot{q}_{cnv,AirOut} \quad [\mathrm{W\ m^{-2}}] \tag{4.1}$$

$$c_{VP_{Air}}\dot{P}_{v,Air} = \dot{m}_{v,CanAir} - \dot{m}_{v,AirCov} - \dot{m}_{v,AirScr} - \dot{m}_{v,AirTop} - \dot{m}_{v,AirOut} \quad [\mathrm{kg\ m^{-2}\ s^{-1}}] \tag{4.2}$$

$$c_{CO2_{Air}}\dot{CO2}_{Air} = \dot{m}_{c,ExtAir} - \dot{m}_{c,AirCan} - \dot{m}_{c,AirTop} - \dot{m}_{c,AirOut} \quad [\mathrm{mg\ m^{-2}\ s^{-1}}] \tag{4.3}$$

The majority of the flows distinguished in a greenhouse originate from convection at surfaces, ventilation processes, conduction at the soil and long-wave infrared radiation (FIR). Forced flows such as the short-wave radiation from the sun, latent heat flows or the sensible heat from supplementary lighting are also considered. A graphical representation of all the flows encountered in a greenhouse is shown in Figure 4.2.

Heat flows

Convection and conduction

Convective heat flows at surfaces are function of the heat exchange coefficient (U_{ij}) and are described by:

$$\dot{q}_{cnv,ij} = U_{ij}(T_i - T_j) \qquad [\mathrm{W\ m^{-2}}] \qquad (4.4)$$

Typically, convective processes in greenhouses are governed by free convection. In this case, the Nusselt (Nu) number describing the convective exchange process can be defined as a function of the Rayleigh (Ra) number [24]. The heat exchange coefficients are therefore modeled based on the Nu-Ra relation, as presented in De Zwart, 1996. In other cases, the convective heat exchange can be considered to be forced. This is the case of the outer side of the greenhouse cover, where convection is driven by wind speed. For the pipes situated close to the canopy and the floor, the heat exchange is considered to be hindered, compared to a pipe in free air. The heat exchange coefficients of these forced processes are modeled by experimental results [23]. The whole heat exchange coefficients are presented in Table 4.1.

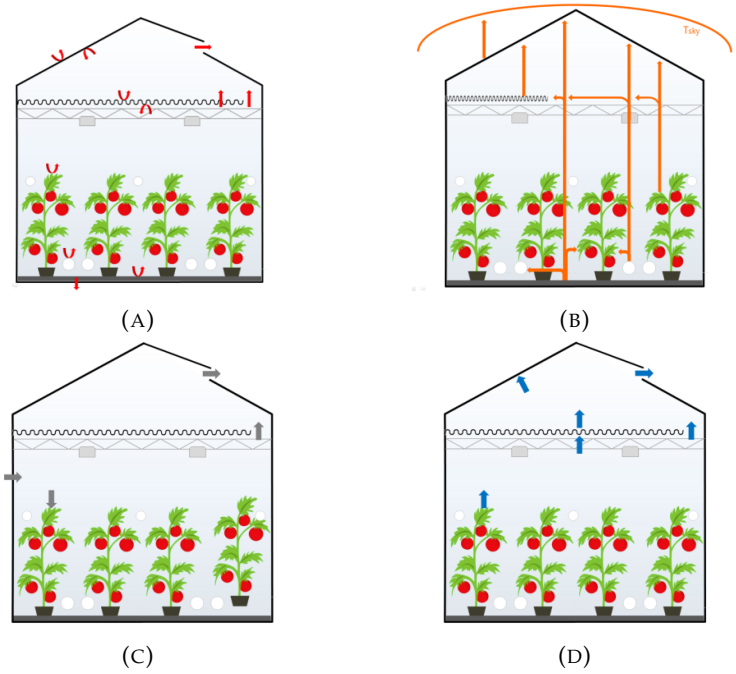

FIGURE 4.2: Graphical representation of the flows present in a greenhouse related to: (A) convection and conduction, (B) long-wave radiation, (C) CO_2 and (D) vapor.

The only conductive flow considered in greenhouse modeling is the conduction through the greenhouse soil. The soil under the greenhouse floor represents a big thermal capacity with a poor thermal conductivity. The floor surface can show temperature variations of 10 K during a day. To be able to describe the temperature gradient, the soil is modeled in several layers. The heat flow between the layers is described by Equation (4.4), using the last heat exchange coefficient from Table 4.1.

TABLE 4.1: Heat exchange coefficients for convective and conductive heat flows

Heat exchange coefficients U_{ij} [W m^{-2} K^{-1}]	**Sources**
$U_{CanAir} = 2\,\alpha_{LeafAir}\,LAI$	[22]
$U_{AirFlr} = \begin{cases} 1.7\,(T_{Flr} - T_{Air})^{0.33} \text{ if } T_{Flr} > T_{Air} \\ 1.3\,(T_{Air} - T_{Flr})^{0.25} \text{ if } T_{Flr} \leq T_{Air} \end{cases}$	[22]
$U_{AirScr} = 1.7 u_{Scr}\,\lvert T_{Air} - T_{Scr}\rvert^{0.33}$	[22]
$U_{ScrTop} = 1.7 u_{Scr}\,\lvert T_{Scr} - T_{Top}\rvert^{0.33}$	[22]
$U_{AirCov} = 1.7\,(T_{Air} - T_{Cov})^{0.33}\cos(\varphi)^{-0.66}$	[22]
$U_{TopCov} = 1.7\,(T_{Top} - T_{Cov})^{0.33}\cos(\varphi)^{-0.66}$	[22]
$U_{CovOut} = \begin{cases} (2.8 + 1.2 v_w)\frac{1}{\cos(\varphi)} \text{ if } v_w < 4\ m\ s^{-1} \\ 2.5 v_w^{0.8}\frac{1}{\cos(\varphi)} \text{ if } v_w \geq 4\ m\ s^{-1} \end{cases}$	[23]
$U_{HinderedPipeAir} = 1.99\,\pi\,\phi_{Pipe}\,l_{Pipe}\,\lvert T_{Pipe} - T_{Air}\rvert^{0.32}$	[23]
$U_{FreePipeAir} = 1.28\,\pi\,\phi_{Pipe}^{0.75}\,l_{Pipe}\,\lvert T_{Pipe} - T_{Air}\rvert^{0.25}$	[22]
$U_{So(j-1)So(j)} = \frac{2}{\frac{h_{So(j-1)}}{\lambda_{So(j-1)}} + \frac{h_{So(j)}}{\lambda_{So(j)}}}$	

Ventilation

The ventilation processes in a greenhouse are mainly driven by natural ventilation between the inside and outside air and between the main and top air zones. Convective flows caused by ventilation processes are modeled based on the air exchange rate f_{ij} between two air volumes i and j, as described by:

$$\dot{q}_{vent,ij} = \rho_{Air}\,c_{p,Air}\,f_{ij}(T_i - T_j) \qquad [\text{W m}^{-2}] \tag{4.5}$$

The air ventilation between the main and top air zones is caused by two mechanisms: the air through the openings in the fabric of the screen and the air through a gap when the screen is opened. Balemans [24] studied the temperature driven air exchange through fully closed screens ($u_{Scr} = 1$) and derived a fitted function through experimental data. When the screen is open ($u_{Scr} < 1$), the air exchanged through the gap, caused by density difference, will dominate the exchange through the screen. This exchange was theoretically modeled by [25] using the Navier-Stokes equation. Combining the air flow through the screen and through the gap, the total air ventilation rate between the air and top zones is described by:

$$\begin{aligned} f_{AirTop} &= u_{Scr} K_{Scr}\,\lvert T_{Air} - T_{Out}\rvert^{0.66} \\ &+ \frac{1 - u_{Scr}}{\overline{\rho}_{air}}\sqrt{0.5\overline{\rho}_{air} W\,(1 - u_{Scr})\,g\,\lvert\rho_{Air} - \rho_{Top}\rvert} \end{aligned} \qquad [\text{m}^3\ \text{m}^{-2}\ \text{s}^{-1}] \tag{4.6}$$

The air ventilation flow caused by natural ventilation with the outside air through the roof windows depends mainly on the windows opening (u_{vent}), and is influenced by the wind pressure coefficient and the coefficient of energy discharge caused by friction at the windows. It is described by [26]:

$$f_{AirOut} = \frac{u_{vent} A_{Roof} C_d}{2 A_{Flr}} \sqrt{g \frac{h_{vent}}{2} \frac{T_{Air} - T_{Out}}{\overline{T}} + C_w v_w^2} \qquad [\mathrm{m^3\ m^{-2}\ s^{-1}}] \qquad (4.7)$$

The ventilation of the greenhouse is influenced by the leakage rate through the greenhouse structure, which is dependent on the wind speed and the leakage coefficient of the greenhouse, characteristic of its structure. It can be described by:

$$f_{leakage} = \begin{cases} 0.25 c_{leakage} & \text{if } v_w < 0.25 \\ c_{leakage}\ v_w & \text{if } v_w \geq 0.25 \end{cases} \qquad [\mathrm{m^3\ m^{-2}\ s^{-1}}] \qquad (4.8)$$

Long-wave radiation

The long-wave infrared radiation flows are modeled by the Stefan-Boltzmann equation:

$$\dot{q}_{rad,ij} = A_i \epsilon_i \epsilon_j F_{ij} \sigma (T_i^4 - T_j^4) \qquad [\mathrm{W\ m^{-2}}] \qquad (4.9)$$

The emission coefficients are characteristic of the surfaces and the view factors of the greenhouse elements are described in [22]. The exchange with the sky, whose temperature is estimated from meteorological data by an approach proposed in [22], is also considered.

Short-wave radiation

Short-wave radiation in a greenhouse can be originated from the sun or from supplementary lighting. Although the contribution of supplementary lighting is very small during summer, in winter it can double the sun input through a day and thus, have an important impact on crop growth.

The solar radiation incident in a greenhouse can be split in three spectral parts: ultra violet (UV, from 0.3 to 0.4 µm), visible light (from 0.4 to 0.7 µm) and near infrared light (NIR, from 0.7 to 3 µm). The visible light has an interest for biological growth and is referred as photosynthetically active radiation (PAR) in greenhouse modeling. The fraction of UV is 6-10% and of PAR is 45-60% of the global radiation [53]. However, for plant growth it is common to assign 50% to PAR, neglect the UV and assign the other 50% to NIR [22]. Besides the spectral division, the solar radiation can be divided in direct and diffuse radiation. As done in [78], the solar model of this work is simplified by making no distinction between diffuse and direct solar

radiation and by assuming that the transmission coefficient of the greenhouse cover does not depend on the solar angle.

The radiation from the sun is partially absorbed by the cover and partially transmitted inside the greenhouse. Part of the transmitted radiation is later absorbed by the canopy and the floor. The PAR and NIR absorbance coefficients of the canopy and the floor depend on their reflection coefficients and on the leaf area index (LAI), defined as the leaf area per unit of ground area, i.e. of greenhouse floor. The rest of the sun radiation is absorbed by the construction elements and then released as long-wave radiation to the air.

Latent heat flows

In the thermal model there are four latent heat flows related to: condensation at the screen and cover, and evaporation at the screen and the canopy leaves. These flows are described by:

$$\dot{q}_{lat,ij} = \Delta H \; M_{v,ij} \qquad [\text{W m}^{-2}] \tag{4.10}$$

Sensible heat from supplementary lighting

Only part of the electric consumption of the supplementary lighting is converted to short-wave radiation. For a high intensity discharge lamp e.g., high pressure sodium (HPS) lamps, 17% of the electrical power is converted to NIR and 25% to visible light [55]. Thus, 58% is released to the greenhouse air.

Vapor flows

The vapor exchange coefficients for condensation and evaporation at the screen and the cover are linearly related to their convective heat exchange coefficients by a conversion factor. The vapor flow from the air to a component is described by:

$$\dot{m}_{v,ij} = \begin{cases} 0 & \text{if } P_{v,i} < P_{v,j} \\ 6.4 \cdot 10^{-9} \; U_{ij}(P_{v,i} - P_{v,j}) & \text{if } P_{v,i} \geq P_{v,j} \end{cases} \qquad [\text{kg m}^{-2}\,\text{s}^{-1}] \tag{4.11}$$

By allowing a mass flow rate from the upper surface of the screen to the top air compartment, the model assumes that the screen is capable of transporting water through its fabric. Water is transported from the lower side to the upper and storage of water in the screen is neglected. Therefore, evaporation from the upper side is only possible when condensation takes place at the lower side.

Mass transfer also occurs in ventilation processes, i.e. between the main and top air zones, and between these and the outside air. The computation of the mass flow

from an air exchange by ventilation is described by:

$$\dot{m}_{v,ij} = \frac{M_{Water} f_{ij}}{R} \left(\frac{P_{v,i}}{T_i} - \frac{P_{v,j}}{T_j} \right) \qquad [\text{kg m}^{-2}\ \text{s}^{-1}] \qquad (4.12)$$

The vapor flow from the canopy to the greenhouse air originates from a phase interface somewhere inside the cavities of a leaf. The resistance to vapor transport from the canopy leaves to the greenhouse air is made of an internal resistance and a boundary layer resistance [27]. According to the latter, the canopy transpiration can be defined as:

$$\dot{m}_{v,CanAir} = \frac{2\,\rho_{Air}\,c_{p,Air}\,LAI}{\Delta H\,\gamma(r_b + r_s)} \left(P_{v,Can} - P_{v,Air}\right) \qquad [\text{kg m}^{-2}\ \text{s}^{-1}] \qquad (4.13)$$

CO_2 flows

In the greenhouse, there are three CO_2 flows associated to the ventilation processes and two forced flows, i.e. the canopy consumption and the CO_2 enrichment. The CO_2 flow accompanying an air flow is function of the air flow rate and can be described by:

$$\dot{m}_{c,ij} = f_{ij} \left(CO_{2,i} - CO_{2,j}\right) \qquad [\text{mg m}^{-2}\ \text{s}^{-1}] \qquad (4.14)$$

The CO_2 flow from the air absorbed by the canopy depends on the canopy photosynthesis rate and respiration processes and is described by the crop yield model.

4.2.2 Crop yield model

A dynamic tomato crop yield model was implemented to account for the effects of the indoor climate on crop growth and thereby on the harvested dry matter. Although crop growth is related to photosynthesis, most of the existent crop models directly relate these two with the absence of a carbohydrate buffer. The function of the buffer is to store the carbohydrates from the photosynthesis (inflow) and to distribute them to the plant organs (outflow). It has a maximum capacity, above which carbohydrates cannot be stored anymore, and a lower limit, below which the carbohydrate outflow stops. Thus, the in- and out-flows depend on the level of carbohydrates in the buffer and thereby, may not be simultaneous. An approach based on not considering the buffer neglects the non-simultaneous character of the flows. For example, it can neglect the crop growth after dusk, when photosynthesis stops but there may still be carbohydrate distribution if the buffer level is higher than its lower limit. The presence of a carbohydrate buffer is thus important when modeling crop growth.

Models with a common carbohydrate buffer are available in the current literature ([56]–[60]). In this work, a recent yield model developed and validated for a variety

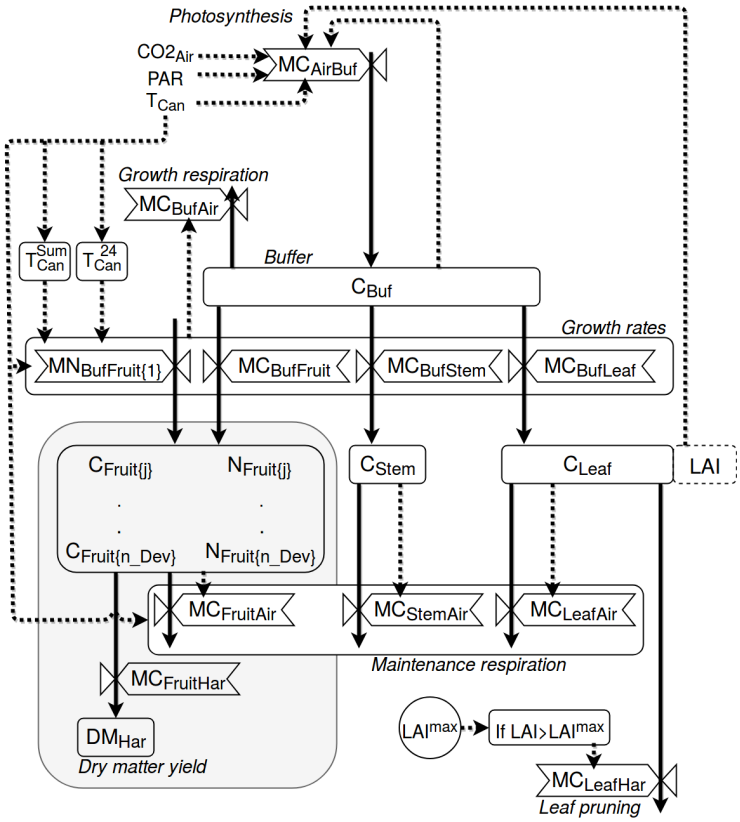

FIGURE 4.3: Schematic representation of the crop yield model. Boxes define state variables (blocks), semi-state variables (dotted blocks) and carbohydrate flows (valves). Arrows define mass flows (solid lines) and information flows (dotted lines). For the purpose of readability, the grey box is a simplified scheme of the mass flow rates related to fruit development. A more detailed scheme of the latter can be found in [78].

of temperatures [78] has been implemented. The model computes the carbohydrates distribution flows in the presence of a buffer, as shown in Figure 4.3. To that end, the model applies carbohydrates mass balances on the buffer, fruits, stems and leaves. The mass balance on the buffer is defined by:

$$\dot{C}_{Buf} = \dot{m}_{C,AirBuf} - \dot{m}_{C,BufFruit} - \dot{m}_{C,BufLeaf} - \dot{m}_{C,BufStem} - \dot{m}_{C,BufAir} \quad [\text{mg m}^{-2}\ \text{s}^{-1}] \tag{4.15}$$

The description of the whole balances can be found in [31]. The inputs of the model are the canopy instantaneous temperature, the CO_2 concentration of the greenhouse air and the PAR absorbed by the canopy. Their values are retrieved from the greenhouse climate simulation model, in which T_{Can} and $CO2_{Air}$ are state variables and PAR_{Can} is a function of the global irradiation and the transmission coefficient of the greenhouse cover. The model takes also into account the 24 hour mean temperature of the canopy (T_{Can}^{24}). The main outputs of the model are the harvested tomato dry matter (DM_{Har}), the LAI and the air CO_2 flow absorbed by the canopy.

4.2.3 Climate control

Greenhouses have high requirements on indoor climate control. The climate controller adjusts heating, ventilation and CO_2 supply to attain the desired climate. In this work, several control systems are developed, based on the control strategies proposed in the literature.

Set-points definition for temperature and CO_2

The determination of set-points is at the top of the functionality of the climate controller. Temperature set-points differ from day-time to night-time and are sometimes adapted to the level of radiation. CO_2 is supplied during daylight to enhance photosynthesis. As measured in [62], different combinations of CO_2 concentration and air temperature lead to different photosynthesis rates. Although a sharp reduction in photosynthesis is measured at non-optimal temperatures, similar values are measured for close-to-optimal temperatures (i.e. optimal temperature ±5ºC). Therefore, temperature and CO_2 set-points can be optimized not only in terms of crop growth but also in terms of energy use. In fact, the definition of temperature set-points for optimal crop growth and energy use has been the subject of a substantial literature (e.g. [63], [64], [66], [71]). However, since this work does not focus on climate set-points optimization, no innovative control is proposed. Instead, the strategy proposed in [64] is implemented in Python and the set-points are inputted as a time-series "txt" file in the model. This strategy consists in minimizing energy consumption while maintaining a crop growth close to the maximal growth rate by:

i) computing a 2-D array of photosynthesis rates for a range of CO_2 and temperature values at a given PAR,

ii) selecting the pairs of CO_2 and temperature that ensure at least 80% of the photosynthesis rate (being 100% the maximum value of the 2-D array), and

iii) defining the temperature and CO_2 set-point ($T_{Air,SP}$ and $CO_{2,Air,SP,th}$) as the pair in ii) with the lowest temperature.

In this work, a PI controller is responsible for adjusting the heating power output by varying the mass flow rate of the heating pipes according to the difference between the air temperature set-point and the actual value. The control strategy for CO_2 is based on a maximal supply rate, defined by the capacity of the CO_2 enrichment system. This capacity is function of the CO_2 source, which is commonly a combination of fossil fuel combustion gases and CO_2 stored in liquid phase. While respecting the enrichment capacity, the supply rate is adapted to attain the CO_2 set-point. However, in high ventilation conditions, CO_2 enrichment is commonly reduced due to the high exchange rate to the outside air. To take this into account, the theoretical CO_2 set-point proposed by the control strategy is modified so that it decreases proportionally with the increase in the ventilation rate. This is done as defined by

Equations (4.16) and (4.17).

$$CO_{2,Air,SP} = f\left(u_{vent}\right)\left(CO_{2,Air,SP,th} - CO_{2,ExtMin}\right) + CO_{2,ExtMin} \quad \text{[ppm]} \quad (4.16)$$

$$f(u_{vent}) = \begin{cases} 1 - \frac{u_{vent}}{u_{vent_{Max}}} & \text{if } u_{vent} < u_{vent_{Max}} \\ 0 & \text{if } u_{vent} \geq u_{vent_{Max}} \end{cases} \quad \text{[-]} \quad (4.17)$$

Supplementary lighting

The most popular lamp type for commercial supplementary lighting in horticulture is high pressure sodium (HPS) lamps. HPS lamps are the most efficient in the PAR spectrum range, with an emission highly concentrated between 500 and 650 nm. HPS lighting is not designed for frequent cycling because it dramatically reduces lamp lifespan. Thus, regardless of the control method, it is best to set up constraints to operate lighting for extended periods. The implemented control strategy for the lighting is based on the following:

- *Lighting window*: allow lights to be turned on between $h_{illu,min,ON}$ and $h_{illu,max,ON}$ (e.g. 5 AM and 10 PM).
- *Lighting set-point*: allow lights to be turned on during the lighting window if light levels decrease below $I_{illu,ON}$ (e.g. 40 Wm^{-2}) and to be turned off when light levels increase above $I_{illu,OFF}$ (e.g. 120 Wm^{-2}).
- *Light accumulation*: turn off lights or do not allow turning them on if the daily accumulated light exceeds $I_{acc,max}$ (e.g. 5 kWh).
- *Proving time*: light levels must be below the set-point for at least $t_{illu,proving}$ (e.g. 30 minutes).
- *Minimum on time*: to prevent cycling, lights must remain on for minimum $t_{illu,min,ON}$ (e.g. 2 hours) once they are turned on, regardless of other conditions.

The strategy sets up a time window for lighting, during which a lighting set-point condition is applied. The proving time and minimum on time strategies are implemented to prevent cycling.

Windows aperture

Windows in the greenhouse can be opened either for dehumidification or for cooling the greenhouse. Excessive humidity can cause fungal diseases or physiological disorders [67]. Humidity in greenhouses is controlled by means of a strategy related to a constraint rather than a specific set-point [22]. The constraint is based on allowing a maximum value of relative humidity in the air, commonly set at 85%. The most common technique for dehumidification is the combination of ventilation and

heating. Although this technique is energy consuming and thus expensive, dehumidifying systems based on refrigerant cycles, e.g. heat pumps, have not proved to be economically feasible [55]. Windows are also used for cooling the air in the case of excessive temperatures, since they have a negative impact on the harvest rate. For example, in [78] the harvest rate at daylight temperatures of 40ºC was 54.5% of that at 25ºC. Moreover, temperatures above 25ºC can penalize fruit quality e.g. size and color [55]. In this work, a proportional (P) controller is used to select the opening of the windows according to the following:

- *Air sanitation*: A maximum value $RH_{vent,ON}$ is allowed for humidity.
- *Air cooling*: A maximum value $T_{vent,ON}$ is allowed for air temperature.

Thermal screen closure

As previously mentioned, thermal losses to the outside can be reduced from 38% to 60% by using a thermal screen [68]. This capability of reducing thermal losses is defined by the screen material, which is selected according to the climate of the region. In fact, depending on the nature of the screen, the light transmission coefficient can vary from 15% to 88%. Thus, when drawn, the screen reduces considerably the transmitted light above the canopy. The most conventional method to operate the screen is therefore to deploy it at sunset, when heating demand becomes significant, and remove it at sunrise, to profit from the available sun light. The removal of the screen must be operated progressively to avoid a thermal shock. A way of further reducing energy consumption is to deploy the screen before sunset or to delay the removal until after sunrise. However, this implies a loss of crop production caused by a reduction on the available light. A good approach would be to study the threshold between energy saving and production loss in order to define the optimal deployment and removing times. However, estimating the reduction of plant growth is a complex task that, although it has been the object of some studies (e.g. [64], [68]), it commonly has many uncertainties and thereby requires many assumptions. A simpler approach is to define the deployment of the screen in function of the outside irradiation. In fact, the photosynthetic activity of the plant achieves its maximal potential about one hour after sunrise and diminishes just before sunset [69]. In Dutch-conditions, deploying the screen after 50 Wm^{-2} (instead of 5 Wm^{-2} usually practiced) allows to decrease energy consumption by an extra 3% without penalizing crop growth [71]. Depending on the night, a small temporary opening of the screen may be necessary to regulate humidity or temperature. As defined by Equation (4.6), screen gaps increase the air exchange between the main and top air zones and therefore decrease temperature and humidity.

In this work, the developed screen control strategy is based on the following:

- *Opening/closing set-point*: the screen is opened (closed) if irradiation increases (decreases) above (below) a certain value $I_{Scr,ON}$ ($I_{Scr,OFF}$) (e.g. 35 Wm^{-2}).

- *Opening/closing time*: the screen is opened progressively by 1% per minute (with an interval pause of 3 minutes) followed by a full opening after 30%. This approach has proven not to generate cold air flows on top of the canopy [69]. As proposed by the latter, the opening percentage and pause time is adapted to the outside weather. The time to fully open the screen is about 45 min to 60 min in cold days and 30 min in mild days.
- *Humidity gap*: the screen is opened in steps of 1% (with an interval of 3 min) up to a maximum of 4% if relative humidity exceeds its set-point. This approach is similar to the one proposed in [71].

4.3 Simulation

4.3.1 Case study

The dynamic model of greenhouse climate is used to simulate the indoor climate of a greenhouse for tomato crop. The model is parameterized based on a real case study of a greenhouse in the Netherlands, whose design parameters were published in [78]. The considered greenhouse structure is that of a Venlo-type greenhouse, typical for mild-temperature conditions. The cover is made of a single glass layer and the considered floor area is 1.4 ha. The greenhouse is only ventilated naturally through the windows on both wind and leeside of the roof. The greenhouse is heated by means of pipe heating and is equipped with a CO_2 enrichment system as well as a movable thermal screen. Any type of cooling equipment is considered. The design parameters related to greenhouse construction, ventilation, heating, CO_2 enrichment and supplementary lighting are presented in Table 4.2.

The tomato yield model is run simultaneously with the greenhouse climate model. The crop initial conditions are established by the case study and are presented in Table 4.3. The climate controller actions are based on the strategies presented in Section 4.2.3, whose inputs are presented in Table 4.3. The simulation period starts in December 10^{th} and ends in November 22^{nd}, being equivalent to a growing period for tomato in mild-climate conditions. Data for a typical meteorological year (TMY) in Brussels is used to describe the outdoor conditions, namely air temperature, relative humidity, pressure, wind speed and global irradiation.

For the purpose of comparison, several simulations are performed:

- *G*: Simulation with the design and control parameters presented in Table 4.2 and Table 4.3.
- *G2*: Simulation similar to *G* but with an opening and closing of the screen at sunrise and sunset ($I_{Scr,ON} = I_{Scr,OFF} = 5\ Wm^{-2}$).
- *G-Scr*: Simulation of a greenhouse without thermal screen.

TABLE 4.2: Greenhouse design parameters for the case study

Greenhouse design parameters	**Parameter**	**Value**	**Unit**
Construction			
Mean greenhouse cover slope	φ	25	^{o}
Surface of the cover including side-walls	A_{Cov}	$1.8{\cdot}10^{4}$	m^2
Surface of the greenhouse floor	A_{Flr}	$1.4{\cdot}10^{4}$	m^2
Height at which the screen is installed	h_{Air}	3.8	m
Mean height of the greenhouse	h_G	4.2	m
Cover			
FIR emission coefficient	$\epsilon_{Cov,FIR}$	0.85	-
NIR reflection coefficient	$\rho_{Cov,NIR}$	0.13	-
PAR reflection coefficient	$\rho_{Cov,PAR}$	0.13	-
NIR transmission coefficient	$\tau_{Cov,NIR}$	0.85	-
PAR transmission coefficient	$\tau_{Cov,PAR}$	0.85	-
Specific heat capacity	$c_{p,Cov}$	$0.84{\cdot}10^{3}$	$J\ K^{-1}\ kg^{-1}$
Density	ρ_{Cov}	$2.6{\cdot}10^{3}$	$kg\ m^{-3}$
Thickness	h_{Cov}	$4{\cdot}10^{-3}$	m
Thermal screen			
FIR emission coefficient	$\epsilon_{Scr,FIR}$	0.67	-
NIR reflection coefficient	$\rho_{Scr,NIR}$	0.35	-
PAR reflection coefficient	$\rho_{Scr,PAR}$	0.35	-
NIR transmission coefficient	$\tau_{Scr,NIR}$	0.6	-
PAR transmission coefficient	$\tau_{Scr,PAR}$	0.6	-
Specific heat capacity	$c_{p,Scr}$	$1.8{\cdot}10^{3}$	$J\ K^{-1}\ kg^{-1}$
Density	ρ_{Scr}	$0.2{\cdot}10^{3}$	$kg\ m^{-3}$
Thickness	h_{Scr}	$0.35{\cdot}10^{-3}$	m
Screen flux coefficient	K_{Scr}	$0.05{\cdot}10^{-3}$	$m^3\ m^{-2}\ K^{-0.66}\ s^{-1}$
Floor			
FIR emission coefficient	$\epsilon_{Flr,FIR}$	1	-
NIR reflection coefficient	$\rho_{Flr,NIR}$	0.5	-
PAR reflection coefficient	$\rho_{Flr,PAR}$	0.65	-
Thermal conductivity	λ_{Flr}	1.7	$W\ m^{-1}\ K^{-1}$
Specific heat capacity	$c_{p,Flr}$	$0.88{\cdot}10^{3}$	$J\ K^{-1}\ kg^{-1}$
Density	ρ_{Flr}	2300	$kg\ m^{-3}$
Thickness	h_{Flr}	0.02	m
Soil			
Thermal conductivity	λ_{So}	0.85	$W\ m^{-1}\ K^{-1}$

TABLE 4.2: Greenhouse design parameters for the case study

Greenhouse design parameters	**Parameter**	**Value**	**Unit**
Volumetric heat capacity	$\rho c_{p,So}$	$1.73 \cdot 10^6$	J K^{-1} m^{-3}
Canopy			
Convective heat exchange coefficient	$\alpha_{LeafAir}$	5	W m^{-2} K^{-1}
FIR emission coefficient	$\epsilon_{Can,FIR}$	1	-
Ventilation properties			
Specific roof ventilation area	A_{Roof} / A_{Flr}	0.1	m^2
Ventilation discharge coefficient	C_d	0.75	-
Ventilation global wind pressure coefficient	C_w	0.09	-
Greenhouse leakage coefficient	$c_{leakage}$	$1 \cdot 10^{-4}$	-
Vertical dimension of a single vent opening	h_{vent}	0.68	m
Heating system			
External pipe diameter	$\varnothing_{pipe}$	51	mm
Pipe length per greenhouse square meter	l_{pipe}	1.875	m m^{-2}
CO_2 enrichment			
Capacity of the external CO_2 source	ϕ_{ExtCO2}	7.5	mg m^{-2} s^{-1}
Supplementary lighting (HPS)			
Capacity of the lamps	$P_{el,illu}$	100	W m^{-2}

TABLE 4.3: Initial crop conditions and climate control inputs for the case study

	Parameter	**Value**	**Units**
Crop conditions			
LAI maximum	$LAI_{\max}$	2.7	m^2 m^{-2}
LAI at the start growing period	LAI_0	0.3	m^2 m^{-2}
Carbohydrate weight of leaves	C_{Leaf}	$40 \cdot 10^3$	mg $\{CH_2O\}$ m^{-2}
Carbohydrate weight of stems and roots	C_{Stem}	$30 \cdot 10^3$	mg $\{CH_2O\}$ m^{-2}
Climate control			
CO_2 enrichment			
Minimum CO_2 concentration enrichment	$CO_{2,ExtMin}$	390	ppm

TABLE 4.3: Initial crop conditions and climate control inputs for the case study

	Parameter	Value	Units
Maximum ventilation for CO_2 enrichment	$u_{vent,Max}$	0.3	-
Supplementary lighting			
Start of light window	$h_{illu,min,ON}$	5	AM
End of light window	$h_{illu,max,ON}$	10	PM
Light set-point for turning ON lights	$I_{illu,ON}$	40	W m^{-2}
Light set-point for turning OFF lights	$I_{illu,OFF}$	120	W m^{-2}
Light accumulation set-point	$I_{acc,max}$	5	kWh
Proving time	$t_{illu,proving}$	1800	s
Minimum ON time	$t_{illu,min,ON}$	7200	s
Windows			
Ventilation set-point for air sanitation	$RH_{vent,ON}$	85	%
Ventilation set-point for air cooling	$T_{air,vent,ON}$	26	ºC
Thermal screen			
Opening set-point	$I_{Scr,OFF}$	50	W m^{-2}
Closing set-point	$I_{Scr,ON}$	50	W m^{-2}

4.3.2 Results

The overall thermal consumption after the simulation period for every case is presented in Table 4.4. If we compare the consumptions after one winter day we can observe that, as expected, the use of a thermal screen results in a reduced thermal consumption, being in G 41% lower than in G-Scr. This value is in agreement with [68], who stated the savings could go between 38 and 60%, and with [69], who attribute savings between 35-40% for non-aluminized screens such as the one used in this simulation. The screen control set-point in G (i.e. 50 Wm^{-2}) enabled savings in thermal consumption up to 11% more than using G2's set-point (i.e. 5 Wm^{-2}). When comparing the consumptions after the whole simulation period, the savings are attenuated, since in summer the thermal screen is barely used. After the whole simulation period, the use of the screen enabled reducing the overall thermal consumption by 18% and the screen set-point in G (i.e. 50 Wm^{-2}) resulted in saving an extra 1.3%. Due to light loss, the harvested dry matter in G is 1.1% lower than in G2. Although the computed overall saving is in agreement with [71], by using the screen set-point of 50 Wm^{-2} they obtain energy savings of 3% with a production loss of 0.5%. The variation on these values is mainly due to the different type of thermal screen used in both studies and the implemented control strategy. The control

strategy of the screen could therefore be improved to further decrease the consumption. The computed total harvested dry matter (Table 4.4) overestimated the values simulated for two Dutch greenhouses in [78]. However, it should be noted that their simulation period was shorter (from December to October). The overestimation on yield could also be explained by a higher 24-hour mean canopy temperature (20.24 in this work, compared to 18.2 in [78]), the differences on the used set-point strategy (unknown in [78]) and/or a possible higher global radiation in the TMY used for this simulation.

TABLE 4.4: Consumption and harvest results for the three simulations (G, G2, G-Scr)

Description	**G**	**G2**	**G-Scr**	**Units**
Consumption after a winter day	1.956	2.203	3.328	kWh m^{-2}
Consumption after the simulation period	368.8	373.7	451.3	kWh m^{-2}
Harvested DM after the simulation period	4.61	4.66	4.68	kg m^{-2}

The differences in the screen operation during a winter day for both treatments G and G2 are shown in Figure 4.4. In a winter day as such, global outside radiation is very low, being above 50 Wm^{-2} only from 12:51 to 14:34 (see irradiation plot). The screen in G is therefore open only for less than two hours, whereas in G2, the screen is open for more than six hours (from 10:21 until 17:01) (see control value plot). The PAR absorbed by the canopy ($I_{PAR,SunCan}$) is lower in G, since having the screen deployed implies a lower light transmittance coefficient. However, this decrease on absorbed PAR decreases crop growth only by 1% over the whole simulation period (Table 4.4) and is therefore negligible. In cold days the solar contribution, being low, is not enough to heat up the indoor air to the set-point. Thus, once the screen is opened, the main and top air zones are mixed, the air temperature decreases and as a consequence, the heating demand increases. The heating demand in G2 is therefore much higher than in G because of its earlier screen opening, as it can be seen in the heat flow plot. In fact, by comparing the instant heating demand curves, differences up to 75 Wm^{-2} are encountered. In cold sunny days, this difference is attenuated due to the higher heat gain from the sun.

Figure 4.5 compares the indoor climate and the climate control variables for three cold and warm days. The irradiation plot shows the importance of supplementary lighting in winter days, in which it can double the total accumulated light from the sun. By looking at the lighting profile, it can be seen that lighting is used constantly during the *lighting window* in winter. However, lighting is barely used in summer, except for cloudy days (e.g. the 22^{nd} of July in Figure 4.5).

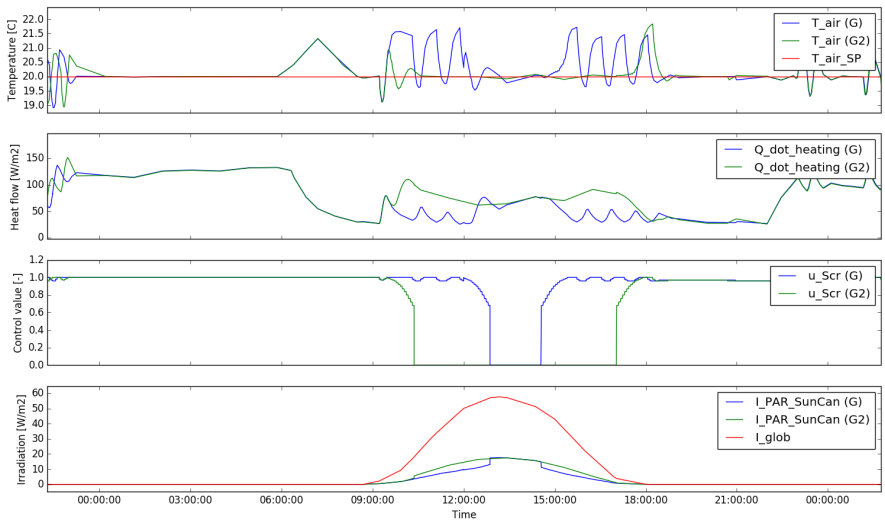

FIGURE 4.4: Comparison of the indoor temperature, heating demand, screen control and absorbed PAR by the canopy for simulations G and G2 in January 27.

In the control variables plot, it can be seen that in winter the screen is used every day and there is almost no ventilation, whereas in summer, ventilation is used constantly and the screen is always open. The control actions are therefore consistent with mitigating losses in cold days and cooling down the indoor air in warm days. As stated by Equation (4.16), high ventilation rates imply a decrease on the CO_2 concentration set-point of the air with respect to the theoretical set-point. This can be seen in the CO_2 plot, where the CO_2 concentration is equal to the theoretical set-point in winter and much lower in summer.

The gaps opened by the screen to control humidity can be seen in the control variables plot. These gaps cause an increase on the air flow rate between the main and top air zones, and thereby a decrease on the humidity of the main air zone. However, temperature is also decreased. This can be seen in the left temperature plot, where temperature fluctuations are synchronized with the screen gaps. Since temperature fluctuations are kept in ±1.5K difference from the set-point, it is assumed that they do not penalize crop growth.

In Figure 4.6, the CO_2 concentrations of the air zones and the main CO_2 flows in the greenhouse are presented for two cold (left) and warm (right) days. As expected, the CO_2 concentration in the top zone is lower than in the main zone when the screen is closed. However, when the screen is open, the air zones are mixed and their concentration is therefore equal. In warm days the screen is always open, whereas in cold days it is only open for some hours after midday (i.e. when solar gain is acceptable), as previously shown in Figure 4.4. It can be noticed that the CO_2 concentration

reaches values up to 1200 ppm in cold days, in which ventilation is limited. In summer, on the contrary, ventilation is enhanced and can reach high flow rates, as it can be seen in the right CO_2 flow plot ($\dot{M}_{c,AirOut}$). Thus, the CO_2 concentration of the air in warm days is much lower, being almost equal than the CO_2 concentration of the outside air.

When the screen is deployed, some fluctuations in the CO_2 concentration of the top air zone are present. This is due to the screen gaps opened for humidity control. The higher exchange between the air and top zones implies a decrease in the CO_2 concentration of the main zone, which is compensated by an increase in CO_2 enrichment. It should be noted that the CO_2 enrichment flow at night is null, since the canopy does not consume CO_2 at this point.

The vapor pressure of water (Figure 4.7), controlled by the screen opening, presents a similar oscillating behavior. This occurs in cold days, since in warm days the screen is always open. In this case, the vapor pressure of water is only controlled by natural ventilation. This control may not be sufficient because, as previously shown in Figure 4.5, relative humidity in the greenhouse may stay above the set-point for several hours, even with the windows fully open. It should be highlighted that the canopy transpiration flow (function of the air temperature, CO_2 concentration, vapor pressure of water and PAR absorbed by the canopy) can reach high values in summer. For example, during the 24th of July, $\dot{M}_{v,CanAir}$ was up to three times higher than in cold days or than in the 22nd of July. This is due to the high solar gain and the excessive air temperature in the greenhouse (as shown in Figure 4.5).

The obtained profiles of temperature, CO_2 concentration and vapor pressure of water of the indoor air are similar to those presented in [78], where a greenhouse is simulated for the summer and winter period in The Netherlands. In [78], the air CO_2 concentration profile is only presented for summer period. Therefore, the temperature and CO_2 concentration profiles are also compared to the results presented [22], in which a greenhouse is simulated in The Netherlands. The simulation results are plotted for three winter days. Although the maximum CO_2 value reached in the indoor air is different because of the different CO_2 supply capacities used in both works, the obtained profiles are very similar.

4.4 Conclusions

The presented modeling framework filled the gap of an inexistent open-source platform for the simulation of greenhouse climate and crop yield including climate control systems. It should be noted that the models can be used for a wide range of purposes, such as the optimal control of the greenhouse actuators, the optimal sizing of the HVAC appliances or the optimal integration of the units in district heating and/or the power system. The models are parametric, thus ensuring its use for a

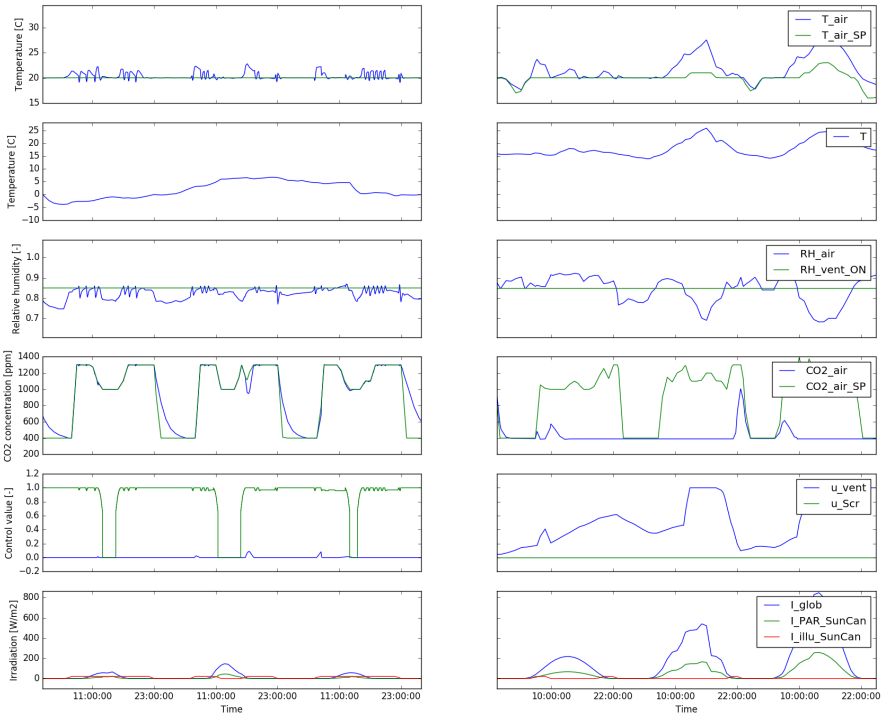

FIGURE 4.5: Comparison of the indoor climate and control variables in simulation G during three cold (22^{nd}-24^{th} January, left) and warm (22^{nd}-24^{th} July, right) days.

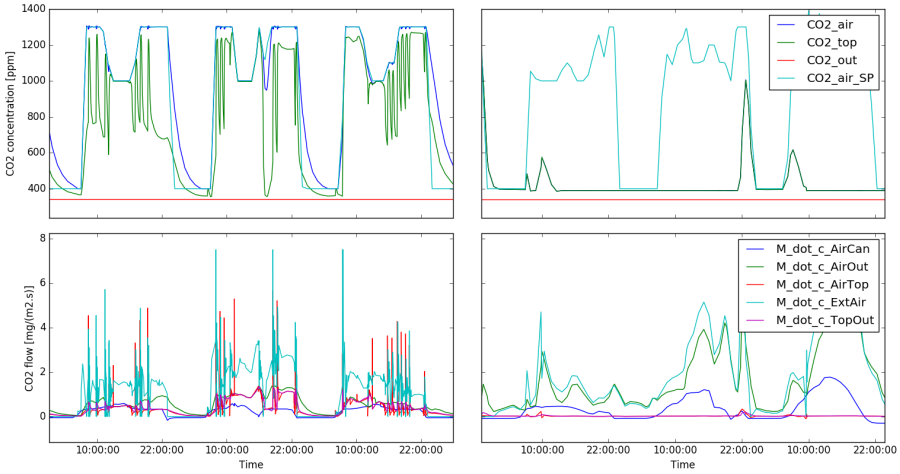

FIGURE 4.6: Comparison of the CO_2 concentrations of the air zones and the main CO_2 flows in the greenhouse in simulation G during three cold (22^{nd}-24^{th} January, left) and warm (22^{nd}-24^{th} July, right) days.

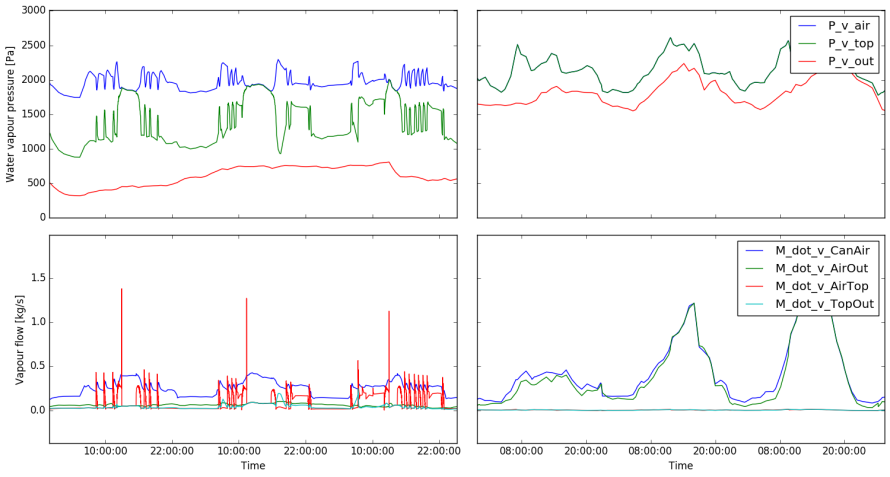

FIGURE 4.7: Comparison of the vapor pressure of water from the different air zones and the main vapor flows in the greenhouse in simulation G during three cold (22nd-24th January, left) and warm (22nd-24th July, right) days.

range of greenhouse designs, climates and cultivation crops. The models are released as open-source in order to ensure a proper reproducibility and reusability of this work (Download from: https://github.com/queraltab/Greenhouses-Library). A detailed description of each model and the required information to run the models is provided in [79].

For the purpose of climate control, several control systems are developed to regulate heating, ventilation, CO_2 enrichment, supplementary lighting and the movable screens in greenhouses. The proposed control strategies are designed based on a literature review. The strategies are then tested in a case study, which is also used to exemplify the use of the greenhouse climate and the tomato yield models. To that end, the models are run for three cases with different screen control strategies. The computed thermal consumption in every case is in agreement with the results presented in the literature ([68], [69], [71]). Although the screen control strategy was proved to function properly, it could be optimized to further decrease the thermal consumption. The harvested dry matter computed in the crop yield model is a bit overestimated with respect to the values presented in [78]. However, the differences in both simulations could justify the overestimation, as discussed in Section 4.3.2. Moreover, the computed profiles of air temperature, CO_2 concentration and vapor pressure of water, illustrated for cold and warm days, are very similar to profiles presented in the literature ([22], [78]). This not only ensures the physical representation of the flows by the implemented greenhouse model, but also the proper functioning of the proposed control strategies for CO_2 enrichment and humidity control.

Nomenclature

Subscripts

Air	Greenhouse main air zone	lat	Latent
b	Boundary	Leaf	Leaves
Buf	Carbon buffer	Out	Outside air
c	CO_2	Pipe	Pipe heating system
C	Carbohydrate	rad	Long-wave infrared radiation
Can	Canopy	Roof	Roof ventilation
cnv	Convection	s	Stomata
Cov	Cover	Scr	Thermal screen
Ext	External source of CO_2	So(j)	The 'j'th soil layer
Flr	Floor	Stem	Stem and roots
Fruit	Fruit	Top	Greenhouse top air zone
Glob	Global radiation	v	Vapor
Har	Harvest	vent	Ventilation
illu	Supplementary lighting	w	Wind

Remaining symbols

α	Absorption coefficient	-
γ	Psychometric constant	Pa K^{-1}
ϕ	Diameter	m
ϵ	FIR emission coefficient	-
ρ	Density or reflection coefficient	kg m^{-3}, -
λ	Thermal conductivity	W m^{-1} K^{-1}
τ	Transmission coefficient	-
σ	Stefan-Boltzmann constant	W m^{-2} K^{-4}
ΔH	Latent heat of evaporation of water	J kg^{-1}
A	Area	m^2
c	Capacity of the associated component	
C	Carbohydrate amount	mg {CH_2O} m^{-2}
c_p	Specific heat capacity	J kg^{-1} K^{-1}
$CO2$	Carbon dioxide concentration	mg m^{-3}
DM	Dry matter	mg {DM} m^{-2}
f	Air flow rate	m^3 m^{-2} s^{-1}
F	View factor	-

h	Thickness or vertical dimension	m
l	Length per square meter	m m^{-2}
$\dot{m}$	Mass flow (vapor, CO_2) averaged per square meter of greenhouse floor	kg m^{-2} s^{-1}, mg m^{-2} s^{-1}
P	Pressure	Pa
$\dot{q}$	Heat flow averaged per square meter of greenhouse floor	W m^{-2}
r	Resistance	s m^{-1}
T	Temperature	K
u	Climate control variable	-
U	Heat exchange coefficient	W m^{-2} K^{-1}
v	Speed	m s^{-1}
W	Width	m

Chapter 5

Exploring Sustainable Alternatives: Integrating Heat Pumps in Greenhouse Horticulture for Operational Costs Reduction

This chapter is a reprint of *Q. Altes-Buch, S. Quoilin, and V. Lemort. "Modeling and control of CHP generation for greenhouse cultivation including thermal energy storage." In Proceedings of ECOS 2018 - The 31st International Conference on Efficiency, Cost, Optimization, Simulation and environmental impact of energy systems, 13. 2018.*

Research Question

How can current greenhouse systems, composed of a CHP unit coupled with TES, be modified to enhance sustainability?

Specifically, is the integration of heat pumps in these systems a sustainable alternative that can potentially reduce overall system costs, and what are the implications and benefits of such integration?

Summary

This article demonstrates the application of the proposed modeling framework through a specific case study. It is crucial to emphasize that for a successful energy transition, focus should extend beyond implementing new systems with RES to include the enhancement of management and decarbonization of existing gas-fired systems.

As outlined in Section 1.1.1, CHP technology predominantly fulfills the energy requirements of greenhouses, with 2.65 GWe installed in the Netherlands in 2021. These CHP units play a contributing role (and are expected to persist in doing so) in the power system (cf. Section 1.1.1). However, due to the specific characteristics of greenhouse demand, these units typically experience a surplus of electricity production that is sold to the grid. For instance, in 2021, 65% of the electricity generated

by CHP units was directed to grid sales. In the absence of subsidies, such surplus is remunerated at a rate closely aligned with the wholesale price of electricity. If the retail price of electricity is significantly higher than the wholesale price, prosumers have a clear advantage at maximizing their level of self-consumption.

To optimize system costs and facilitate decarbonization, this study suggests incorporating a heat pump to enhance electrical self-consumption while meeting heating demands. The analysis evaluates the impact on overall system costs and the yield of harvested dry matter.

To that end, employing the models detailed in Chapter 2 and 3, two simulations were instantiated. Initially, a greenhouse model was built by interconnecting the components from the Greenhouses Library. Subsequently, for comparative analysis, this greenhouse model was integrated in two distinct systems. The first simulation emulated a conventional greenhouse system coupled with CHP and TES. The second simulation incorporated a heat pump in series with the CHP. Dedicated controllers were developed for each strategic simulation.

Contributions

This work has two primary contributions focused on current greenhouse systems composed of CHP and TES to enhance the energy transition. First, it demonstrates that greenhouse owners with such systems can significantly maximize self-consumption. This represents a departure from current practices, where the control of generation units does not prioritize self-consumption, leading to excess energy being sold to the market. Second, it proposes an innovative energy solution: the integration of heat pumps into the traditional CHP-TES system. While this configuration has been previously studied in the building/thermal field, there is no record of its application in the greenhouse sector. This work evaluates the viability of such a system, demonstrating that greenhouse load is well-suited to this design and noting that energy markets might influence the economic viability of such systems.

An additional contribution is the integration of the two performance-based CHP and heat pump models into the Greenhouses Library. These models can also be utilized by researchers in thermal studies not necessarily related to greenhouses.

Moreover, this work includes the integration of the two global models developed for this study (one for greenhouse-CHP-TES, and another for greenhouse-CHP-TES-HP), including all parameters and input data) into the Greenhouses Library, making them readily available for researchers interested in developing case studies with similar configurations.

Finally, for these simulations, two control units for the thermal systems were developed to manage the operation of the CHP and HP based on the TES state of charge and the greenhouse demand. The control units are also included in the library to ensure reproducibility.

Reading tips

The methodology elucidated in Section 5.2, 5.3, and 5.4 (detailing the primary energy balances within a greenhouse, the crop yield model, and the heating system models, respectively) has been partially revisited and expanded upon in a later publication in Building Simulation (cf. Chapter 2). Consequently, readers who have already perused that chapter may encounter some redundancy. Nonetheless, specific sub-sections introduce novel information, notably pertaining to the graphical user interface (5.2.3), the description of the heating distribution system (5.4.1), and the methodology employed for modeling a heat pump in a performance-based model (5.4.3).

This approach aims to address the economic advantages enjoyed by prosumers in maximizing their level of self-consumption, particularly in the context of the notable difference between retail and wholesale electricity prices. Nevertheless, recent events have demonstrated a surge in electricity prices in the power market, promoting the sale of electricity rather than prioritizing self-consumption. It is noteworthy that the utility of this paper remains intact, as its primary objective was to showcase the model's capabilities.

5.1 Introduction

In the past years, greenhouse horticulture market has been directly affected by the fluctuations of the price of fossil fuels. Attention must therefore be paid to the choice of the energy sources that ensure a sustainable development while being competitive and environmentally friendly. In the current literature and current practice, the use of Combined Heat and Power (CHP) is proposed as an efficient technology for that purpose. In a country like The Netherlands, for example, the CHP capacity dedicated to agriculture and horticulture was 3000 MW (for a peak load of 18000 MW) and represented 63.7% of the CHP installations in the country in 2012 [39]. CHP systems present the advantage of higher energy efficiency, but, when coupled to thermal storage, they can also be valuable for the power system, by providing services such as load balancing, ancillary services or decentralised storage capacity [38]. The limited electrical load of greenhouses implies an excess electricity generation when using CHP units, which have a power-to-heat ratio usually close to one. This excess electricity is fed to the grid and, in the absence of subsidies, remunerated at a price close to the wholesale price of electricity. Because the retail price of electricity is significantly higher than wholesale price, prosumers have a clear advantage at maximizing their level of self-consumption [20].

To evaluate the potential of such activities, detailed models coupling the greenhouse, the thermal storage and the CHP are required. The goal of this work is therefore to:

- Propose an open modelling framework for greenhouse climate simulation. Such models are not available in the current literature. The proposed platform includes the modelling of the greenhouse indoor climate, heating systems, climate controller and crop yield.
- Propose an open modelling framework capable of simulating the complex interactions and energy flows relative to systems coupling the greenhouse, the thermal storage and the CHP unit.
- Illustrate the use of the proposed simulation through the particular case of maximizing the self-consumption level of such systems through the addition of a heat pump. A control strategy is designed to optimize the operational cost of the system.

The models are written in the Modelica language, a language based on non-causal modeling and object-oriented constructs to facilitate reuse of modeling knowledge. The proposed model can be used for multiple purposes, such as the optimal control of the greenhouse actuators, the optimal sizing of the heating appliances, or the optimal integration of the units in the power system. The models are released as open-source and are run within the Dymola simulation platform.

5.2 Greenhouse climate model

5.2.1 Model overview

In recent decades, greenhouse climate models have been the object of a substantial literature. While many models have been developed ([22], [23], [50]–[52]), most of them can only be used for a single location and for a specific construction design and climate. Recently, a more generic greenhouse model [78] combining the work of Bot [23] and De Zwart [22] was developed. The model was validated for a range of climates and greenhouse designs. For the purpose of this work, the model in [78] has been implemented in the Modelica language, which is flexible and allows simulating system integration through the connection with other components such as thermal generators. The models are open-source and are run within the Dymola simulation platform.

This section contains a description of the greenhouse climate model. The model describes the indoor greenhouse climate resultant from a greenhouse design, outdoor climate and specific control. The greenhouse air is divided into two zones, separated by a thermal screen (waved line in Figure 5.1). In each zone, the air temperature, the vapor partial pressure and the CO_2 concentration are considered to be homogeneous. The model includes a climate controller which adapts the indoor climate to the needs of the crop. The controller actuates by comparing the desired indoor air conditions to the actual values. Temperature, relative humidity and CO_2 concentration are the main controlled variables. The simulation model therefore allows describing accurately the impact of control actions such as heating input or CO_2 supply.

5.2.2 Main model variables

The state variables and boundary conditions of the model are shown in Figure 5.1. State variables are denoted with capital letters that define the type of variable and a subscript that states its related component. Three types of state variables can be distinguished: temperature (T), partial vapor pressures (VP) and CO_2 concentration (CO2). The subscripts are described at the caption of Figure 5.1. The state variables are characterized by the fact that they appear differentiated in the system of equation. The time derivatives are indicated by a dot above the state variable symbol. Heat capacities of the components are denoted with a lower-case c followed by a subscript that states the corresponding component. Fluxes are denoted by capital letters that define the type of flux and two subscripts that indicate its direction from one component to another. Five types of fluxes are considered in the model: heat fluxes, which are mainly sensible heat fluxes (H) driven by convective or conductive processes, latent heat fluxes caused by condensation or evaporation (L) and long-wave radiation fluxes (R); mass vapor fluxes (MV) and mass CO_2 fluxes (MC).

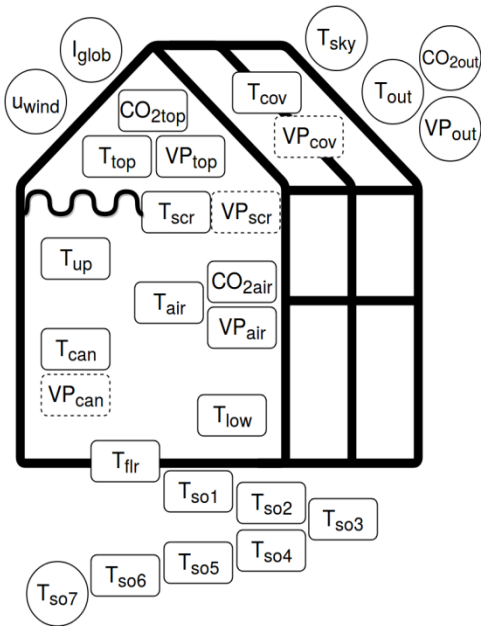

FIGURE 5.1: Graphical representation of the state variables (blocks), semi-state variables (dotted blocks) and boundary conditions (circles) of the greenhouse climate simulation model. Variables: Temperature (T), partial vapor pressures (VP) and CO_2 concentration (CO2). Subscripts: main air zone (air), top air zone (top), upper (up) and lower (low) heating circuits, thermal screen (scr), canopy (can), floor (flr), soil layers (so(j)), outside air (out) and sky (sky). Adapted from [22].

The greenhouse air temperature of the main zone, i.e. air volume below the thermal screen, is described by:

$$\begin{aligned} c_{Air}\dot{T}_{Air} = R_{SunAir} + H_{UpAir} + H_{LowAir} + H_{CanAir} - H_{AirFlr} \\ -H_{AirCov} - H_{AirScr} - H_{AirTop} - H_{AirOut} \end{aligned} \tag{5.1}$$

where R_{SunAir} is the global short-wave radiation absorbed by the greenhouse components and later released as long-wave radiation to the air. Sensible heat is exchanged between the air and the upper H_{UpAir} and lower H_{LowAir} heating pipes, the floor H_{AirFlr}, the canopy H_{CanAir}, the cover H_{AirCov}, the thermal screen H_{AirScr}, the top air zone H_{AirTop} and the outdoor air H_{AirOut}. The exchange between the two air zones through the thermal screen occurs because of the porosity material, nature of the latter. The exchange with the outside air accounts for infiltration/exfiltration and natural ventilation through the greenhouse vents.

Canopy temperature is defined by:

$$\begin{aligned} c_{Can}\dot{T}_{Can} = R_{SunCan} + R_{UpCan} + R_{LowCan} - H_{CanAir} \\ -L_{CanAir} - R_{CanCov} - R_{CanFlr} - R_{CanScr} \end{aligned} \tag{5.2}$$

where R_{SunCan} is the photosynthetically active radiation (PAR) and near infrared radiation (NIR) short-wave radiation absorbed by the canopy. Long-wave radiation fluxes are exchanged between the canopy and the upper R_{UpCan} and lower R_{LowCan} heating pipes, the cover R_{CanCov}, the floor R_{CanFlr} and the thermal screen R_{CanScr}. The canopy also exchanges sensible H_{CanAir} and latent L_{CanAir} heat with the main air zone.

The temperature of the cover is defined by:

$$\begin{aligned} c_{Cov}\dot{T}_{Cov} = R_{SunCov} + H_{TopCov} + L_{TopCov} + H_{AirCov} + L_{AirCov} + R_{LowCov} + R_{UpCov} \\ + R_{CanCov} + R_{FlrCov} + R_{ScrCov} - H_{CovOut} - R_{CovSky} \end{aligned} \tag{5.3}$$

where R_{SunCov} is the global short-wave radiation absorbed by the cover. Sensible heat fluxes caused by convection are mainly exchanged with the top air zone H_{TopCov}, main air zone in the absence of a thermal screen H_{AirCov} and the outside air H_{CovOut}. Latent fluxes L_{TopCov} and L_{AirCov} caused by condensation may appear in the inner side of the cover. The cover exchanges long-wave radiation with the upper R_{UpCov} and lower R_{LowCov} heating pipes, the canopy R_{CanCov}, the floor R_{FlrCov}, the thermal screen R_{ScrCov} and the sky R_{CovSky}.

Floor temperature is determined by:

$$\begin{aligned} c_{Flr}\dot{T}_{Flr} = R_{SunFlr} + R_{UpFlr} + R_{LowFlr} + H_{AirFlr} \\ + R_{CanFlr} - H_{FlrSo1} - R_{FlrCov} - R_{FlrScr} \end{aligned} \tag{5.4}$$

where R_{SunFlr} is the PAR and NIR short-wave radiation absorbed by the floor. Long-wave radiation is exchanged between the floor and the upper R_{UpFlr} and lower R_{LowFlr} heating pipes, the canopy R_{CanFlr}, the thermal screen R_{FlrScr} and the cover R_{FlrCov}. Sensible heat is exchanged with the air H_{AirFlr} by convection and with the first soil layer H_{FlrSo1} by conduction.

Because of the high thermal capacity, the ground is divided into several layers, whose thickness increases with the depth. The model is written in general equations so that the first ground layers (i.e. the layers in contact with the floor surface) can be made of concrete or soil, according to the floor material. The temperature of the ground layer 'i' is described by:

$$c_{So(i)}\dot{T}_{So(i)} = H_{So(i-1)So(i)} - H_{So(i)So(i+1)} \tag{5.5}$$

for $i = 1, 2 \dots 7$, where $c_{So(i)}$ is the heat capacity of each soil layer function of the material and the thickness. $H_{So(i-1)So(i)}$ and $H_{So(i)So(i+1)}$ are the conductive heat fluxes from layer 'i-1' to layer 'i' and from layer 'i' to layer 'i+1', respectively.

The temperature of the thermal screen is described by:

$$\begin{aligned} c_{Scr}\dot{T}_{Scr} = R_{UpScr} + R_{LowScr} + R_{CanScr} + R_{FlrScr} + H_{AirScr} \\ + L_{AirScr} - H_{ScrTop} - L_{ScrTop} + R_{ScrCov} \end{aligned} \tag{5.6}$$

Long-wave radiation is exchanged with the upper R_{UpScr} and lower R_{LowScr} heating pipes, the canopy R_{CanScr}, the floor R_{FlrScr} and the cover R_{ScrCov}. H_{AirScr} and H_{ScrTop} are the sensible heat fluxes caused by convection of the top and main air compartments. L_{AirScr} and L_{ScrTop} are the latent heat fluxes caused by condensation beneath the screen or evaporation above the screen.

The greenhouse air temperature of the top zone i.e. the compartment above the thermal screen is described by:

$$c_{Top}\dot{T}_{Top} = H_{ScrTop} + H_{AirTop} - H_{TopCov} - H_{TopOut} \tag{5.7}$$

Sensible heat fluxes caused by convection occur to the thermal screen H_{ScrTop} and the cover H_{TopCov}. H_{TopOut} is the natural ventilation flux to the outside air and H_{AirTop} is the air exchange through the thermal screen.

The greenhouse air vapor pressure is defined by:

$$c_{VP_{Air}}\dot{VP}_{Air} = MV_{CanAir} - MV_{AirCov} - MV_{AirScr} - MV_{AirTop} - MV_{AirOut} \tag{5.8}$$

where MV are the vapor fluxes exchanged between the air and the cover MV_{AirCov}, the thermal screen MV_{AirScr}, the top air compartment MV_{AirTop} and the outside air MV_{AirOut}. MV_{CanAir} is the mass flux caused by canopy transpiration. The latter depends on the resistance to vapor transfer from the leaves to the air. Its determination is based on the tomato crop stomata model of Stanghellini [27].

The top air compartment vapor pressure is defined by:

$$c_{VP_{Top}}\dot{VP}_{Top} = MV_{AirTop} + MV_{ScrTop} - MV_{TopCov} - MV_{TopOut} \tag{5.9}$$

where MV_{AirTop}, MV_{ScrTop}, MV_{TopCov} and MV_{TopOut} are the vapor fluxes exchanged with the main air compartment, the thermal screen, the cover and the outside air.

The CO_2 concentration of the greenhouse main air compartment is described by:

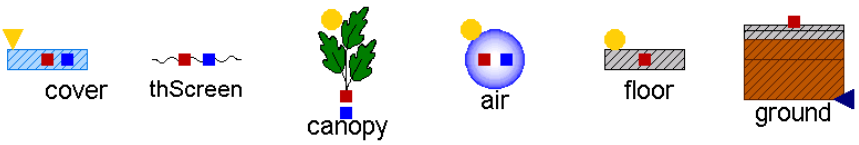

FIGURE 5.2: Components sub-models (left to right): cover, thermal screen, canopy, air, floor and ground.

$$c_{CO2_{Air}} \dot{CO2}_{Air} = MC_{ExtAir} - MC_{AirCan} - MC_{AirTop} - MC_{AirOut} \tag{5.10}$$

where MC_{ExtAir} is the carbon dioxide exchanged between the air and the external CO_2 source. MC_{AirTop} and MC_{AirOut} are the CO_2 fluxes between the air and the top air compartment and the outside air, respectively. The CO_2 fluxes caused by canopy activity MC_{AirCan}, are computed in the crop yield model from Section 5.3.

The CO_2 concentration of the top air compartment is described by:

$$c_{CO2} \dot{CO2}_{Top} = MC_{AirTop} - MC_{TopOut} \tag{5.11}$$

where MC_{AirTop} and MC_{TopOut} are the CO_2 fluxes between the top air compartment and the main air compartment and the outside air, respectively.

5.2.3 Graphical user interface

The developed modeling framework, being object-oriented, is made of independent models for each greenhouse component (Figure 5.2) and exchanged flow (Figure 5.3). From top to bottom, the greenhouse comprises the following components: cover, top air compartment, thermal screen, main air compartment, upper heating pipes, canopy, lower heating pipes, floor and ground. Although most of the fluxes are the result of a difference between the levels of state variables, some are forced by climate control actions or by boundary conditions. Heat and mass fluxes related to the same components are lumped into a single flux sub-model. For example, the air and the cover exchange heat by convection with possible condensation. Thus, H_{AirCov} and MV_{AirCov} are lumped into the model H_MV_AirCov (Figure 5.4), which is based on the model convection_cd (Figure 5.3).

The greenhouse model (Figure 5.4) is built by interconnecting of all of those models, called sub-models from this point forward. The top air zone uses a simplified version of the main air zone model. The model of the heating pipes is explained in Section 5.4.1. The sub-models interact together through standard interfaces called ports. Three types of ports are distinguished: heat, water mass and CO_2 transfer. As shown in Figure 5.2-5.4, these ports are graphically represented by red, blue and grey filled squares, respectively. Yellow ports are radiation inputs from the sun or artificial illumination.

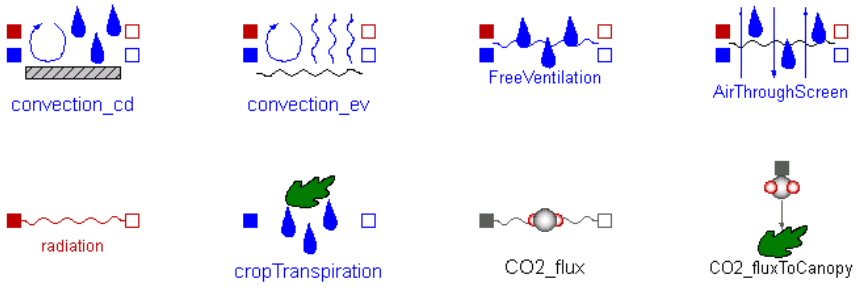

FIGURE 5.3: Flux sub-models for convection with possible condensation or evaporation, free ventilation, air exchange through the thermal screen, radiation, canopy transpiration and CO_2 fluxes.

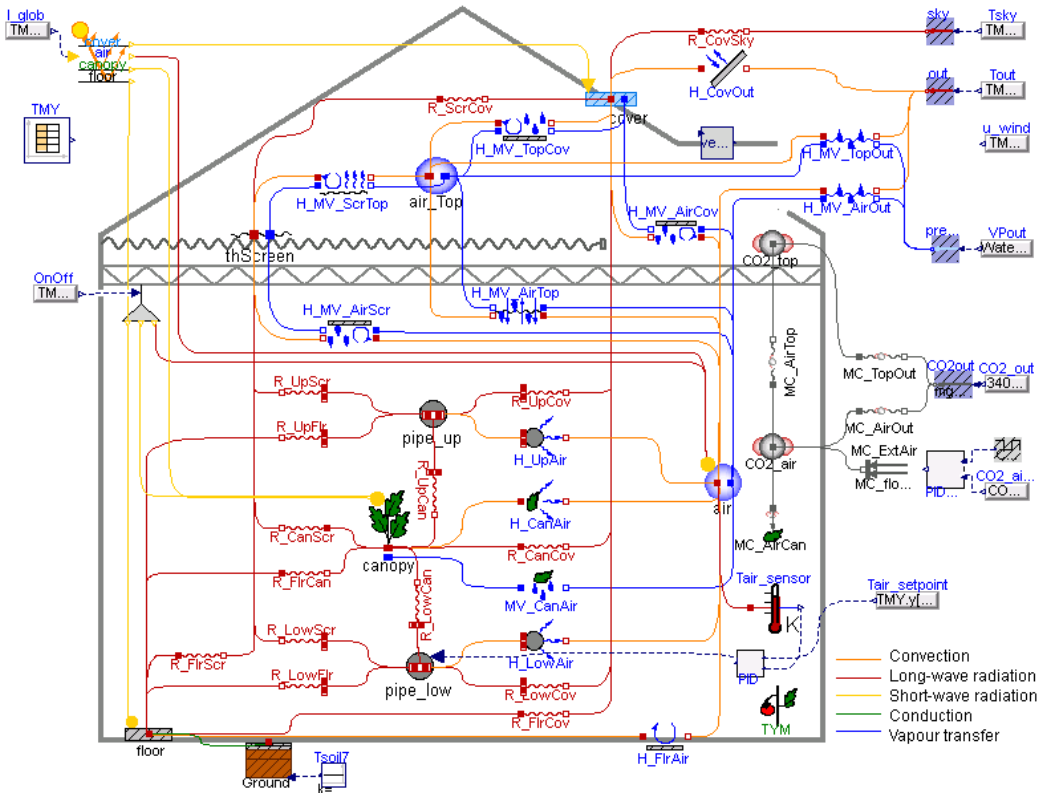

FIGURE 5.4: Graphical interface of the greenhouse climate simulation model. Fluxes: sensible heat (H), long-wave radiation (R), vapor mass (MV) and CO_2 mass (MC). The subscripts meaning can be found in the caption of Figure 5.1

5.3 Tomato yield model

5.3.1 Model overview

A dynamic tomato crop yield model was implemented to account for the effects of the indoor climate on crop growth and thereby on the harvested dry matter. Although crop growth is related to photosynthesis, most of the existent crop models directly relate these two with the absence of a carbohydrate buffer. The buffer function is to store the carbohydrates from the photosynthesis (inflow) and to distribute them to the plant organs (outflow). The carbohydrate flows depend on the availability of carbohydrates in the buffer, which has a maximum capacity, above which carbohydrates cannot be stored anymore, and a lower limit, below which the carbohydrate outflow stops. The outflow and inflow may not be simultaneous. An approach based on not considering the buffer therefore neglects the crop growth at night, when there is no photosynthesis. The presence of a carbohydrate buffer is thus important when modeling crop growth. Models with a common carbohydrate buffer are available in the current literature (e.g. [56]–[60]).

In this work, a recent yield model developed and validated for a variety of temperatures [78] has been implemented. The model computes the carbohydrates flows to the plant organs in the presence of a buffer, as shown in Figure 5.5. The inputs of the model are the canopy instantaneous temperature, the CO_2 concentration of the greenhouse air and the PAR absorbed by the canopy. Their values are retrieved from the greenhouse climate simulation model, in which T_{Can} and $CO2_{Can}$ are state variables and PAR_{Can} is function of the global irradiation. The model takes also into account the 24 hour mean temperature of the canopy ($T_{Can}{}^{24}$). The tomato yield model is used together with the greenhouse model. Its graphical interface is shown in Figure 5.4, where it is indicated by TYM.

5.3.2 Main model variables

The availability of carbohydrates in the buffer is described by:

$$\dot{C}_{Buf} = MC_{AirBuf} - MC_{BufFruit} - MC_{BufLeaf} - MC_{BufStem} - MC_{BufAir} \tag{5.12}$$

where MC_{AirBuf} is the carbohydrate flow coming from the photosynthesis rate; $MC_{BufFruit}$, $MC_{BufLeaf}$ and $MC_{BufStem}$ are the carbohydrate flows distributed to the fruits, leaves and stems, respectively; and MC_{BufAir} is the growth respiration of the plant.

The fruit growth period, defined as the time between fruit set and fruit harvest, is modeled using the "fixed boxcar train" method [61]. Several successive development stages are distinguished. The carbohydrates stored in a fruit development stage j are described by:

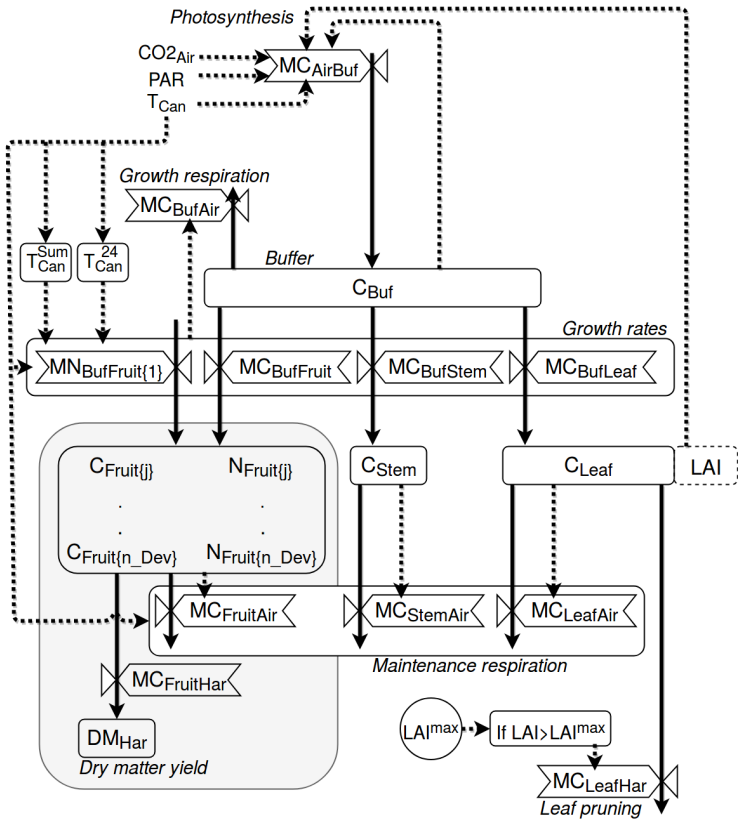

FIGURE 5.5: Schematic representation of the crop yield model adapted from [78]. Boxes define state variables (blocks), semi-state variables (dotted blocks) and carbohydrate flows (valves). Arrows define mass fluxes (solid lines) and information fluxes (dotted lines). For the purpose of readability, the grey box is a simplified scheme of the mass fluxes in the fruit development stages. A more detailed scheme of the latter can be found in [78].

$$\dot{C}_{Fruit\{j\}} = MC_{BufFruit\{j\}} + MC_{Fruit\{j-1\}Fruit\{j\}} - MC_{Fruit\{j\}Fruit\{j+1\}} - MC_{FruitAir\{j\}} \tag{5.13}$$

for $j = 1, 2 \ldots n_{Dev}$, where n_{Dev} is the total number of fruit development stages. $MC_{BufFruit\{j\}}$ is the carbohydrates flow from the buffer to a fruit development stage j. $MC_{Fruit\{j-1\}Fruit\{j\}}$ and $MC_{Fruit\{j\}Fruit\{j+1\}}$ are the flows from the previous and to the next fruit development stage, respectively. For the first stage, $MC_{Fruit\{j-1\}Fruit\{j\}}$ is zero. For the last stage, $MC_{Fruit\{j\}Fruit\{j+1\}}$ equals $MC_{FruitHar}$. $MC_{FruitAir\{j\}}$ is the maintenance fruit respiration of the development stage j.

The evolution of the number of fruits at a fruit development stage j is described by:

$$\dot{N}_{Fruit\{j\}} = MN_{Fruit\{j-1\}Fruit\{j\}} - MN_{Fruit\{j\}Fruit\{j+1\}} \tag{5.14}$$

for $j = 1, 2 \ldots n_{Dev}$. $MN_{Fruit\{j-1\}Fruit\{j\}}$ and $MN_{Fruit\{j\}Fruit\{j+1\}}$ are the fruit number flows from the previous and to the next fruit development stage.

The evolution of the carbohydrates stored in the leaves is described by:

$$\dot{C}_{Leaf} = MC_{BufLeaf} - MC_{LeafAir} - MC_{LeafHar} \tag{5.15}$$

where $MC_{LeafAir}$ is the leaf maintenance respiration and $MC_{LeafHar}$ is the leaf pruning.

The Leaf Area Index (LAI), defined as the leaf area per unit of ground area, i.e. of greenhouse floor, is a semi-state variable of the model and determined by:

$$LAI = SLA \cdot C_{Leaf} \tag{5.16}$$

where SLA is the specific leaf area, whose value can be found in the literature.

The evolution of carbohydrates stored in the stems and roots is defined by:

$$\dot{C}_{Stem} = MC_{BufStem} - MC_{StemAir} \tag{5.17}$$

where $MC_{StemAir}$ is the stem maintenance respiration.

The harvested tomato dry matter (DM) is assumed to evolve with a continuous harvest rate. Thus, the accumulated DM equals the carbohydrate outflow from the last fruit development stage:

$$\dot{DM}_{Har} = \eta_{C\_DM} \cdot MC_{FruitHar} \tag{5.18}$$

where η_{C_DM} is a conversion factor from carbohydrate to dry matter.

The development stages of the crop are defined by the evolution of the canopy temperature:

$$\dot{T}_{Can}^{Sum} = 86400^{-1} \cdot T_{Can} \tag{5.19}$$

where T_{Can}^{Sum} defines the transition from the vegetative to the generative stage. Its value is zero when the generative state starts.

Finally, the 24 hour mean canopy temperature is determined by a 1st order approach:

$$\dot{T}_{Can}^{24} = \tau^{-1}(T_{Can} - T_{Can}^{24}) \tag{5.20}$$

where τ is the time constant (24 h).

5.4 Heating systems models

This section details the modeling of the greenhouse heating system chosen for heat distribution. Regarding heat generation, performance-based models of a heat pump and a CHP unit have been developed. Because of the decrease in CHP efficiency when working in part-load, the simulation system includes a thermal energy storage unit, whose model is presented in this section. For the purpose of compatibility with the climate and crop yield models, the models here presented are written in the Modelica language.

5.4.1 Greenhouse heating system

The greenhouse heating system is made of two heating circuits, the lower and the upper. The lower circuit is the primary heating circuit, which works at high temperature (between 50 and 90ºC) and it is usually made of several loops. It is placed some centimeters above the floor and below the canopy. Heat is transferred by long-wave radiation to the canopy, floor and greenhouse cover, and by convection to the air. This circuit is always in operation in the presence of heat demand. The upper circuit is the secondary heating circuit, which works at low temperature (lower than 50ºC) and is used as a peaker to complement the primary circuit. It is installed at a higher level, in between the thermal screen and the canopy. Because of the lower emitted long-wave radiation flux, the circuit is placed close to the vegetation.

The heating circuits are modeled by means of the discretized incompressible flow model from the ThermoCycle Modelica Library [29]. The discretization is achieved by connecting the desired number of cells in series. In each cell, the flow is described with enthalpy as a state variable. Dynamic energy balance and static mass and momentum balances are applied in each cell. Uniform velocity through the cross section

and constant pressure in the cell are assumed. Axial thermal energy transfer is neglected. Since the resistance to heat transport to the air from the outer pipe surface is about 100 times greater than the resistance from the inner surface to the outer one [22], it is assumed that the temperature of the pipe surface is equal to the water temperature. The heat flow is finally computed by an ideal heat transfer model with constant heat transfer coefficient.

5.4.2 CHP

The CHP model is a performance-based model that assumes constant natural gas consumption and total efficiency. The electrical power is computed by:

$$\dot{W}_{CHP} = \eta_{el}\ \dot{M}_{nom,gas}\ LHV\ U_{ONOFF} \tag{5.21}$$

where η_{el} is the electrical efficiency of the CHP unit, $\dot{M}_{nom,gas}$ is the nominal gas mass flow rate, LHV is the low heating value of the gas and U_{ONOFF} is a boolean control variable that defines the ON/OFF status of the CHP. The electrical efficiency is described by:

$$\eta_{el} = \eta_{II}\ \eta_{Carnot} \tag{5.22}$$

where η_{II} is the second-law efficiency, which is assumed constant, and η_{Carnot} is the Carnot efficiency, which is function of the high and low temperatures of the cycle. The thermal power $\dot{Q}_{CHP}$ is described by its thermal efficiency η_{th}:

$$\eta_{th} = \eta_{tot} - \eta_{el} \tag{5.23}$$

where η_{tot} is the total efficiency, which is assumed to be constant.

5.4.3 Heat pump

The heat pump modeling approach is similar to that of the CHP. The operational coefficient of performance (COP) and heat flows are computed with respect to the nominal performance data. The latter is used to derive a second-law efficiency, which is assumed to remain unchanged in part-load operation (5.24) and (5.25). The nominal heat flow is an input of the model, characteristic of the size of the heat pump. In order to account for the lower heat capacity of the heat pump at lower evaporating temperature, a linear relation between these two variables is assumed (5.26). The electrical consumption is determined by the heat flow and the COP. Equation (5.25) can also be used for off-design operation conditions.

$$COP = \eta_{II}\ COP_{Carnot} \tag{5.24}$$

$$\dot{W}_{nom} = \dot{Q}_{nom}/COP_{nom} \tag{5.25}$$

$$\frac{\dot{Q}}{\dot{Q}_{nom}} = \frac{T_c}{T_{c,nom}} \tag{5.26}$$

5.4.4 Thermal energy storage

For the purpose of the simulation, a thermal energy storage model has been developed. It is a nodal model applied to a stratified tank with an internal heat exchanger. Ambient heat losses are taken into account, and it is assumed that there is no heat transfer between the different nodes. The basic component models (nodes, heat exchanger) are developed according to the formulation proposed in the ThermoCycle Modelica Library [29]. The internal heat exchanger is discretized in the same way as the tank, i.e. each cell of the heat exchanger corresponds to one cell of the tank and exchanges heat with that cell only. The fluid is assumed incompressible in both the tank and the heat exchanger. The energy balance of the fluid in the heat exchanger is described by:

$$V_i \rho \frac{dh}{dt} + \dot{M}(h_{ex} - h_{su}) = A_i \dot{q} \tag{5.27}$$

where V_i is the internal volume of a single cell of the heat exchanger, ρ is the fluid density, h is the fluid specific enthalpy at the cell, $\dot{M}$ is the fluid mass flow rate, h_{ex} and h_{su} are the enthalpy at the outlet and inlet nodes of the cell, A_i is the heat exchange surface of a cell in the heat exchanger and $\dot{q}$ is the heat flux at a cell. The model also includes a heating resistance and a temperature sensor whose height can be adjusted. The energy balance of the fluid in the tank is described by:

$$\frac{V_{tank}}{N} \rho \frac{dh}{dt} + \dot{M}\left(h_{ex} - h_{su}\right) - A_{hx}\dot{q}_{hx} = \frac{A_{amb}}{N}\dot{q}_{amb} + \dot{Q}_{res} \tag{5.28}$$

where V_i is the total capacity of the tank, N is the number of cells, A_{hx} is the exchange surface of a cell in the heat exchanger, $\dot{q}_{hx}$ is the heat flux at a cell of the heat exchanger, A_{amb} is the total heat exchange area from the tank to the ambient and $\dot{Q}_{res}$ is the input power from the heating resistance.

5.5 Case study and results

In this work, it is proposed to illustrate the use of the model with the purpose of fostering electrical self-consumption. The diagram of the considered configuration is shown in Figure 5.6a. The system (case (A)) consists of a greenhouse connected to a thermal energy storage tank, which acts as an open buffer. On its primary side, it serves the greenhouse, and on its secondary side, it is supplied by a heat pump and

a CHP unit in series. The heating demand is provided by both the CHP unit and the heat pump. The electrical demand is provided by the CHP, which at the same time is used to power the heat pump. For the purpose of comparison, a second case study (case (B)) similar to the first one but with only the CHP as a generation unit is also simulated (Figure 5.6b). With the exception of the heat pump, both models have the same parameters and inputs.

The dynamic model of the greenhouse climate presented in Section 5.2 is used to simulate the indoor climate of a greenhouse for tomato crop. A climate controller adapts the heat flow input to the greenhouse so that the radiation level, the temperature, the relative humidity and the CO_2 concentration of the air fulfill the required conditions for the crop. In case these conditions are not satisfied, the harvest rate from the yield model is affected. Greenhouse heating circuits are typically controlled by temperature regulation, which is done by a mixing valve at the beginning of the heating circuit [22]. However, because the heat flow in this work is provided directly from the storage tank, the selected regulation strategy is the water mass flow rate. The primary circuit pump (i.e. *pump_1ry* in Figure 5.6) runs at a variable speed regulated by the climate controller. The pump of the secondary circuit (i.e. *pump_2ry* in Figure 5.6) runs at a constant speed. The performance-based models for each generation unit and the storage unit are also included. According to the greenhouse demand and the level of the storage, a control strategy (i.e. controller box in Figure 5.6) decides when to run the generation units. For the purpose of minimizing the amount of electricity bought from the grid, the heat pump is never running independently.

The size of the considered systems can be found in Table 5.1. The total installed capacity for thermal generation is equal for both simulations. Case (A) consists of a CHP unit of 92 kW_{th} and a heat pump of 33 kW_{th}. Case (B) consists of a CHP unit of 125 kW_{th}. For the former, the heat pump capacity is based on a nominal COP and the nominal electric capacity of the CHP. A thermal energy storage tank of 10 m^3 is used in both cases. The greenhouse design characteristics are based on the values from [78] for typical low-tech greenhouses in The Netherlands. The studied greenhouse is a Venlo-type structure with a roof slope of 25° and a mean height of 4.2 m. The air is naturally ventilated through the vents mounted on the roof. The simulation is run for a floor surface of 192 m^2 and the simulated time period is one year.

As shown in Table 5.2, both systems generated a total thermal load of approximately 133 MWh, used to supply the greenhouse demand. While in case (B) it is 100% covered by the CHP, in case (A) 75% is covered by the CHP and 25% by the heat pump. The evolution in time of the accumulated generated power is steeper in winter months, where the heat demand is higher (Figure 5.7a). Because of the lower CHP capacity, the gas consumption is about 1.3 times lower in case (A) than in case (B) (Figure 5.7b). In a similar way, the total net electrical generation of case (A) is also lower. As expected, the heat pump reduces the amount the electricity sold back

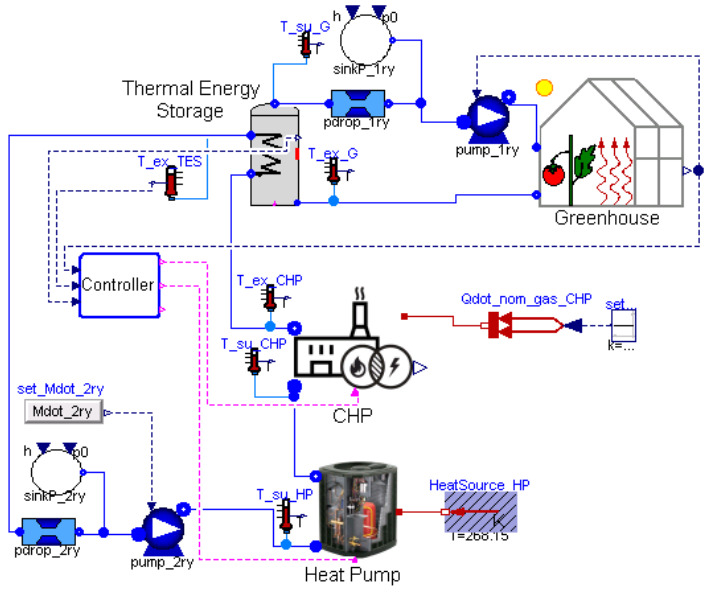

(A)

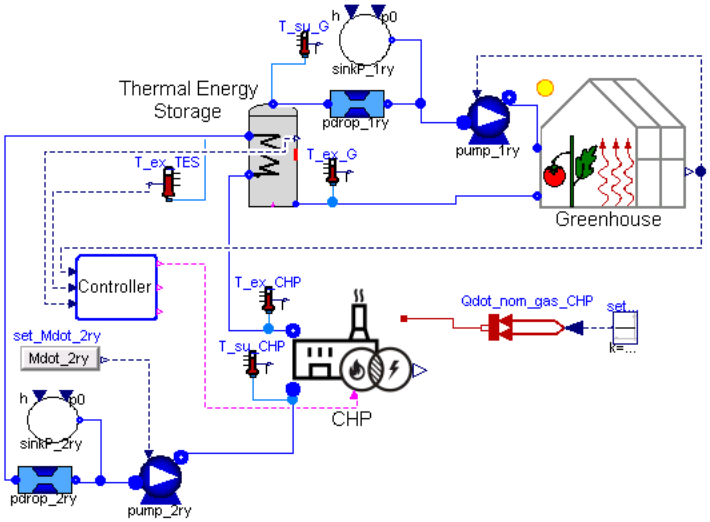

(B)

FIGURE 5.6: Diagram of the studied configurations: (A) Greenhouse connected to a thermal energy storage tank, which is filled by a heat pump and a CHP unit in series; (B) same as (A) without the heat pump.

to the grid by a factor close to 3.2 (Figure 5.8a). The costs of the gas consumption and electricity are computed with their associated average prices for non-household consumers of year 2017. These prices, extracted from Eurostat in February 2018, are stated in Table 5.1. The use of a heat pump diminishes the total yearly operational cost by 9.1% (i.e. 431 €). Results finally show that the tomato yield is not affected by the new control strategy and configuration (Figure 5.8b).

TABLE 5.1: Main parameters of the models

Description	*Variable*	*Case (A)*	*Case (B)*	*Units*
Thermal Energy Storage	V_{TES}	10	10	m^3
CHP capacity	P_{CHP}	92	125	kW_{th}
HP capacity	P_{HP}	33	0	kW_{th}
Greenhouse surface	A_{floor}	192	192	m^2
CHP total efficiency	$\eta_{tot,CHP}$	0.9	0.9	-
CHP second-law efficiency	$\eta_{II,CHP}$	0.4	0.4	-
COP of the HP	COP_{HP}	3.5	3.5	-
Price of natural gas	π_{gas}	35.5	35.5	€ MWh^{-1}
Price of electricity	π_{el}	141.5	141.5	€ MWh^{-1}
Selling price of electricity	$\pi_{el,sell}$	47.2	47.2	€ MWh^{-1}

TABLE 5.2: Results

Description	*Variable*	*Case (A)*	*Case (B)*	*Units*
Greenhouse thermal load	Q_G	132.7	132.7	MWh_{th} y^{-1}
Total thermal generation	Q_{TOTAL}	132.9	132.7	MWh_{th} y^{-1}
CHP generation	Q_{CHP}	99.3	132.7	MWh_{th} y^{-1}
HP generation	Q_{HP}	33.6	0	MWh_{th} y^{-1}
Greenhouse electrical load	W_G	0.187	0.187	MWh_{el} y^{-1}
CHP electrical generation	W_{CHP}	29.9	40.3	MWh_{el} y^{-1}
HP electrical consumption	W_{HP}	17.1	-	MWh_{el} y^{-1}
Harvested tomato dry matter	DM_{Har}	755.2	755.6	g m^2 y^{-1}
Gas consumption	Q_{gas}	143.5	192.2	MWh_{th} y^{-1}
Electricity sold to the grid	W_{sell}	12.6	40.1	MWh_{el} y^{-1}
Electricity bought from the grid	W_{buy}	0	0	MWh_{el} y^{-1}
Cost of gas	C_{gas}	5094	6823	€ y^{-1}
Cost of sold electricity	C_{sell}	-595	-1893	€ y^{-1}
Cost of bought electricity	C_{buy}	0	0	€ y^{-1}
Total yearly cost	C_{TOTAL}	4499	4930	€ y^{-1}

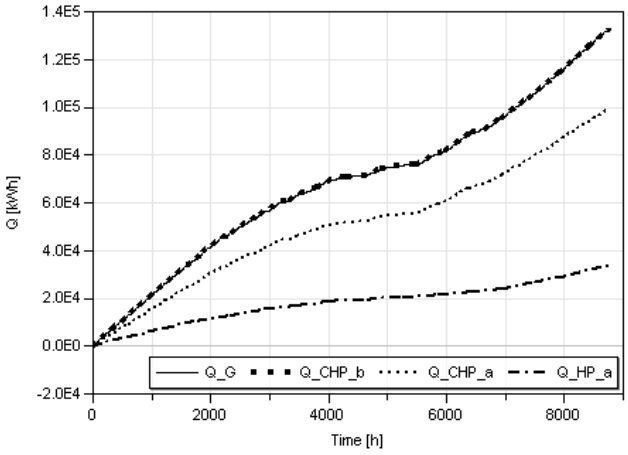

(A)

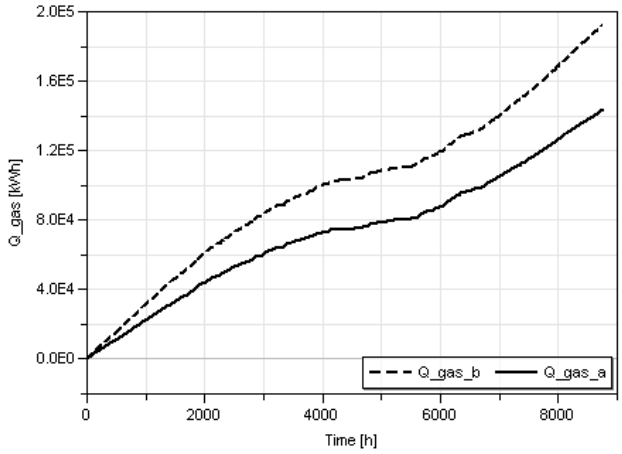

(B)

FIGURE 5.7: Evolution in time of the (A) accumulated generated energy and (B) gas consumption.

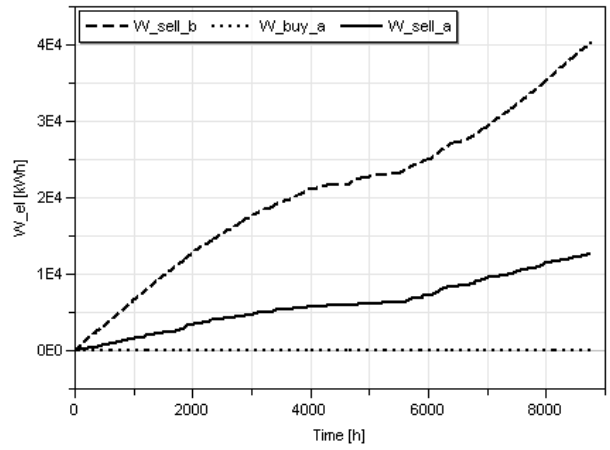

(A)

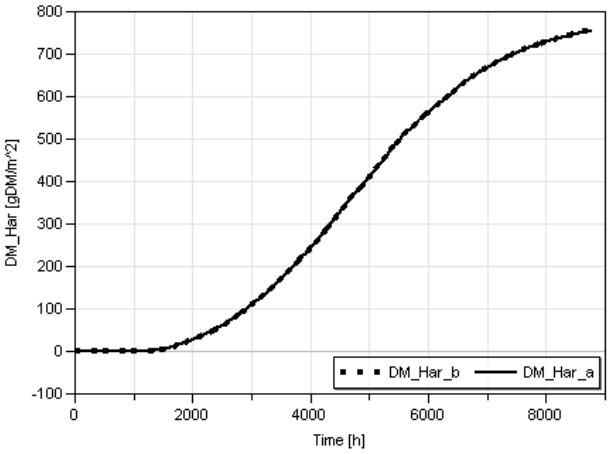

(B)

FIGURE 5.8: Evolution in time of the accumulated: (A) electrical energy sold and bought, (B) dry matter of harvested tomato.

5.6 Conclusions

The presented modeling framework filled the gap of an inexistent simulation platform readily available for the simulation of greenhouse climate and its system integration with e.g. thermal generators. The models are released as open-source, thus ensuring a proper reproducibility and re-usability of this work [72]. Moreover, the development of the main greenhouse climate model with an object-oriented approach offers a high degree of flexibility to the user because: (i) the greenhouse structure is not predefined, i.e. the model can easily be adapted to match required greenhouse characteristics (e.g. number of heating circuits, the existence of side vents, the use of a thermal screen, the existence of forced ventilation, etc.) and (ii) the model is parametrizable (e.g. material of the floor, type of cover, dimensions of the heating circuits, etc.).

In this work, the case study is presented to exemplify the use of the greenhouse climate and the tomato yield model. Nonetheless, these models can be used for a wide range of purposes such as the optimal control of the greenhouse actuators, the optimal sizing of the heating appliances, or the optimal integration of the units in the power system.

For the particular case of fostering electrical self-consumption, results show that adding a heat pump with a proper control strategy increases the self-consumption level and reduces the operational costs. The heat pump consumed 57% of the electricity generated by the CHP, leaving only 42% to be sold back to the grid. The system with the heat pump allowed having a smaller CHP capacity. The gas consumption was therefore reduced by 25%. Total operational costs were reduced by 9%.

Chapter 6

Optimizing Energy Management Strategies in Greenhouse Horticulture: Control of Screen Deployment and CHP Units

This chapter is a reprint of the case study, results and discussion parts in *Q. Altes-Buch, S. Quoilin, and V. Lemort. "A modeling framework for the integration of electrical and thermal energy systems in greenhouses." Building Simulation, 15: 779–797. 2022. doi:10.1007/s12273-021-0851-2*

Research Question

What are the optimal energy management strategies for enhancing energy efficiency in greenhouse horticulture, with a specific focus on screen deployment control and the operation of CHP units, and what are the potential benefits associated with these optimizations?

Summary

This study exemplifies the capabilities of the modeling framework in achieving energy savings and operational cost reduction, utilizing a specific case study. The case study undergoes simulation under six distinct control strategies, associated with two sensitivity studies. The first evaluates the impact of energy savings through the control of greenhouse appliances, with a particular focus on the thermal screen. The second assesses the impact on both energy savings and operational costs through the control of generation units, specifically a CHP unit coupled to TES.

To that end, the models detailed in Chapter 2 and 3 were utilized to build a system that was simulated under six control strategies. Initially, a greenhouse model was built by interconnecting the components from the Greenhouses Library. This greenhouse model is characterized by increased complexity and incorporates more

advanced control strategies in comparison to those employed in Chapter 4 and 5. Subsequently, this greenhouse model was integrated into a broader system, interconnecting it to a CHP unit and a TES tank, forming a circuit that faithfully represents real-world systems. Six dedicated controllers were developed, with each assigned to a specific strategic simulation.

The case study is sized to a real system in the Netherlands, with documented characteristics available in the literature. As a result, the outcomes from these simulations are anticipated to align with real-world conditions. This case study underscores the significant influence that tuning the climate controller or controlling heat generation units can have on operational costs. Additionally, it highlights the substantial dependency of these costs on energy market prices.

Contributions

The main contribution of this work is the proposal of two strategies that demonstrably increase the energy efficiency of traditional greenhouse systems coupled with CHP and TES, thereby advancing towards the decarbonization of the greenhouse sector.

The first strategy introduces an innovative screen control method, where the opening of the screen is regulated by temperature in addition to irradiation. Although this practice is commonly employed by greenhouse growers[1], it has rarely been simulated. This work quantifies the resulting reduction in energy consumption.

The second strategy assesses the variations resulting from the use of heat-driven, electrical-driven, or mixed-driven strategies for the thermal units. This article demonstrates that applying different control methods leads to varying levels of energy purchases from external sources to meet the greenhouse demand. Consequently, this analysis shows that depending on the energy sources or energy market prices, different strategies may be more effective for different systems and identifies the optimal strategy for the classic CHP-TES system.

Reading tips

For readers beginning with this chapter, it is advisable to peruse the introduction and modeling details pertinent to this work, as they are covered in Chapter 2.

[1]Knowledge of common practices has been acquired throughout the course of this thesis. This has been achieved through information published in the literature and discussions with other researchers in the field, including those from the Gembloux campus of the University of Liege, the Geel campus of KU Leuven, Thomas More, Warmtekracht Ondersteunings Maatschappij, Wageningen University & Research, A-net, Hankyong National University, Seoul National University, Samsung Electronics, EZFarm, FARM8, Spacewalk, and ioCrops.

6.1 Case study

In this work, various energy management strategies are defined and simulated to demonstrate the capabilities of the proposed modeling framework. To that end, a tomato-growing greenhouse is selected as case study. The greenhouse is connected to a thermal energy storage unit and to a CHP unit. A simplified scheme of the system is shown in Figure 6.1. The generated heat can be either stored in a large water tank or directly bypassed to the greenhouse heating distribution circuit. In order to obtain an horizontally-homogeneous indoor climate, the heat input to the greenhouse is controlled by temperature regulation. A three way valve is used for that purpose, allowing to mix the return to lower down the supply temperature. The generated electricity from the CHP can either be self-consumed or fed back to the grid.

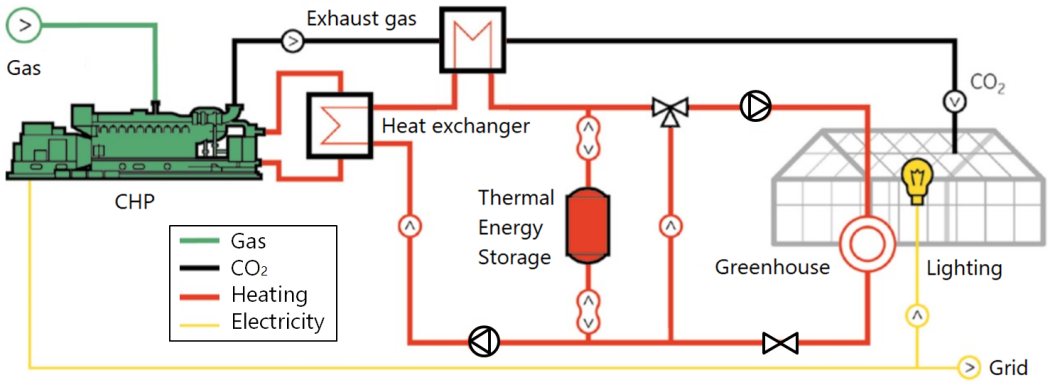

FIGURE 6.1: Scheme of the simulation model (adapted from [80])

The model is parametrized according to the case study. The selected greenhouse has a Venlo-type structure with a single glass layer cover, typical for mild-temperature conditions. The floor area is 2.3 ha. Ventilation only occurs naturally through the roof windows. Heating is distributed by a pipe rail system. The greenhouse is equipped with a CO_2 enrichment system connected to the CHP exhaust gases, HPS lamps and a movable thermal screen. No cooling equipment is considered. The design parameters related to the greenhouse construction, ventilation, heating, CO_2 enrichment and supplementary lighting are presented in Table 6.1. The climate controller actions are based on the strategies presented in Section 2.2.4, whose inputs are presented in Table 6.2.

TABLE 6.1: Main parameters of the model.

Parameters	**Value**	**Units**
Construction		
A_{flr}	$2.3{\cdot}10^4$	m^2
φ_{cov}	25	°
h_{air}	3.8	m

Parameters	Value	Units
h_{gh}	4.2	m
Cover		
ε_{cov}	0.85	-
ρ_{cov}^{NIR}	0.13	-
ρ_{cov}^{PAR}	0.13	-
τ_{cov}^{NIR}	0.85	-
τ_{cov}^{PAR}	0.85	-
c_{cov}	840	J K^{-1} kg^{-1}
ρ_{cov}	2600	kg m^{-3}
e_{cov}	$4{\cdot}10^{-3}$	m
Thermal screen		
ε_{scr}	0.67	-
ρ_{scr}^{NIR}	0.35	-
ρ_{scr}^{PAR}	0.35	-
τ_{scr}^{NIR}	0.6	-
τ_{scr}^{PAR}	0.6	-
c_{scr}	1800	J K^{-1} kg^{-1}
ρ_{scr}	200	kg m^{-3}
e_{scr}	$0.35{\cdot}10^{-3}$	m
K_{scr}	$0.05{\cdot}10^{-3}$	m^3 m^{-2} $K^{-0.66}$ s^{-1}
Floor		
ε_{flr}	1	-
ρ_{flr}^{NIR}	0.5	-
ρ_{flr}^{PAR}	0.65	-
λ_{flr}	1.7	W m^{-1} K^{-1}
c_{flr}	880	J K^{-1} kg^{-1}
ρ_{flr}	2300	kg m^{-3}
e_{flr}	0.02	m
Soil		
λ_{so}	0.85	W m^{-1} K^{-1}
$\rho \cdot c_{so}$	$1.73{\cdot}10^{6}$	J K^{-1} m^{-3}
Canopy		
ε_{can}	1	-
$U_{leaf,air}$	5	W m^{-2} K^{-1}
Ventilation		
A_{ven}/A_{flr}	0.1	m^2
K_d	0.75	-
K_w	0.09	-
K_{leak}	$1{\cdot}10^{-4}$	-
h_{ven}	0.68	m
Heating		

Parameters	Value	Units
d_{pip}	0.051	m
l_{pip}	1.36	m m^{-2}
CO_2 supply		
$\dot{m}_{ext}^{c,max}$	7.5	mg m^{-2} s^{-1}
Supp. lighting		
P_{el}	100	W m^{-2}
External systems		
V^{tes}	1100	m^3
$\dot{Q}_{gas}^{chp}$	3.92	MW
η_{el}^{chp}	0.4	-
η_{tot}^{chp}	0.9	-

The tomato yield model is run simultaneously with the greenhouse climate model. The crop initial conditions are shown in Table 6.2.

The CHP unit has a nominal capacity of 3.92 MW. The nominal electrical and thermal efficiencies are 40% and 50%, respectively. The thermal efficiency lumps the heat provided directly by the CHP and heat recovered from the exhaust gases. The storage volume is 1100 m^3.

The simulation period is one year and starts on December 10th, being equivalent to the start period for tomato growth in mild-climate conditions. Data for a typical meteorological year (TMY) in Brussels is used to describe the outdoor conditions, namely air temperature, relative humidity, pressure, wind speed and global irradiation.

In order to demonstrate the capabilities of the model, two sensitivity analyses with different energy management strategies are performed. The first intends to show the difference in energy consumption and the impact on crop growth caused by applying different control rules on the greenhouse thermal screen. To that end, three different deployment methods are tested:

- C05: The first and simpler approach, consists in deploying and removing the screen at sunset and sunrise. In the model, these are set at the threshold of 5 W m^{-2}.
- C30: given that photosynthetic activity of the plant achieves its maximal potential about one hour after sunrise and diminishes just before sunset [69], the second approach consists in remomving the screen after outside irradiation reaches 30 W m^{-2}.
- VAR: The third approach consists in deploying the screen in function of an outside temperature dependent radiation criterion. As shown in Figure 6.2,

TABLE 6.2: Main inputs of the model

Parameters	Value	Units
Crop conditions		
LAI^{max}	2.7	$m^2\ m^{-2}$
LAI^{0}	0.3	$m^2\ m^{-2}$
m^{ch}_{leaf}	$40{\cdot}10^3$	mg $\{CH_2O\}\ m^{-2}$
m^{ch}_{stem}	$30{\cdot}10^3$	mg $\{CH_2O\}\ m^{-2}$
Climate control		
CO_2 supply		
$\gamma^{c,min}_{air,SP}$	390	ppm
u^{max}_{ven}	0.3	-
Supp. lighting		
h_{start}	5	AM
h_{end}	10	PM
$I_{Off\rightarrow On}$	40	$W\ m^{-2}$
$I_{On\rightarrow Off}$	120	$W\ m^{-2}$
I^{max}_{acc}	5	kWh
t_{prove}	1800	s
t^{min}_{On}	7200	s
Ventilation		
RH_{ven}	85	%
T_{ven}	$T_{air,SP} + 2$	°C
Thermal screen		
t_{open}	30	min
$u_{scr,open}$	0.5	-
RH_{gap}	85	%
T_{gap}	$T_{air,SP} + 1$	°C
Energy prices		
π_{gas}	35.5	€ MWh^{-1}
π^{buy}_{el}	141.5	€ MWh^{-1}
π^{sell}_{el}	47.2	€ MWh^{-1}

the screen is removed when crossing the following threshold:

$$I_{thr}^{G} = \max\{0,\ 290 - 19.33 \cdot T_{out}\} \tag{6.1}$$

where T_{out} is expressed in Celsius. In other words, the screen is open/deployed when the combination of outside temperature and solar radiation is above/below the set-point.

The second study intends to show the difference on the system operational cost for different controls on the CHP unit. The operational cost is obtained by:

$$C_{tot} = C_{gas}^{chp} + C_{el}^{buy} - B_{el}^{sell} \tag{6.2}$$

where C_{gas}^{chp} is the gas cost, C_{el}^{buy} is the cost of the electricity consumed from the grid and B_{el}^{sell} is the remuneration from the electricity fed back to the grid. The cost of CO_2 could be added to the equation in case the latter was purchased instead of recovered from the CHP exhaust gases. Electricity is purchased if there is an electrical demand and the CHP is not running, or the system is short (i.e. the CHP is running but its output power is lower than the consumption). In a similar manner, electricity is fed back if the system is long. In the absence of subsidies, fed back electricity is remunerated at a price close to the wholesale price of electricity. Given that the retail price of electricity is significantly higher than the wholesale price, prosumers have a clear advantage at maximizing their level of self-consumption [20]. To evaluate the impact this can have on the total operational cost, three state diagram controls are implemented:

- Heat-driven control (HDC): This control ensures the heating demand regardless of the electrical demand. The CHP is run to heat up the TES and/or to provide the greenhouse heating demand. Since there is heating demand almost every day of the year, the TES is not allowed to go below a certain temperature. Its storage level is controlled by keeping the temperature at the middle cell in between boundaries.
- Electrical-driven control (EDC): This control maximizes electrical self-consumption regardless of the heating demand. The CHP is operated only when there is an electrical consumption, i.e. when the lamps are turned On. As explained in Section 2.2.4, the lower the solar radiation, the higher the hours the lamps operate and viceversa. Therefore, the EDC runs the CHP for longer periods in the days with a lower heat input from the sun, i.e. the days with a higher heating demand.
- Mix-driven control (MDC): This control maximizes electrical self-consumption while ensuring the heating demand. The CHP can be operated by the EDC or the HDC. Therefore, the CHP is always run when the lamps are On, and

can also be started up if the lamps are Off but the conditions of the HDC are satisfied.

The gas and electrical prices used for this study are stated in Table 6.2. All simulations of the first sensitivity analysis use the HDC. Simulations of the second sensitivity analysis use the VAR set-point in the screen control. Therefore, there are a total of five simulations (VAR and HDC being the same).

6.2 Results and discussion

6.2.1 Optimizing screen use

Table 6.3 summarizes some key results obtained for the C05, C30 and VAR simulations. The first three columns evaluate the share of time over the total simulation time during which the air temperature is:

- t_{in}: well controlled (T_{air} in $T_{air,SP} \pm 1.5$ °C)
- t_{uh}: underheated ($T_{air} < T_{air,SP} - 1.5$ °C)
- t_{oh}: overheated ($T_{air} > T_{air,SP} + 1.5$ °C)

TABLE 6.3: Main results of the sensitivity analysis on screen use

	t_{in} [%]	t_{uh} [%]	t_{oh} [%]	E_{th}^{gh} [kWh m^{-2}]	E_{el}^{gh} [kWh m^{-2}]	m_{har}^{DM} [kg m^{-2}]
C05	75.6	0.55	23.9	373.4	227.4	4.74
C30	75.8	0.65	23.6	362.6	227.4	4.72
VAR	76.9	0.64	22.5	356.9	227.4	4.58

By looking at the numbers in Table 6.3, one can see the air temperature control has similar efficiencies for the three simulations. This is justified by a fast control, which adapts the heating input and the opening of the windows to the constantly changing dynamics. Independent of the screen operation, the control manages to keep the air temperature well controlled for in average 76% of the time. The rest of the time, the greenhouse climate is rarely underheated (less than 1% of the time) and mostly overheated (in average 23% of the time). Although overheating can be caused by an excessive input from the heating units, it is primarily caused by excessive solar gains. In mild-weather regions like Belgium, the temperature inside the greenhouse can reach 40°C in hot sunny days. As quantified in Section 2.2.4, excessive temperatures have a negative impact on the harvest rate and must be avoided. However, since this event only occurs occasionally, investing in a cooling system is not justified.

As previously stated, in order to keep the temperature within boundaries, the climate control adapts the heating input and the opening of the windows. Simulation C05 has therefore the highest heating consumption (373 kWh m^{-2}). Delaying the opening from 5 to 30 W m^{-2} in C30, allows decreasing the heating consumption by 2.9% without penalizing crop growth (-0.5% of harvested DM). Moreover, the

outside temperature dependent radiation criterion (VAR) allows decreasing heating consumption by 4.4% but at the expense of a more significant decrease in harvested DM (-3.3%). The screen opening for each simulated point of the latter control strategy are plotted in Figure 6.2. It should be noticed that the screen is never closed above the threshold, but it is sometimes open below it (i.e. blue points below the I^G_{thr} curve). These points do not reflect a control failure but instead, follow the humidity control, which is at the top of the screen control hierarchy.

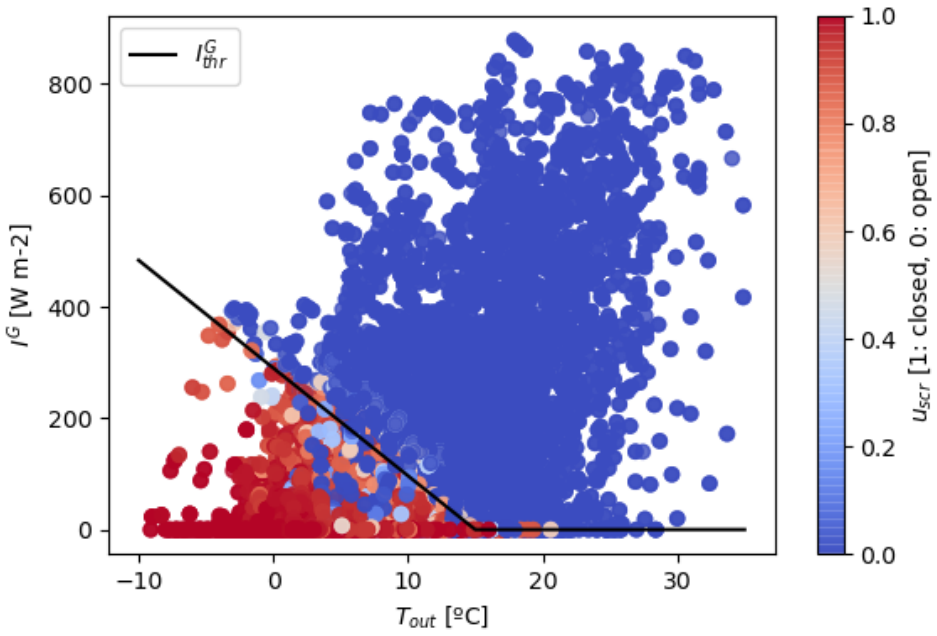

FIGURE 6.2: VAR's screen deployment criterion (I^G_{thr}) and simulation points

Overall, the VAR method is an improved version of the simpler radiation-only dependent approaches (C05 and C30) by promoting energy savings in cold cloudy days and avoiding overheating in warm mornings.

6.2.2 Optimizing operational costs

Some key characteristics of the results obtained for the heat, electrical and mix-driven controls are presented in Table 6.4. The HDC and MDC present similarities in terms of performance. They succeed in controlling indoor temperature during 76.9% and 76.1% of the simulation period, respectively. The greenhouse is underheated during only 0.64% and 0.67% of the total time, the remainder 22.5% and 23.2% of the time is overheated. The EDC, on the contrary, keeps the temperature within boundaries during only 46% of the time. Running the CHP only in case of electrical demand (i.e. 2 233 hours, corresponding to hours of supplementary lighting) is not sufficient to fulfill the heating demand. The greenhouse is underheated 44% of the time.

TABLE 6.4: Main results of the sensitivity analysis on operational costs

	t_{in} [%]	t_{uh} [%]	t_{oh} [%]	E_{gas}^{chp} [MWh]	E_{th}^{chp} [MWh]	E_{el}^{chp} [MWh]	E_{el}^{buy} [MWh]	E_{el}^{sell} [MWh]	C_{gas} [k€]	C_{el}^{buy} [k€]	B_{el}^{sell} [k€]	C_{tot} [k€]
HDC	76.9	0.642	22.5	16 477	8 271	6 509	3 413	4 691	585	483	221	846
MDC	76.1	0.671	23.2	16 820	8 408	6 680	1 826	3 276	597	258	155	700
EDC	46.0	44.0	9.94	8 754	4 321	3 558	1 672	0.125	311	237	0.006	547

In terms of operational strategy, the HDC and MDC run the CHP unit for a similar accumulated time (4 203 and 4 291 hours, respectively) and thus, have similar gas consumptions. However, the time of the day where the CHP is run differs for both controls. Its impact is mainly reflected in the electrical consumption. For instance, the HDC runs the CHP independently of the operation of supplementary lighting. The generated electricity is therefore either consumed or sold depending on the lighting status at the moment. From the generated 6 509 MWh_{el}, only 28% is consumed by the greenhouse, the rest 4 691 MWh_{el} being fed back to the grid and remunerated at 221 k€. To cover the greenhouse electrical demand, this leads to 3 413 MWh_{el} bought from the grid with an associated cost of 483 k€. Considering the gas cost, the final operational cost at the end of the simulation period is 846 k€.

By prioritizing the operation of the CHP during supplementary lighting hours, the MDC allows decreasing the amount of electricity bought from the grid by 46% with respect to the HDC, saving 225 k€. Nonetheless, since the instant power produced by the CHP is smaller than the electrical consumption of the lamps, the system is often short and the remainder 54% (1826 MWh_{el}) are still bought from the grid. Since the CHP is also run when lamps are Off because of heat-driven conditions, the MDC feeds back to the grid 3276 MWh_{el}, which are remunerated at 155 k€. This is 49% of its electrical production, compared to 72% in the HDC. In total, the operational cost of the MDC at the end of the simulation period is 700 k€. Therefore, compared to the HDC the MDC allows reducing total operational costs by 17%.

Figure 6.3 shows three Sankey diagrams of the accumulated energy flows in the MDC simulation for the whole simulation period, the month of January and the month of July. By comparing the diagrams, it appears that only 1.8% of the yearly solar radiation is received in January, versus 16% in July. For January, this implies a higher use of heating (12% of the yearly consumption, versus 5% in July) and a higher use of supplementary lighting (15% of the yearly consumption, versus 1.9% in July).

As expected, most of the energy losses happen through long-wave radiative heat transfer with the sky, by convection from the outer side of the cover or by ventilation from the indoor air to the outside air. In January, ventilation is limited and the loss by convection from the cover is substantial. On the contrary, in July, ventilation is used intensively to decrease the indoor air temperature.

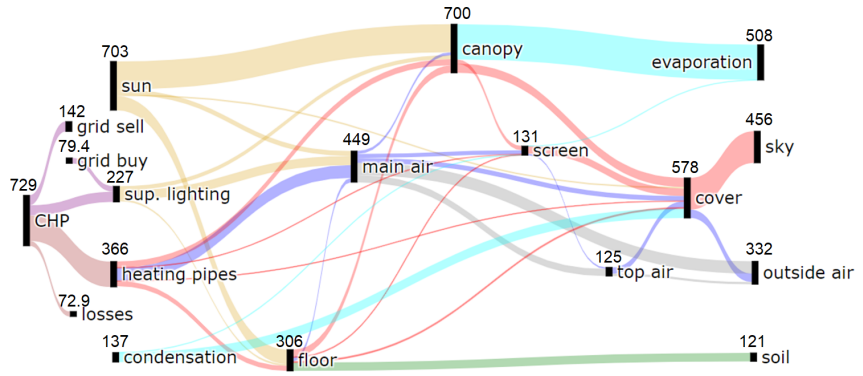

(A) Year

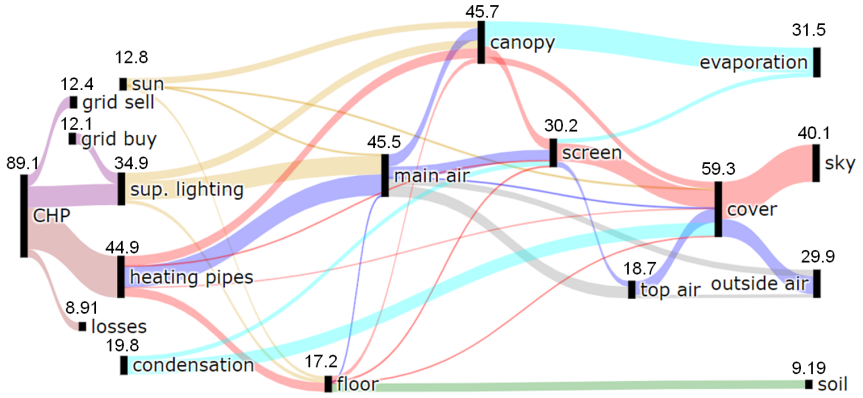

(B) January

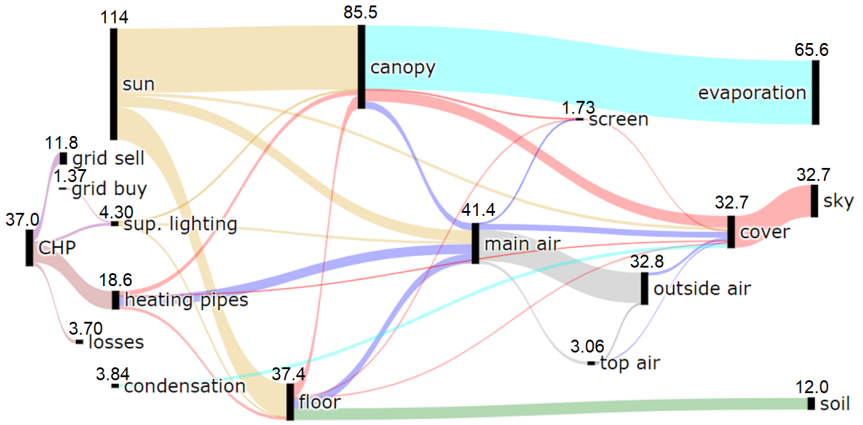

(C) July

Electrical energy (E_{el}) | Long-wave radiation (E^{rad}) | Conduction (E^{cnd})
Thermal energy (E_{th}) | Convection (E^{cnv}) | Latent heat (E^{lat})
Short-wave radiation (E^{swr}) | Ventilation (E^{sens})

FIGURE 6.3: Sankey diagrams of the accumulated sensible energy flows in the MDC simulation

Latent heat gains from condensation on the inner side of the cover mainly occur in January due to the cold outside air. In July, condensation is minimal in the greenhouse. However, the canopy is warmer than the air and has high latent heat losses due to transpiration. In January, on the contrary, given the smaller short-wave radiation intake (among others), the canopy is colder than the air and presents lower latent heat losses.

Finally, it should be remarked that the screen is a key participant in the sensible energy balance in January, whereas it is barely participating in July.

6.3 Conclusions

In this work, the proposed models are used to investigate the influence of control strategies on the greenhouse energy consumption and crop yield through two case studies. The first case study focuses on intrinsic greenhouse components. For the particular case of the thermal screen, results indicate that just by delaying the deployment of the screen, heating consumption can be reduced by 3% with no loss of productivity. Moreover, outside temperature dependent radiation criterion can further reduce energy use with a small decrease on harvest.

The second case study illustrates the impact of the control of the generation units on the operational costs. Results show that a mix electrical-heat-driven control that fosters electrical self-consumption can decrease operational costs by 17% with respect to a purely heat-driven control. It is also demonstrated that purely electrical-driven control strategies are not suitable for this kind of systems since they do not cover a sufficient share of the heating demand.

In conclusion, the presented open-source modeling framework can be used for a wide range of possibilities that can contribute to the necessary energy transition. Apart from optimizing the control strategies to drive productivity while reducing energy use, it can also evaluate the potential use of renewable energy sources (e.g. solar, geothermal), the use of energy-related emissions (e.g. waste-heat or CO_2 emissions) or even the impact in the power grid by using existing CHP units for ancillary services.

Part III

Integration of Sustainable Energy Solutions for Greenhouses

Chapter 7

Assessment of Short-Term Aquifer Thermal Energy Storage for Energy Management in Greenhouse Horticulture: Modeling and Optimization

This chapter is a reprint of *Q. Altes-Buch, T. Robert, S. Quoilin, and V. Lemort. "Assessment of short-term aquifer thermal energy storage for energy management in greenhouse horticulture: modeling and optimization." In Proceedings of the 7th International High Performance Buildings Conference, 2022.*

Research Question

What sustainable energy solutions are viable for greenhouses, and how can the developed modeling framework contribute to exploring these integrated systems?

Specifically, what is the energy recovery potential of greenhouses with thermal storage in shallow alluvial aquifers in Atlantic climates, and what are the advantages and implications of such integration?

Summary

In this work, the established modeling framework was utilized to assess the feasibility of low-carbon energy sources. Specifically, the exploration focused on the potential of thermal energy storage in alluvial aquifers as a sustainable solution for greenhouse energy needs. Still in the early stages of development with limited foundational groundwork, this application, known as aquifer thermal energy storage (ATES), contributes merely 6% to the existing renewable energy generation in the Netherlands. The ATES concept involves cooling greenhouses in the summer to

store excess energy in an underground seasonal buffer. This stored energy is later utilized for heating during the winter, facilitated by a heat pump.

In the presented case study, the aquifer is characterized by a deterministic 3D groundwater flow and heat transport numerical model. Evaluating the benefits of implementing ATES in greenhouse energy systems required the development and integration of new models into the Greenhouses Library. Notably, models for a water-to-water heat pump and a heating and cooling coil were introduced. Together with the models detailed in Chapter 2 and 3, these models were utilized to build the simulation system. Initially, a greenhouse model was built by interconnecting the components from the Greenhouses Library. Notably, this greenhouse model differs from the one utilized in Chapter 6, featuring distinct heating distribution systems and controllers. The climate control actions, however, though also characterized by increased complexity and incorporate more advanced strategies akin in Chapter 6, as opposed to those implemented in Chapter 4 and 5. Subsequently, the greenhouse is interconnected with a heat pump model and sources models representing the evaporator side and the cold wells. Controllers based on state graph representations were developed to ensure the proper functioning of the system.

The models were sized for a specific case study, focusing on a 100 m thick aquifer situated in the Cretaceous chalk region of Wallonia, Belgium. The simulations cover a two-year period, revealing that shallow alluvial aquifers can prove highly advantageous, providing a sustainable solution for both heating and cooling in greenhouse applications.

Contributions

The primary contribution of this work is the demonstration that ATES is a viable energy source for greenhouses. This is significant because ATES is an emerging energy solution, as discussed in Section 1.1.4. Moreover, this study is the first to explore this technology for a Cretaceous chalk aquifer in Belgium.

An additional contribution of this article is the proposal to transform a pipe-only heating distribution system into a combination of heating pipes and heating/cooling coils to meet the cooling needs of greenhouses. The code for the heating and cooling coil models is released as open-source, enabling researchers to replicate the work. The pipes model was improved as explained in Chapter 2, by employing a discretized approach that segments the pipes into multiple cells to model the flow. This approach replaces the originally used isothermal hypothesis for heat transfer from the heating pipes within the greenhouse.

A third contribution is the development of a water-to-water heat pump model that can operate under both partial- and full-load conditions, fitted according to manufacturer data.

Additionally, during this work a control unit for a greenhouse system coupled to ATES and a HP was developed. The control unit manages the extraction/injection to the aquifer wells, the operation of the HP, and the distribution of heating/cooling through pipes and/or coils. The control units are also included in the library to ensure reproducibility.

All these models are included in the Greenhouses Library, allowing researchers to utilize them for greenhouse systems. These models also contribute to other fields, such as building energy simulation, due to their universal characteristics.

Finally, a minor contribution is the demonstration of the library's utility for both sizing and simulating systems.

Reading tips

Readers interested in a detailed exploration of greenhouse modeling can turn to Chapter 2 for more in-depth information.

The part-load performance curve given in Figure 7.3 does not assume a constant water temperature at the condenser supply. Indeed, this curve is drawn according to AHRI standard 550-590 1998. In an improved version of the work, part-load data with constant water temperature at the condenser supply could be considered, leading to the following values of the parameters of Equation (7.13): $\delta_0 = 0.0180278$, $\delta_1 = 0.972543$, $\delta_2 = 0$. It is noteworthy, however, that such a modification would solely impact the control algorithm of the heat pumps and would not exert any discernible influence on the overall results. Specifically, introducing a marginal reduction in performance during part-load conditions would prioritize the utilization of a single heat pump at higher load over multiple units at part-load.

For clarification, the two different cooling capacities given in Section 7.3.4 (366 kW versus 324.2 kW) correspond to two distinct submodels of the chiller offered by the manufacturer (Standard efficiency (SE) versus High efficiency (XE)).

7.1 Introduction

Glass greenhouses are a well established technology used to cultivate crops. By heating and increasing the exposure to light via lamps, they allow colder regions for cultivating breeds of flowers and vegetables that naturally grow in temperate or tropical climates. One of the many benefits of technologically equipped greenhouses is the potential they offer for optimizing crop production. On the one hand, the focus on climate control has enabled maximizing crop production both quantitatively and qualitatively. The latter has lead countries such as the Netherlands to be the largest exporter of tomatoes in Europe, even above Spain [81]. On the other hand, climate control comes at a high energy cost. To maintain the optimal temperature, light and CO_2 levels that maximize the crop yield, greenhouses may consume (prohibitively) substantial amounts of energy for heating, electricity, CO_2 and cooling.

Even in the Atlantic and Central European regions, cooling is needed because greenhouses have a surplus of thermal energy in summer that must be removed to avoid yield reduction and crop diseases [82]. The most established cooling method in these regions is natural ventilation. However, when ventilating the thermal energy surplus is lost to the environment. In addition, if the target temperature is lower than the outside (dry or wetbulb) temperature, non-passive cooling is required. Most of the existing mechanical cooling methods for greenhouses have been developed for hot, dry climate regions whose primary energy consumption is cooling. Based on evaporative cooling, these systems are not suited to the Atlantic and Central European climates. With an increased need for active cooling during summer in regions with mainly heating requirements, sustainable technologies that allow for seasonal energy recovery in greenhouses have become a relevant scope of research.

In a greenhouse with reduced ventilation, active cooling in summer allows for storing the thermal energy surplus in an underground seasonal buffer that can later be used for heating in winter [82]. Among the available underground storage technologies, aquifer thermal energy storage (ATES) is the most suitable for that purpose. The high percentage of heat recovery makes ATES useful for demand-side management applications such as greenhouses [83].

The main goal of this work is to assess the energy recovery potential of greenhouses with thermal energy storage in shallow alluvial aquifers in the Atlantic climate. To that end, this work models and simulates a case study based on a greenhouse coupled to a 100 m thick synthetic chalk aquifer mimicking a real Cretaceous chalk aquifer in the Mons area in Wallonia (Belgium). The aquifer is characterized by a slow ambient groundwater flow. The flows are at 10-15°C for heating and at 5-10°C for cooling. While heating requires the use of a heat pump, cooling is possible directly at the aquifer temperature. The greenhouse is used for growing tomato crop and is equipped with lighting and a CO_2 enrichment system. The aquifer is assumed to supply the thermal demand at all times.

The greenhouse and the thermal distribution and generation systems are modeled by means of the Greenhouses Library [79], an open-source Modelica library for the dynamic simulation of greenhouse climate and energy systems. The Greenhouses library also provides control strategies for the heating, ventilation and other appliances (e.g. CO_2 enrichment and lighting), which determine the combined demand of the greenhouse during the simulation period. The aquifer is modeled by a deterministic 3D ground water flow and heat transport numerical model in the presented case study.

The case study is simulated for a period of two years. Results show that shallow alluvial aquifers can be very valuable and can provide a sustainable solution when heating and cooling greenhouses. However, to achieve so, the greenhouse climate controller must be correctly calibrated. In fact, to maintain a balanced system, greenhouses in the latitude of Belgium are forced to increase their cooling consumption. Otherwise, the system is imbalanced due to the higher needs of heating.

7.2 Modeling

The evaluation of the benefits arising from using ATES for supplying the energy demand in greenhouse applications requires to model several thermal systems, namely: a greenhouse climate model, heating distribution systems (i.e. heating pipes, heating and cooling coils), generation systems (i.e. heat pump) as well as the ATES system.

7.2.1 Greenhouse climate

Greenhouse climate models are useful to quantify the energy performance and the crop production given a greenhouse design, outdoor climate and a specifc control. Similar to building energy modeling, greenhouse climate models compute the indoor climate of a greenhouse by describing the flows between its components and solving their respective energy balances. Since in greenhouses the indoor climate is described by three variables (i.e. the temperature, the humidity and the CO_2 concentration in the air), the greenhouse model also includes moisture and CO_2 mass balances on the air.

The sensible energy balances are written in the form of Equation (7.1) and are applied to all components of the greenhouse. As shown in Figure 7.1, the greenhouse model consists of the air, the canopy, the envelope (i.e. the cover and the floor), the heating pipes and the thermal screen. The thermal screen is an horizontally movable membrane used to reduce the far-infrared radiative losses to the cover and to the sky. When the screen is deployed, the air of the greenhouse is divided in two zones, i.e. below and above the screen. These zones are modeled separately and their respective climate is assumed to be homogeneous [84].

$$\rho c_p V \frac{dT}{dt} = \sum \dot{Q} + \sum \dot{H}_{sens} \tag{7.1}$$

Apart from the energy flows exchanged within the forementioned greenhouse components, the model takes into account the moisture exchanged by natural ventilation with the outside air, the condensation at the cover and thermal screen, as well as the transpiration and photosynthesis (CO_2 consumption) from the canopy.

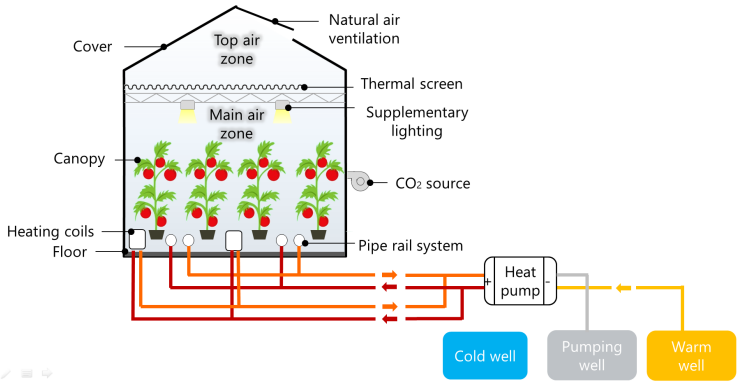

(A) Heating

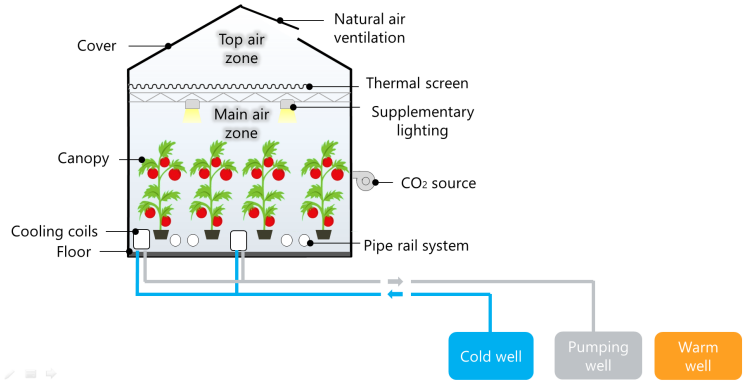

(B) Cooling

FIGURE 7.1: Sketch of the system

7.2.2 Heat distribution systems

In order to have an optimal thermal energy recovery, the thermal energy distribution systems inside the greenhouse must be selected by taking into account potential constraints from the supply source, such as the supply temperature, and from the crop [55]. For instance, in order to keep crop yield at an optimal level, it has been proven that, the temperature of the canopy is of utmost importance, not the temperature of the air that surrounds it. To that end, radiative systems (e.g. water pipes) are preferred over purely convective systems, since not only they heat the air through convection, but also they heat the canopy through long-wave radiation. As an illustration, in [84] it is demonstrated that in winter the canopy absorbs as much radiative heat flow from the pipes than convective heat flow from the air.

In this work, water pipes are selected as the primary heating distribution system. Water pipes are the most established technology for distributing heat in regions with high heating requirements. They usually cover the entire greenhouse floor through parallel loops that go along the crop rows. Therefore, despite their high investment cost, they allow for an horizontal temperature distribution of the highest quality. In order to be used as transport rails for the harvest, they are plain pipes (i.e. without fins) placed some centimeters above the ground. The installed capacity (diameter and length) follows greenhouse crop rows setup standards. Depending on the heat generation system that supplies them, they work between 45°C and 90°C.

Contrary to the case of heating, radiative systems are less adequate for cooling greenhouses. The plain nature of the water pipes implies a low heat transfer coefficient to the air. For the given aquifer supply temperature and the standard piping installed capacity (restricted to increase due to the crops setup), the water pipes are not able to meet the peak cooling demand. Additionally, the radiative exchange decreases the canopy temperature below the optimal range, which implies substantial yield reduction. It is therefore not desirable to lower supply temperature by means of a chiller to meet the peak demand. In order to be able to meet the peak demand without production losses, purely convective systems are a preference. Out of the available convective distribution systems, only water-to-air units are suitable for ATES applications. This work proposes the use of coils.

Given that the standard installed piping capacity is insufficient to supply the peak heating demand in winter (cf. Section 7.3.3), the coils are also used for heating distribution. They are used during peak heating demand hours as an accessory to the pipe system. This combination allows maintaining the canopy temperature at an optimal level both when heating and cooling to avoid yield reduction.

Heating pipes

The pipes heat the greenhouse air through hindered convection, but also the canopy, the floor and the greenhouse cover through long-wave radiation. Because of their length, a constant heat transfer coefficient cannot be assumed along the pipe. As a consequence, the heating pipes are modeled using a finite volume approach by means of a discretized model that divides the pipes into several cells, each one connected in series by a node [29]. In each cell, the flow is described with enthalpy as a state variable. The dynamic energy balance and static mass and momentum balances are applied in each cell. The model assumes uniform speed through the cross section as well as constant pressure. Axial thermal energy transfer is neglected. The heat flow is computed by an ideal heat transfer model with constant heat transfer coefficient. The energy balance on the fluid for a cell i is described by:

$$V_i \, \rho_i \, \frac{dh_i}{dt} + \dot{M}(h_{ex,i} - h_{su,i}) = A_i \, \dot{q}_i, \quad i = 1, 2...N_{cell} \tag{7.2}$$

where h_i is the fluid specific enthalpy at cell i, and h_{ex} and h_{su} are the enthalpy at the cell's outlet and inlet nodes, respectively.

Heating and cooling coils

Coils can work in dry, partially wet or wet regimes. In most cases, cooling and drying are done simultaneously with the coil working in a wet regime. In a partially wet regime, condensation appears in a point where the contact temperature is lower than the dew point temperature of the air. In this case, a part of the coil works in dry regime, while the rest works in a wet regime.

Over the past decades, water cooling coil models have been the subject of a substantial literature. Many models using different approaches have been developed and validated, the most common ones being:

- Single zone epsilon-NTU models ([30], [85]),
- Variable boundary models ([86]), and
- Finite elements ([87]) and lumped models.

In this work, the model proposed in [30] is implemented because of its increased robustness for similar levels of accuracy in comparison to the rest of the models, as reviewed in [88]. The model is characterized by three main hypothesis. The first one is that it assumes the cooling coil either completely dry or completely wet. In reality, both options underestimate the heat transfer rate. On the one hand, if the coil is assumed completely dry, the latent heat transfer is neglected. On the other hand, if the coil is assumed completely wet, the model predicts air moisture in the dry part of the coil, which means it considers a negative latent heat transfer rate. Given that both descriptions underestimate the total exchange, the model sets the cooling power to the one with the highest exchanged power:

$$\dot{Q}_{ccoil} = \max\left(\dot{Q}_{dry}, \dot{Q}_{wet}\right) \tag{7.3}$$

The heating coil is modeled in a simpler manner since only the dry regime must be described.

The second hypothesis states that in the energy balance in wet regime (which takes into account the latent heat), the air can be subtituted by a ficticious fluid the enthalpy of which is completely defined by the wet temperature of the fluid. Therefore, the energy balance described by Equation (7.4) is equivalent to Equation (7.5).

$$\dot{Q}_{wet} = \dot{M}_{air} \cdot (h_{air,su} - h_{air,ex,wet}) - \dot{M}_{air} \cdot (w_{air,su} - w_{air,ex,wet}) \cdot c_w \cdot T_{air,ex,wet} \tag{7.4}$$

$$\dot{Q}_{wet} = \dot{M}_{air} \cdot c_{p,airf} \cdot (T_{wb,su} - T_{wb,ex,wet}) \tag{7.5}$$

Finally, in order to compute the state in which the air exits the coil, the model defines a semi-isothermal exchanger that takes the air as one fluid and the external surface of the coil as the other, as described by:

$$h_{air,su} - h_{air,ex,wet} = \varepsilon_{c,wet} \cdot (h_{air,su} - h_{c,wet}) \tag{7.6}$$

$$w_{air,su} - w_{air,ex,wet} = \varepsilon_{c,wet} \cdot (w_{air,su} - w_{c,wet}) \tag{7.7}$$

$$\varepsilon_{c,wet} = 1 - exp(-NTU_{c,wet}) \tag{7.8}$$

$$NTU_{c,wet} = \frac{1}{R_{air} \cdot \dot{C}_{air}} \tag{7.9}$$

7.2.3 Water-to-water heat pump

The heat pump model implemented in this work predicts the performance at both full- and partial-load operation for different working conditions by means of three polynomial laws fitted through manufacturing data [74]. The first law describes the coefficient of performance (COP) at full load as a function of the temperatures at the evaporator inlet and at the condenser outlet:

$$EIRFT = \frac{COP_n}{COP_{fl}} = \alpha_0 + \alpha_1 \cdot \Delta T + \alpha_2 \cdot \Delta T^2 \tag{7.10}$$

where

$$\Delta T = \frac{T_{su,ev}}{T_{ex,cd}} - \frac{T_{su,ev,n}}{T_{ex,cd,n}} \tag{7.11}$$

with the temperatures values being in Kelvins.

The second law describes the heating power at full load as a function of the temperatures at the evaporator inlet and at the condenser outlet:

$$CAPFT = \frac{\dot{Q}_{cd,fl}}{\dot{Q}_{cd,n}} = \beta_0 + \beta_1 \cdot (T_{su,ev} - T_{su,ev,n}) + \beta_2 \cdot (T_{ex,cd} - T_{ex,cd,n}) \tag{7.12}$$

Finally, the third law describes the performance at partial load:

$$EIRFPLR = \frac{\dot{W}_{pl}}{\dot{W}_{fl}} = \delta_0 + \delta_1 \cdot PLR_{cd} + \delta_2 \cdot PLR_{cd}^2 \tag{7.13}$$

where the part load ratio is described by:

$$PLR_{cd} = \frac{\dot{Q}_{cd,pl}}{\dot{Q}_{cd,fl}} \tag{7.14}$$

and the electrical power required at the compressor at full load operation is described by:

$$\dot{W}_{fl} = \frac{\dot{Q}_{cd,fl}}{COP_{fl}} \tag{7.15}$$

7.2.4 Aquifer thermal energy storage

The synthetic model used to simulate groundwater flow and heat transport represents a 100 m thick aquifer typical of the Cretaceous chalk area located in Mons, in Belgium. These aquifers are very productive and are good targets for ATES systems. As an example, pumping rates can reach up to 300 m^3/h. This model was built with the MODFLOW [89] and MT3DMS [90] suites. For the latter code simulating only solute transport, we took advantage of the analogy between the equations of heat transport and solute transport, as previously shown and validated in [91].

The modeled ATES system consists of three wells, the so-called triplet. The first well (the pumping well) always supplies water at 10°C. The other two wells are used to store (1) cold water (at about 5°C) when the greenhouse is heated and (2) hot water (at about 15°C) when the greenhouse is air-conditioned. These two wells are called the cold well and the warm well respectively. The inputs of the model depend on the direction of pumping. When pumping from the pumping well, the inputs are the pumping rate in the pumping well and the injection rates at the cold and warm well with their associated temperatures. When pumping from the warm and cold wells, the input is still the pumping rates at the different wells (which are defined by the greenhouse demand). However, the water temperature of the pumped water from the cold and warm wells is now an output of the model.

The hydraulic conductivity is the main parameter for groundwater flow simulation. The hydraulic conductivity is set to 10^{-4} m s^{-1}, which is a mean value for this kind of aquifer. As for the thermal parameters that do not vary in great proportion in aquifers, we took the same parameters that can be found in [91].

The ATES system was designed according to Dutch best practice. This means for example that the distance between the different wells is sufficiently large to avoid any thermal interaction between the thermal plumes stored in the aquifer [92], [93].

7.3 Sizing of the components

The simulation of the case study requires the sizing of the modeled components. This section summarizes the sizing of all of the models presented in Section 7.2.

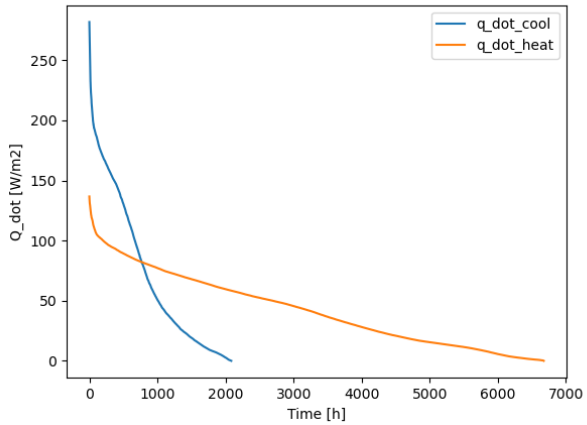

FIGURE 7.2: Yearly load duration curves of cooling and heating

7.3.1 Greenhouse sizing

The greenhouse is sized to the geological site. The alluvial plain from this case study allows for a construction of a 1 ha greenhouse. In order to size the greenhouse energy systems, the greenhouse model described in Section 7.2.1 has been simulated for a period of one year. The goal is to obtain the peak heating and cooling powers required by the greenhouse. The climate set-points are computed as proposed in [73] and are suited to the crop needs. The obtained yearly load duration curves for heating and cooling are shown in Figure 7.2.

Results show that energy for heating purposes is demanded about three quarters of the year, with a peak demand of 137 W m^{-2}. Cooling is required only in summer and has a higher peak demand at 278 W m^{-2}. This is, as expected, due to the greenhouse effect on sunny warm summer days.

7.3.2 Heating pipes sizing

As previously mentioned, water pipes are placed along the crop rows to keep a homogeneous climate on an horizontal axis and to serve as rails for harvest transport. The installed capacity of the pipes is therefore defined by the setup of the crop rows over the greenhouse floor area. In a classic Venlo type greenhouse, crop rows are separated by 1.6 m [22]. Therefore, the required installed capacity for a greenhouse of 1 ha, assuming 200 m over 50 m, is 125 loops of 100 m.

Given the considerable length of each pipe loop, two conditions must be respected in order to have a homogeneous climate on an horizontal axis. First, the power output is adjusted by temperature control. The mass flow rate is therefore constant to the nominal value. Second, small temperature differences from the supply to the exhaust are desired. Typical controls aim for a temperature difference of about 5 to 7 degrees.

Assuming a loop completion time of 20 min [22] and a standard pipe diameter of 51 mm [55], the nominal mass flow rate is computed to be 0.14 kg s^{-1}. Considering a 6 degrees temperature difference supply-exhaust, the maximum power output of the pipes is around 46 W m^{-2}, which is 42% of the the peak demand (assuming the peak at 110 W m^{-2} instead of 137 W m^{-2}, given the low frequency of the points above 110 W m^{-2}). As a reminder, the rest of the heat is supplied by the coils.

7.3.3 Coils sizing

The coils are used for both heating and cooling. Given that the cooling demand is higher than the heating demand, the coils have been sized for cooling. When observing the steepness of the load duration curve, one may conclude that it is not cost-efficent to size the system according to the peak demand. Indeed, demand values above 200 W m^{-2} are only required few hours per year. However, the installed capacity must be high enough to allow for maintaining the air temperature below a certain threshold defined by the crop. The main reason is that the crop has temperature and humidity thresholds that, if exceeded, lead to crop yield reduction and potentially to crop diseases. For instance, many diseases are favored by temperatures between 24°C and 35°C [55]. Additionnaly, the harvest rate at a maximum day temperature of 30°C, 35°C and 40°C is 91%, 79% and 52% of the one at 25°C [78]. In this work, the maximum acceptable air temperature has been established at 32°C. To comply with the later, the cooling coils must be able to supply 250 W m^{-2}. Given the characteristics of the modeled coils, the greenhouse must be equipped with 192 units (i.e. a share of 52 m^2 of greenhouse floor per unit).

As previously mentioned, coils are also used as an accessory to the heating pipes in case the heating demand is higher than the pipes installed capacity. Considering a heating peak demand of 110 W m^{-2} and the pipes maximum output of 46 W m^{-2}, the heating coils must be able to supply 64 W m^{-2}. Therefore, only a quarter of the installation (sized according to cooling needs) is required to provide the heating demand.

7.3.4 Heat pump sizing

Manufacturer data are necessary to fit the performance laws of the heat pump model. The heat pump must be able to provide the total heat demand, which is translated to a power of 1.13 MW at the condenser. The peak power can either be achieved by a single unit or by several smaller units working in parallel or series (e.g. 4 units of 283 kW). Manufacturer data that fits the size range useful for our case study could only be obtained for a water-to-water chiller. The characteristics at nominal load are displayed in Table 7.1. The coefficient of performance (COP) of a machine working in heat pump mode can be assumed as its energy efficiency ratio (EER) plus one:

$$COP = EER + 1 \tag{7.16}$$

Given the specifications and together with Equation (7.15), we compute an equivalent nominal heating power of 445 kW, which allows for supplying the peak demand by three units in parallel. The nominal cooling capacity and the power input are based on $\Delta T = 5$K entering/leaving condenser water temperature. The chiller's working temperature range is:

- Evaporator outlet: from 4°C to 9°C, with 7°C as nominal operation.
- Condenser inlet: from 25°C to 45°C, with 30°C as nominal operation.

TABLE 7.1: Characteristics of chiller *ECOPLUS XE - ST 100.2*

Specifications	Values	Units
$\dot{Q}_{ev,n}$	366	kW
EER_n	4.62	-
$T_{ev,ex,n}$	7	°C
$T_{ev,su,n}$	12	°C
$T_{cd,su,n}$	30	°C
$T_{cd,ex,n}$	35	°C

The chiller is a water-cooled machine equipped with 2 single-screw compressors and working with HFC-134a. Each compressor, integrated in 2 separate refrigerant circuits, can modulate continuously its capacity down to 25% by means of capacity slides, offering a cooling capacity reduction of the chiller down to 12.5%. Evaporator and condenser are shell-and-tube heat exchangers.

Equations (7.10) and (7.12) were fit with the data at full load operation and the working $\Delta T = 5$K. Equation (7.13) was fit with the data at part load operation (shown in Figure 7.3), which is given for a cooling power of 324.2 kW and a compressor input of 84.3 kW. As it can be observed, the chiller performance are higher at part load operation, with a peak at 40% of load. The obtained calibration parameters are displayed in Table 7.2.

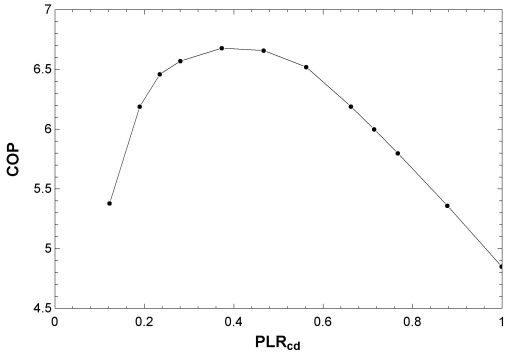

FIGURE 7.3: Performance at part load as a function of the part load ratio at the condenser

TABLE 7.2: Coefficients of the heat pump model

Coefficient	Value
α_0	0.99777
α_1	-8.9186
α_2	39.826
β_0	1.00145
β_1	0.026347
β_2	-0.0026717
δ_0	0.0898214
δ_1	0.186482
δ_2	0.710761

7.3.5 ATES sizing

The ATES wells must be sized to the extraction volumes required by the greenhouse. These are the volumes needed at the heat pump evaporator and the cooling coils to provide the greenhouse demand. The volumes are computed by means of Simulation 1 in the experimental protocol. The simulation details are described in Section 7.4.1 and the results are later discussed in Section 7.5.

7.4 Case study

In order to quantify the energy recovery potential of the study site, the modeled system is simulated for two years:

- First year: the goal is to recover energy from the greenhouse and store it underground, thus forming a warm and a cold plume in the aquifer. To that end, the greenhouse demand for both heating and cooling is provided by flows extracted from a pumping well at 10°C (i.e. the temperature of the site). The flows to the greenhouse are controlled such that the return temperature is $\pm$5K with respect to the supply temperature. The greenhouse heating and cooling returns are injected in two separate locations, the goal being to create a warm plume at 15°C around the warm well and inversely, a cold plume at 5°C around the cold well.
- Second year: the goal is to exploit the energy stored in the warm and cold wells as shown in Figure 7.1. To that end, the greenhouse demand flows are extracted from the warm and cold wells for heating and cooling (respectively). Both returns are injected to the pumping well.

Because of crop constraints, the start of the simulation must be equivalent to the start of the growing year. Since the studied crop is tomato, the simulation starts on December 10th, as proposed in [69]. In the greenhouse model, a typical meteorological year of Brussels is used to represent the outdoor climate.

7.4.1 Experimental protocol

The overground models (i.e. the greenhouse climate model, the heat pump model, the water pipes model and the coils model) cannot be simulated simultaneously with the ATES model because they are based on two different simulation software. Therefore, the simulation of the global system requires iterations between the two platforms. To tackle the iteration process, the following experimental protocol is followed:

- **Simulation 1**: simulate the overground models over the first year

  Goal: compute the greenhouse demand at the ATES level (i.e. the heat pump and coils flow rates and their return temperature)

  To that end, the models have been interconnected as follows. The greenhouse climate model, in which the water pipes and coils models are integrated, is coupled to three heat pump models connected in parallel. The aggregated condensers' outlet/inlet are connected to the inlet/outlet of the water pipes and heating coils. The evaporators' and cooling coils' inlets are connected to a supply source model representing the pumping well of the ATES. The flows of the source model are regulated by the climate controller and are assumed at 10°C (i.e. the ATES extraction temperature). Since the demand must be met at all times, the supply source has no flow restriction. Given an ATES target temperature of 15°C and 5°C, the models have been calibrated to ensure that the return temperature from the evaporator and the cooling coils is at $\pm$5K from the supply.

- **Simulation 2**: simulate the ATES model over the first year

  Goal: compute the cold and warm plume formations and their status after the one year of injection.

  In the first year, the ATES model is made of one extraction well and two injection wells. The injection flows and temperatures are imposed to the profiles computed in step one. For the cold well, these are the heat pump evaporator flows and return temperature. For the warm well, these are the cooling coils flows and their return temperature. The extraction flow is equivalent to the addition of the latter.

- **Simulation 3**: simulate the ATES model over the second year

  Goal: compute the temperature evolution of the warm and cold wells over the year as a function of extracted volume.

  In the second year, the ATES model is made of two extraction wells and one injection well. The model initialization conditions are set to the status at the end of one year of injection (i.e. the simulation from step two). Given that the greenhouse is assumed to have the same consumption, the same flow

profiles are used. Over the second year, these are not injection but extraction flows: the cooling coils flows are the cold well extraction, the heat pump evaporator flows are the warm well extraction. The extraction temperature profile evolves due to the storage level and the losses to the environment. The temperature profile as a function of the extracted volume is the main result of the simulation.

- **Simulation 4**: simulate the overground models over the second year

  Goal: compute the greenhouse demand with a supply from the cold and warm wells. Assess the energy efficiency of the global system in the ex-post.

  The interconnected overground models are simulated for one year. The evaporator and cooling coils inlets are connected to two supply source models representing the warm and cold wells of the ATES. The temperature of the sources evolve as a function of the extracted volume given the results from step three.

7.5 Results and discussion

The main results of the overground models simulations (i.e. simulations 1 and 4) are summarized in Table 7.3. As it can be observed, for both simulations the climate controller succeeds in maintaining the air temperature within one degree of difference from the set-point during 82-83% of the time. The air temperature is outside the acceptable temperature range for the crop less than 1% of the time. This can be seen in Figure 7.4, which displays quarter-hourly data of the air temperature as a function of the set-point together with the thresholds of acceptable temperatures defined by the crop. The colors indicate whether the greenhouse was being heated, cooled or none of the above. It is observable that most of the points outside a 2 degrees range from the set-point value are on the upper side. This is because as explained in Section 7.3.3, the cooling system is not sized to supply the peak cooling demand but to respect the maximum acceptable threshold.

During the first simulation year, the greenhouse recovers 2338 MWh at the evaporator and 1546 MWh at the cooling coils. The accumulated volumes used in these exchangers are 403 dam^3 and 308 dam^3, respectively. The evolution of the accumulated volumes over the year is shown in Figure 7.5 (blue curves). The maximum extraction volumetric flow rate, which used to size the ATES, is 180 $m^3\ h^{-1}$. The return temperatures of the heat pumps and coils circuits are well controlled at ± 5 degrees with respect to the supply. After one year of simulation (Simulation 2), the warm and cold wells temperature is stable at 14.5°C and 5.7°C, respectively.

In Simulation 3, the recovered temperatures over a year as a function of the extraction volumes are obtained (Figure 7.5, red curves). As a reminder, Simulation 3 assumes that the greenhouse has the same demand profile as Simulation 1. As

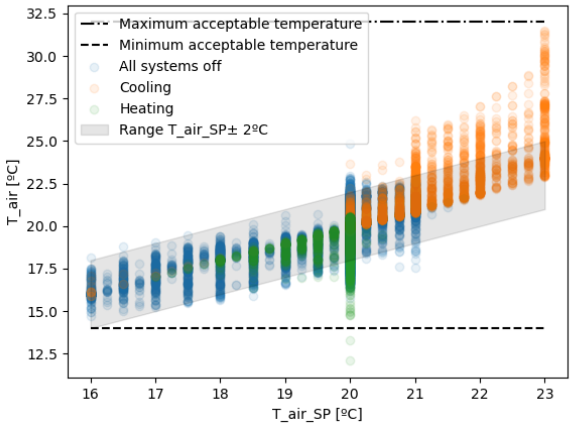

FIGURE 7.4: Comparison of the air temperature with respect to its set-point (quarter-hourly data points of simulation 1)

expected, the amount of energy stored decreases proportionally to the increase in extraction. In the warm well, the recovered temperature decreases over the year by a linear trend that follows the more or less linear demand profile. In the cold well, on the contrary, the absence of cooling demand at the begining of the year allows for the temperature to be impacted by diffusion losses to the underground flows. When the cooling demand becomes stable throughout summer, the recovered temperature increases in a linear fashion.

In Simulation 4, the second simulation year in which the greenhouse demand is produced by the warm and cold wells (assumed at the temperature profiles from Simulation 3), the greenhouse recovers 3127 MWh at the evaporator and 1599 MWh at the cooling coils. On the one hand, and as expected since the climate set-points remain unchanged, these values are very similar to the ones from Simulation 1. On the other hand, given that the supply temperatures at the evaporator and the cooling coils are different, the required volumes for producing a heating or cooling capacity differ from the ones considered in Simulation 1. The volumes consumed at the evaporator and the cooling coils are now 437 dam^3 and 216 dam^3, respectively. This means that the heat volume consumed from the warm well in the second year (437 dam^3) is higher than the volume stored in the first year (308 dam^3). Similarly, the cooling volume consumed from the cold well in the second year (216 dam^3) is lower than the volume stored in the first year (403 dam^3). Over the years, this may lead to a system imbalance, mainly in the cold well side, since more energy is stored than consumed.

A way to avoid this imbalance is through the flexibility offered by greenhouses. Among the available measures that would help balancing the system, the ones that generate the most impact are:

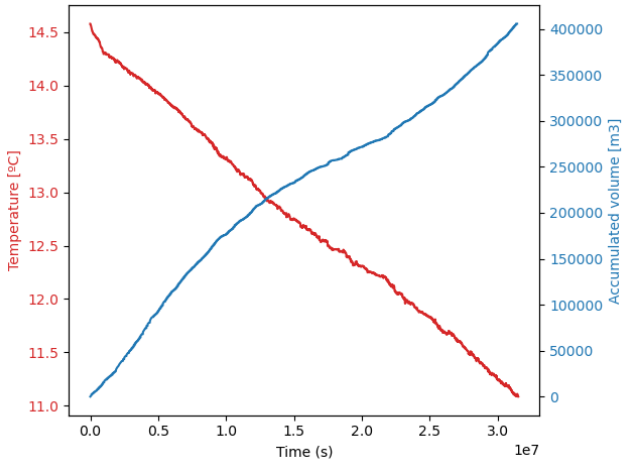

(A) Warm well

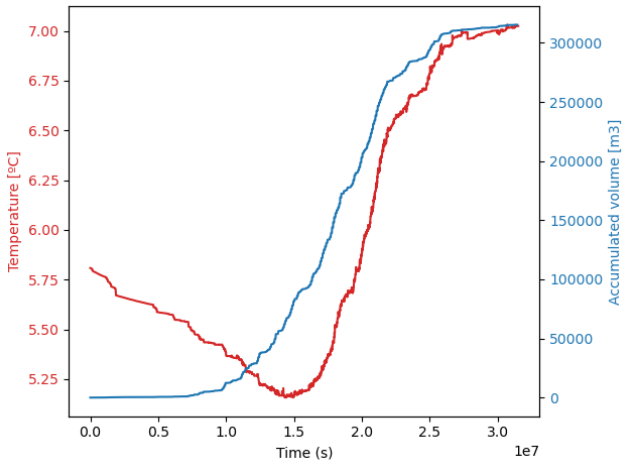

(B) Cold well

FIGURE 7.5: Evolution of the recovered temperature at the wells over one extraction year

i) Reducing ventilation for temperature control: The greenhouse climate controller of Simulations 1 and 4 is programmed to use natural ventilation to cool the greenhouse when the outside temperature is lower than the targetted set-point. The greenhouse cooling consumption could therefore be increased by not opening the vents and using active cooling instead.

ii) Decreasing the air temperature set-point to reduce heating in winter: As previously mentioned in this work, extreme temperatures are not optimal for crop yield and must be avoided. However, there is a range of near-optimal temperatures that allow for similar values of crop production rate. For instance, the harvest rate at a mean temperature of 14°C is 18% of the harvest rate at a mean temperature of 22°C. At the same time, the harvest rate at a mean temperature of 18°C is 87% of the one at 22°C [78].

iii) Increasing the air relative humidity ventilation threshold: natural ventilation is used when the air relative humidity increases above a threshold mainly to

reduce the risk of crop diseases. Higher levels of humidity do not necessarily imply that the crop is affected by diseases, but because the risk on such diseases increases as humidity becomes higher, growers try to avoid such high moisture contents.

In order to illustrate the impact of these measures, Simulation 4 has been repeated twice producing variants 4b and 4c. The first, Simulation 4b, applies all three methods in the following fashion. The ventilation threshold for temperature control is increased from 1.5 to 2 degrees when heating is used, and from 1 to 2 degrees when no heating is used (i). The temperature set-point is modified in such way that the average temperature set-point is decreased by 2 degrees with respect to the original simuation, but the lowest temperature set-point remains unchanged (ii). The threshold of ventilation for humidity control is increased from 85% to 90% from sunset until midnight (iii). The second, Simulation 4c, applies measures (ii) and (iii), and forbids ventilation for temperature control. That means, the vents can only open for humidity control. Measures (ii) and (iii) are applied as in Simulation 4b.

The obtained results, displayed in Table 7.3 and Figure 7.6, indicate that the measures can have a substantial impact on the greenhouse energy consumption. The modified set-points (measures ii and iii) decrease the heating needs down to 2502 MWh and increase the cooling demand up to 1995 MWh. In other words, measures (ii) and (iii) allow for increasing the cold well extraction by 40% (304 dam^3) and decreasing the warm well extraction by 29% (311 dam^3). A reduction on the ventilation for temperature control (measure i) as an additional measure allows for increasing the cold well extraction by 72% (371 dam^3) and decreasing the warm well extraction by 45% (241 dam^3), with respect to Simulation 4. Therefore, both methods decrease the system imbalance considerably, with measure (i) being the one with the most impact. However, as shown in Figure 7.7, when using measure (i) (Simulation 4c) the air relative humidity is above 90% during long periods, amounting for 30% of the year. The higher risk of diseases, although not quantifiable by the model, must be kept in mind and considered a drawback of this type of measure. In Simulation 4c, the integrated cooling rate (2561 MWh) is higher than the integrated heating rate (2012 MWh). This implies that, even in the Atlantic climate, the greenhouse can become a major cooling consumer.

7.6 Conclusions

In this work, the use of the thermal energy storage in shallow alluvial aquifers is proposed as a sustainable solution for supplying the energy demand of greenhouses. Air-conditioning greenhouses in summer allows for storing their energy surplus in an underground seasonal buffer that can later be used, in winter, for heating via a heat pump. The evaluation of the benefits arising from using ATES for supplying

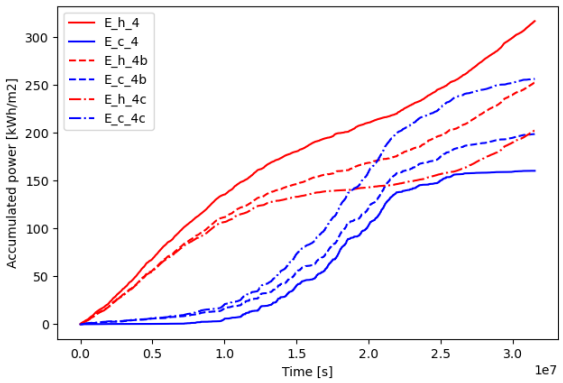

(A) Heat transfer rate

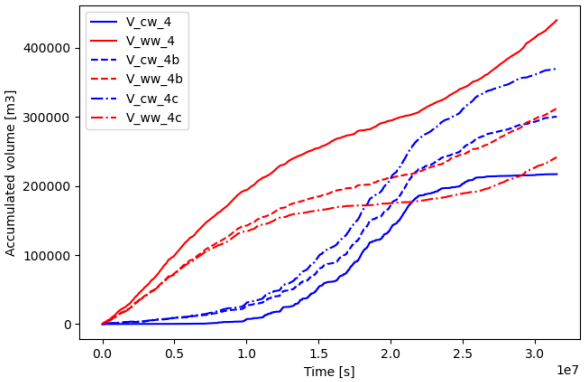

(B) Volume

FIGURE 7.6: Accumulated heat transfer rate and volumes for simulations 4 and 4b

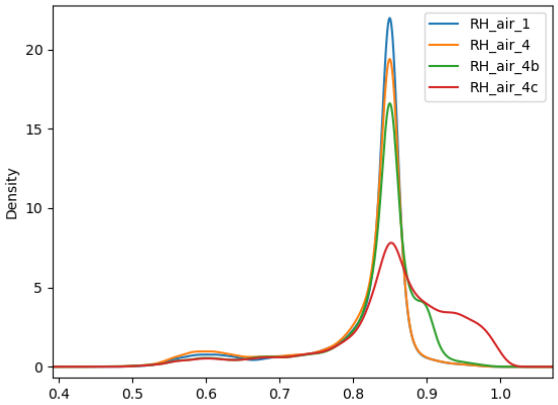

FIGURE 7.7: Density distribution of the air relative humidity over one year

the energy demand in greenhouse applications requires the modeling of a greenhouse climate model, heating/cooling distribution and emission systems (i.e. heating pipes and coils), a heat pump and the ATES system. The models have been sized

TABLE 7.3: Simulation results

Variable	Unit	Sim 1	Sim 4	Sim 4b	Sim 4c
Simulation year	-	First	Second	Second	Second
Time T_air is within T_air_sp $\pm$ 1°C	%	82.12	83.70	84.57	86.84
Time T_air is within [14, 32]°C	%	100	100	99.40	99.45
Time RH_air is below 90 %	%	98.27	98.32	94.11	70.38
Average air temperature	%	20.04	20.02	18.36	18.39
Average air relative humidity	%	81.59	80.85	82.72	85.29
E_heat_total	MWh	2885	3127	2502	2012
E_heat_pipes	MWh	2117	2236	1979	1630
E_heat_coils	MWh	768.2	891.3	523.2	381.8
E_cool_total	MWh	1546	1599	1995	2561
E_el_total	MWh	3341	2802	2674	2589
E_el_lamps	MWh	2809	2265	2267	2272
E_el_hp	MWh	532.6	536.5	406.9	316.8
E_ev	MWh	2338	2595	2068	1661
V_ev	dam^3	403.3	436.9	310.8	241.6
V_cc	dam^3	307.8	216.4	304.1	371.3
V_ww	dam^3	307.8	436.9	310.8	241.6
V_cw	dam^3	403.3	216.4	304.1	371.3
Direction	-	Injection	Extraction	Extraction	Extraction
V_pw	dam^3	711.1	653.3	614.9	612.9
Direction	-	Extraction	Injection	Injection	Injection

to the presented case study, which is based on a 100 m thick aquifer in the Cretaceous chalk, located in Wallonia (Belgium).

The case study has been simulated for two years. Due to the nature of the models, the experimental protocol is iterative and consists of 4 simulations. Results show that the recovered energy and volumes for heating and cooling are not in equilibrium. Greenhouses located in the Belgian latitude can be primarily considered as consumers of heating energy. Although energy is recovered during 3 months per year from cooling the greenhouse, the total energy consumed for heating is much higher. This results in a system imbalance on the cold well, since more energy is stored than consumed.

Despite this fact, a sustainable system can be achieved if the greenhouse climate controller is correctly calibrated. On the one hand, the great potential of flexibility offered by greenhouses allowed for improving the results in two extra simulations in which the greenhouse is forced to increase its cooling consumption. On the other hand, we observed a higher risk for crop diseases since a reduction of the ventilation to the outside air lead to a higher moisture content in the greenhouse. Not authorizing the opening of the vents for temperature control is therefore not desirable unless the greenhouse is equipped with a dehumidifier.

At this stage, the coupling between the two models (the aquifer and greenhouse ones) is not perfect. The results of one model are simply injected as inputs into the second and vice versa. This prevents us from going beyond the second year or simulating more complex (but probably more efficient) strategies. Therefore, a more tight coupling between the two models would be the natural continuation of this

work for tackling optimisation strategies that lead to a sustainable, self-sufficient system.

Nomenclature

α	polynomial coefficient	(–)
β	polynomial coefficient	(–)
δ	polynomial coefficient	(–)
ε	efficiency	(–)
ρ	density	(kg m^{-3})
A	surface	(m^2)
c	specific heat capacity	(J kg^{-1} K^{-1})
COP	coefficient of performance	(–)
E	accumulated energy	(MWh)
EER	energy efficiency ratio	(–)
h	specific enthalpy	(J kg^{-1})
$\dot{H}$	heat flow associated to a mass transfer	(W)
$\dot{M}$	mass flow	(kg s^{-1})
$\dot{Q}$	heat flow	(W)
$\dot{q}$	specific heat flow	(W m^{-2})
RH	relative humidity	(–)
T	temperature	(°C)
t	time	(s)
V	volume	(dam^3)
$\dot{W}$	electrical power	(W)
w	absolute humidity	(kg kg^{-1})

Subscript

air	air
c	contact
cc	cooling coils
cd	condenser
cool	cooling
cw	cold well
dry	dry
el	electricity
ev	evaporator
ex	exhaust
f	ficticious
fl	full-load
heat	heating
hp	heat pump
n	nominal
p	pressure
pl	part-load
pw	pumping well
su	supply
sens	sensible heat
sp	set-point
total	total
w	water
wb	wet-bulb
wet	wet
ww	warm well

Conclusion

Chapter 8

Conclusion

This chapter reviews the principal contributions of this thesis, concludes the work and proposes future research avenues that derive as natural continuation of the presented work.

8.1 Review of Contributions

The principal contributions of this work are summarized as follows:

- The **integration of validated models from diverse fields**: the greenhouse model (building simulation), a crop yield model (biology), thermal systems models (thermodynamics), and greenhouse climate control (control).
- The **release of a single modeling framework** that enables the dynamic simulation of greenhouses connected to thermal and electrical systems, with **open-source release of the code** for all models, including the default values for all model parameters, to facilitate reproducibility.
- The demonstration that the **greenhouse model reproduces physical results** consistent with the validated models from the literature upon which it is based.
- The demonstration of the **library's utility for both sizing and simulating** systems.
- The release as a **Modelica language-based library: the Greenhouses Library**. This enables researchers in related fields to utilize the library directly, thereby saving the considerable time required to implement such a complex model and allowing them to focus on investigating energy solutions involving greenhouses.
- The publication of the **online documentation and user guide**, providing researchers and other users with an attractive interface to access information about the models and enabling them to quickly commence their studies.
- The introduction of **solutions for numerical aspects in the Modelica language** to ensure the model's computational efficiency and robustness:

  - Because of the important time constants involved in some parts of the model (e.g. the vapor content of the air within the greenhouse), most **equations are initialized in steady-state**. While this adds some complexity to the initialization problem, it avoids long and unnecessary transients at the beginning of the simulation.
  - As previously seen in Chapter 2, some equations of the model include conditional statements (in the form of Equation (2.17), (2.29), (2.30), (2.49)) which, during integration, generate state events and thus decrease the computational efficiency of the model. To enhance computational efficiency, these **conditional statements have been replaced by a differentiable switch function**.
  - The **transformation of the control units of the screen from discrete steps (as done in practice) to continuous functions**, to avoid the computational overhead linked to *events* during the simulation [70]. This transformation is applied to both the screen removal/deployment processes and the screen's gap for humidity control.

- The **improvement of the greenhouse model**, which originally utilized an isothermal hypothesis for heat transfer from the heating pipes within the greenhouse. To improve model accuracy, a more detailed approach has been implemented, wherein the water flow through the pipes is represented by a discretized model that segments the pipes into multiple cells.
- The **innovative method for computing temperature and CO_2 set-points**. This work combines the set-point computation method from [64] for daylight periods, with an optimization of the set-point during nighttime based on the literature review of temperature effects on crop growth. The computation of the set-point for nighttime depends on the previous daylight hours and considers an average temperature and a maximum spread between the maximum and minimum temperatures over 24 hours. This model, employed in the Autonomous Greenhouses Challenge (2nd Edition), demonstrated significant improvements in tomato growth and reductions in energy consumption compared to traditional set-point definitions, greatly contributing to our success in achieving second position.
- The **proposal of various strategies for screen usage**, illustrating the potential energy savings achievable through different approaches.
- The **demonstration that greenhouse owners with such systems can significantly maximize self-consumption** (this represents a departure from current practices, where the control of generation units does not prioritize self-consumption, leading to excess energy being sold to the market), and the subsequent proposal of an **innovative energy solution: the integration of heat pumps into**

the traditional Combined Heat and Power - Thermal Energy Storage (CHP-TES) system. While this configuration has been previously studied in the building/thermal field, there is no record of its application in the greenhouse sector. This work evaluates the viability of such a system, demonstrating that greenhouse load is well-suited to this design and noting that energy markets might influence the economic viability of such systems.

- The **integration of the two performance-based CHP and Heat Pump (HP) models** into the Greenhouses Library. These models can also be utilized by researchers in thermal studies not necessarily related to greenhouses.
- The **integration of the two global system models** developed for this study (one for greenhouse-CHP-TES, and another for greenhouse-CHP-TES-HP), including all parameters and input data) into the Greenhouses Library, making them readily available for researchers interested in developing case studies with similar configurations.
- The development of **control units for the thermal systems** to manage the operation of the CHP and HP based on the TES state of charge and the greenhouse demand. The control units are also included in the library to ensure reproducibility.
- The proposal of a strategy that introduces an **innovative screen control method**, where the opening of the screen is regulated by temperature in addition to irradiation. Although this practice is commonly employed by greenhouse growers, it has rarely been simulated. This work quantifies the resulting reduction in energy consumption.
- The implementation of a strategy that assesses the variations resulting from the use of **heat-driven, electrical-driven, or mixed-driven strategies for the thermal units**. This article demonstrates that applying different control methods leads to varying levels of energy purchases from external sources to meet the greenhouse demand. Consequently, this analysis shows that depending on the energy sources or energy market prices, different strategies may be more effective for different systems and identifies the optimal strategy for the classic CHP-TES system.
- The **demonstration that Aquifer Thermal Energy Storage (ATES) is a viable energy source for greenhouses**. This is significant because ATES is an emerging energy solution, as discussed in Section 1.1.4. Moreover, this study is the first to explore this technology for a Cretaceous chalk aquifer in Belgium.
- The proposal to transform a pipe-only heating distribution system into a **combination of heating pipes and heating/cooling coils** to meet the cooling needs of greenhouses. The code for the heating and cooling coil models is released as open-source, enabling researchers to replicate the work.

- The **development of a water-to-water HP** model that can operate under both partial- and full-load conditions, fitted according to manufacturer data.
- The development of **a control unit for a greenhouse system coupled to ATES and a HP**, which manages the extraction/injection to the aquifer wells, the operation of the HP, and the distribution of heating/cooling through pipes and/or coils. The control units are also included in the library to ensure reproducibility.
- The addition of all thermal systems models in the Greenhouses Library, allowing researchers to utilize them for greenhouse systems. These models also **contribute to other fields**, such as building energy simulation, due to their universal characteristics.

8.2 Conclusion

Part I

This study introduces a comprehensive modeling framework that addresses critical gaps in the literature, providing a simulation platform for evaluating the potential contribution of greenhouses to the broader energy transition. The developed modeling framework stands as a pioneering contribution, furnishing a user-friendly, open-source platform for simulating and optimizing greenhouse climate, crop yield, and intricate energy flows between the greenhouse and its generation and storage units. Its parametric and object-oriented approach provides unmatched flexibility for adapting to diverse greenhouse designs and climates. This flexibility extends beyond the customization of the systems within the greenhouse; it facilitates a wide array of applications such as exploring sustainable energy sources, emissions reduction or energy efficiency measures, operational cost optimization under diverse control strategies, and the potential services of existing CHP to the power system. Indeed, the utilization of the Modelica language proves benefitial for formulating this problem, given its acausal characteristic language that enables the interconnection of the models in a 'physical' way [44]. Additionally, the full compatibility (connector-wise) between the library and other specialized Modelica libraries dedicated to modeling thermal systems or the power system increases the simulation possibilities of the Greenhouses library.

Additionally, the inclusion of ready-to-simulate pre-configured greenhouse systems, parametrized to the classic Venlo-type greenhouse designs, enhances the versatility of the framework. This feature allows researchers from diverse energy fields to seamlessly employ a greenhouse model with standardized parameters and control strategies. Consequently, they can directly integrate the greenhouse into their modeled systems, e.g. a district heating network, as done by [48]. This obviates the need for them to delve into the intricacies of developing a greenhouse model or resorting

to average consumption figures, which do not capture the dynamic energy flows inherent to the coupling of these systems.

The release of these models as open-source ensures a proper reproducibility and re-usability of this work.

Part II

As outlined in the Introduction, Part II aims to demonstrate the practical application of the modeling framework. Consequently, three case studies are presented to effectively illustrate how users can derive benefits from employing this library to address the following current research questions:

- Chapter 4: How can climate control strategies in technologically equipped greenhouses be optimized to enhance energy efficiency, i.e. maximize crop production while minimizing energy consumption?
- Chapter 5: How can current greenhouse systems, composed of a CHP unit coupled with TES, be modified to enhance sustainability?

  Specifically, is the integration of heat pumps in these systems a sustainable alternative that can potentially reduce overall system costs, and what are the implications and benefits of such integration?
- Chapter 6: What are the optimal energy management strategies for enhancing energy efficiency in greenhouse horticulture, with a specific focus on screen deployment control and the operation of CHP units, and what are the potential benefits associated with these optimizations?

The exhaustive analysis of climate control variables in Chapter 4 elucidates both the physical representation of the flows within the implemented greenhouse model and the proper functioning of the proposed control strategies for CO_2 enrichment and humidity control. The screen deployment strategies delineated in Chapter 4 do not purport to be revolutionary but rather aim to reflect prevalent practices, and how can the developed modeling framework be used to model these practices. Furthermore, the chapter's conclusion suggests that optimization of screen control could further decrease thermal consumption, a notion subsequently addressed in Chapter 6.

In Chapter 5, the evaluation centers on the advantages arising form the integration of heat pumps into conventional greenhouse systems, which include a CHP unit and TES, as a viable solution for the decarbonization of such systems. In the context of enhancing electrical self-consumption, the findings indicate that the incorporation of a heat pump, coupled with an appropriate control strategy, increases the self-consumption levels and concurrently diminishes operational costs. The addition of a heat pump allows for a reduction in the required CHP capacity, leading to a consequent decrease in environmental emissions. Notably, gas consumption is thereby

reduced by 25%. This operation results in an overall reduction of total operational costs by 9%. These findings are subject to the energy prices at the time of the study.

Recent events have demonstrated a surge in electricity prices in the power market, promoting the sale of electricity rather than prioritizing self-consumption. Nevertheless, it is noteworthy that the utility of this paper remains intact, as its primary objective was to showcase the model's capabilities.

Lastly, Chapter 6 concentrates on enhancing the energy efficiency of greenhouses, achieved either through the control of intrinsic components or by regulating external units. For the particular case of the thermal screen, findings reveal that a mere postponement in the deployment of the thermal screen results in a 3% reduction in heating consumption, without acompanying productivity losses. Moreover, the incorporation of an external temperature-dependent radiation criterion further diminishes energy consumption, albeit with a minor reduction in crop harvest.

The second case study illustrates the impact of the control of the generation units on the operational costs. Findings indicate that a hybrid electrical-heat-driven control, designed to enhance electrical self-consumption, can yield a 17% reduction in operational costs compared to a control strategy solely heat-driven. Furthermore, the study demonstrates that exclusively electrical-driven control strategies are not suitable for conventional CHP-TES systems, as they fail to adequately cover a significant portion of the heating demand.

The case studies in Chapters 4 and 5 were initiated during the early phases of this research, and consequently, they may exhibit certain limitations. For instance, the climate control strategies employed in Chapter 4 for windows aperture and screen deployment were not as sophisticated as those presented in Chapter 6. In particular, the latter features novel controls for windows (previously under fixed temperature control) and screens (formerly contingent solely on radiative dependence). Despite their simpler approach, the strategies used in Chapters 4 and 5 remain relevant, as they align with commonly used practices in low-tech greenhouses.

Furthermore, Chapter 5 features a system design with simplified interconnections, potentially deviating from real-world representations. Notably, the CHP unit's inability to directly supply the greenhouse, necessitating passage through the TES, represents a simplification. Similarly, the regulation of heat power supplied to the greenhouse through mass-flow rate control, while common in thermal systems, contrasts with conventional practices in greenhouse horticulture, where it may compromise the attainment of a homogeneous climate.

These simplifications were subsequently addressed and refined in the later stages of this research, as demonstrated in the final case study presented in Chapter 6. This case study incorporates system design and climate control strategies that closely mirror real-world scenarios.

The exploration of control strategies in these case studies reveals, as expected, their profound impact on energy consumption and crop yield. Strategic control of intrinsic greenhouse components and generation units emerges as a potent tool for reducing operational costs without compromising productivity. This holds paramount significance, as deliberated upon Section 1.1.5, because the competitiveness of the greenhouse sector, a pivotal objective outlined in the sector's roadmap, is contingent upon the reduction of costs linked to energy consumption.

In conclusion, the model proves to be a versatile tool for assessing the feasibility of energy efficiency measures, contributing to the decarbonization of the greenhouse horticulture sector and concurrently accelerating the energy transition.

Part III

In Part III, the developed modeling framework has been employed to examine the viability of innovative low-carbon energy sources for greenhouses. In the prevailing context of hastening the energy transition, a primary research question emerges:

- What sustainable energy solutions are viable for greenhouses, and how can the developed modeling framework contribute to exploring these integrated systems?

  Specifically, what is the energy recovery potential of greenhouses with thermal storage in shallow alluvial aquifers in Atlantic climates, and what are the benefits and implications of such integration?

In this work, the utilization of thermal energy storage in shallow alluvial aquifers, which is still in its nascent stages of development and lacks well-established foundations, is suggested as a sustainable solution for meeting the energy requirements of greenhouses. To that end, Chapter 7 delves into the intricate interplay of greenhouse climate models, heating and cooling distribution systems, heat pumps and ATES.

The case study, based on a Belgian aquifer, elucidates the challenges and potential benefits of this approach. The findings indicate that in Atlantic climate, where greenhouses predominantly require heating and have a minor cooling demand, the ATES system experiences an imbalance. This discrepancy arises due to a considerable disparity in the total energy consumption for heating, leading to an excess storage of energy in the cold well. However, rectifying this equilibrium can be achieved by forcing the greenhouse to augment its cooling consumption, within the confines of the crop's requirements and constraints. Certainly, refraining from permitting the opening of vents for temperature control is not a viable option unless the greenhouse is equipped with a dehumidifier.

While not explicitly addressed in the chapter, alternative approaches to attaining equilibrium could involve the addition of a dehumidifier, the utilization of a peaker

heating supply source, or the incorporation of nearby cooling consumers into the system, such as local industries, thereby establishing an integrated system.

At this stage, the coupling between the two models (the ATES and greenhouse ones) is not perfect. The results of one model are simply injected as inputs into the second and vice versa. This prevents us from going beyond the second year or to explore more intricate (yet potentially more efficient) strategies. Consequently, a more robust coupling between the two models emerges as the logical progression of this work. Such enhanced integration would enable the exploration of optimization strategies aimed at establishing a sustainable, self-sufficient system.

8.3 Paths for Future Research

In paving the way for future investigations, the modeling framework proposed by this research work reveals a range of opportunities.

First, in order to enhance the modeling framework's versatility, continuing to strengthen compatibility with external Modelica libraries that model district heating networks, dwellings, solar cycles, HVAC systems, and the power system is crucial. Additionally, broadening the spectrum of energy system models to encompass a more extensive array of heating, cooling, and lighting solutions is essential, reflecting the technological diversity and latest innovations in practical application. For instance, in recent years there has been a growing focus on assessing the suitability of Light-Emitting Diodes (LEDs) for lighting in greenhouses. Consequently, it is advisable to incorporate models of LED lighting within the existing library.

Second, there is a need for further investigation into solutions such as temperature integration for set-point definition. Notably, crops exhibit robustness to temperature control, and studies have demonstrated that maintaining temperatures within the minimum and maximum tolerated limits, achieving an average, and ensuring a controlled delta between the maximum and minimum temperatures per day can lead to similar crop performance. Considering that photosynthesis increases with absorbed irradiance, implementing strategies akin to those proposed in Section 2.2.4 for extended periods (3 to 5 days) has shown potential for increasing crop yield and reducing energy consumption compared to single day optimization. Moreover, the crops robustness to temperature control demonstrate a high suitability for demand-side management applications.

Third, investigating the integration of artificial intelligence (AI) algorithms into the modeling framework for intelligent control of greenhouse components is a promising avenue. This aspect was preliminarily explored in the present work utilizing the dymola Python library. The library enabled the coupling of Dymola with Python, facilitating the execution of optimizations and the training of AI algorithms through iterative simulations of a Dymola model. Although these specific studies were not

pursued in this thesis due to being beyond its scope, the accomplished integration of the Greenhouses library with Python establishes a broad spectrum of potential research avenues and applications.

Last but not least, actively involving greenhouse growers to obtain insights into practical challenges is instrumental to accelerate the energy transition. Research constitutes the fundamental prerequisite for identifying sustainable solutions. However, the implementation of these solutions is an essential step for the realization of the energy transition.

Similarly, fostering active collaboration between greenhouse growers, local communities, and industry stakeholders to formulate cross-sectoral solutions proves benefitial for facilitating the energy transition. Exemplary instances, such as the Warmtesysteem Westland (Westland Heating System) project (refer to Section 1.1.4), serve as valuable models. The successes and lessons learned from their practical implementation should be leveraged to advocate for the initiation of similar projects.

In conclusion, this thesis not only sheds light on the exploration and integration of sustainable energy solutions in greenhouse horticulture but also serves as a launchpad for a myriad of future research endeavors. The path ahead beckons researchers and practitioners to investigate, innovate and collaborate to usher in a greener and more sustainable era in greenhouse horticultural practices.

Appendix A

Modeling assumptions

A.1 Chapter 2 - Long-Wave Radiation View Factors

As discussed in Section 2.2.1, long-wave radiation flows between all greenhouse components and between the cover and the sky are modeled by the Stefan-Boltzmann equation. This section describes the application of this equation to each opaque surface in the greenhouse, including a description of the computation of the view factors.

A.1.1 The Stefan-Boltzmann Equation

The Stefan-Boltzmann equation describes the emission of radiation by a black body (E [W m^{-2}]) as follows:

$$E_{black} = \sigma\, T^4 \tag{A.1}$$

where σ is the Stefan-Boltzmann constant ($5.67 \cdot 10^{-8}$ W m^{-2} K^{-4}) and T the absolute temperature of the surface (K). In general, bodies are not black and therefore radiate less. The ratio over the amount of energy actually radiated by a body over the total emission if the body was black is called the emissivity factor. The emissivity factor of a body is not constant but function of the wave length. In greenhouse modeling, since the radiative exchanges occur in a limited spectrum (5 - 50 µm), it is common to assume emission factors as constants [94]. Therefore, for a natural body of finite surface, the emitted radiation (E [W]) is defined as:

$$E_i = A_i\, \varepsilon_i\, \sigma\, T_i^4 \tag{A.2}$$

Apart from emission, another important phenomenom in radiative heat exchange is absorption. Black bodies absorb all incident radiation, regardless of the spectrum or direction. This is not the case for natural bodies, which consequently have an absorption coefficient smaller than one, which is also function of the wave length and direction. Kirchhoff's law proves that for a gray and diffuse body, the absorption

coefficient is equivalent to the emission coefficient for any spectrum [95]:

$$\alpha_i = \varepsilon_i \tag{A.3}$$

The radiative energy that is not emitted or absorbed is either reflected or transmitted.

When computing the radiative flow between two finite surfaces, one must take into account that the radiative energy of the surfaces is emitted to the whole hemisphere but the surfaces intersect only partially with the hemisphere. The fraction of total emitted energy by a surface A_i to which a surface A_j is exposed to is called the view factor of A_i to A_j, commonly notated as $F_{i,j}$. Considering the emission of a surface A_i, and the subsequent absorptions and reflections flows, the radiative energy from A_i to A_j can be described as [22]:

$$\dot{q}_{i,j}^{rad} = \alpha_j \, \rho_j^n \, \rho_i^n \, F_{i,j}^{n+1} \, F_{j,i}^n \, E_i, \quad n = 0, 1...N \tag{A.4}$$

With $0 < \rho_i \rho_j F_{i,j} F_{j,i} < 1$, and together with Equations (A.2) and (A.3), it reduces to:

$$\dot{q}_{i,j}^{rad} = \frac{\varepsilon_j \, F_{i,j} \, A_i \, \varepsilon_i \, \sigma \, T_i^4}{1 - \rho_i \, \rho_j \, F_{i,j} \, F_{j,i}} \tag{A.5}$$

However, the flow described in Equation (A.5) is only a fraction of the net radiation flow from i to j, which must also include to the substraction of the flow from j to i. The latter can be computed analogue from Equation (A.5). Consequently, the net radiation flow from i to j is described by:

$$\dot{q}_{i,j}^{rad} = \frac{\varepsilon_i \, \varepsilon_j \, A_i \, F_{i,j} \, \sigma}{1 - \rho_i \, \rho_j \, F_{i,j} \, F_{j,i}} (T_i^4 - T_j^4) \tag{A.6}$$

If the reflection coefficients and/or the view factors are small enough (which is the case for all greenhouse bodies), the denominator of Equation A.6 is close to one and can be omitted. Equation A.6 is therefore reduced to the following (i.e. Equation 2.18, presented in Section 2.2.1):

$$\dot{q}_{i,j}^{rad} = \varepsilon_i \, \varepsilon_j \, A_i \, F_{i,j} \, \sigma (T_i^4 - T_j^4) \tag{A.7}$$

It should be noted that for finite bodies the reciprocity theorem ([95]) can be applied:

$$A_i F_{i,j} = A_j F_{j,i} \tag{A.8}$$

Additionally, if the temperature between the two surfaces is very close, Equation (A.6) may be linearized into:

$$\dot{q}_{i,j}^{rad} = \frac{\varepsilon_i \, \varepsilon_j \, A_i \, F_{i,j} \, \sigma}{1 - \rho_i \, \rho_j \, F_{i,j} \, F_{j,i}} 4 \, \bar{T}^3 (T_i - T_j) \tag{A.9}$$

where $\bar{T}$ is the average temperature between i and j.

A.1.2 Application to Greenhouses

In greenhouses, radiative flows occur between the greenhouse opaque surfaces (namely the canopy, heating pipes and floor and the cover), and between the cover and the sky. To compute the radiative energy flows between these surfaces, the greenhouse model applies Equation (A.6). To be consistent with the rest of the manuscript, all radiative heat flows in this section are described per square meter of greenhouse.

Starting with the cover, the radiative heat exchange between the cover and the sky can be therefore written as follows:

$$\dot{q}_{cov,sky}^{rad} = A_{cov} \, \varepsilon_{cov} \, \varepsilon_{sky} \, F_{cov,sky} \, \sigma \, (T_{cov}^4 - T_{sky}^4) \tag{A.10}$$

As the cover is tilted, the view factor $F_{cov,sky}$ is smaller than one. Nonetheless, as the sky encloses the cover, the product $F_{cov,sky} A_{cov}$ is equal to one, leading to:

$$\dot{q}_{cov,sky}^{rad} = \varepsilon_{cov} \, \sigma \, (T_{cov}^4 - T_{sky}^4) \tag{A.11}$$

The outer coefficient for ordinary glass is estimated at 0.84 [22]. It should be noted that the emission coefficient of the cover could differ between the inner and outer surfaces in the presence of coated cladding materials.

When the screen is closed, the inner side of the cover only exchanges energy with the screen. The radiative heat flow from the screen to the cover can be described by:

$$\dot{q}_{scr,cov}^{rad} = \frac{\varepsilon_{scr} \, \varepsilon_{cov} \, A_{scr} \, F_{scr,cov}}{1 - \rho_{scr} \, \rho_{cov} \, F_{scr,cov} \, F_{cov,scr}} \sigma \, (T_{scr}^4 - T_{cov}^4) \tag{A.12}$$

As the cover englobes all the hemisphere from the screen, $F_{scr,cov}$ equals to one. $F_{cov,scr}$ can be computed by means of Equation (A.8):

$$F_{cov,scr} = F_{scr,cov} \frac{A_{scr}}{A_{cov}} \tag{A.13}$$

which, considering that the cover has a certain tiltness (φ) and that the screen surface interacting is function of the screen closure (u_{scr}), can be reduced to:

$$F_{cov,scr} = F_{scr,cov} \frac{A_{flr} u_{scr}}{A_{flr} cos(\varphi)^{-1}} = F_{scr,cov}\, u_{scr}\, cos(\varphi) \tag{A.14}$$

The emission coefficient of the screen depends on the material of the thermal screen. For a classic thermal screen in Dutch greenhouses, this coefficient can be assumed to be 0.67 [78]. The reflection coefficient, in this case, is estimated at 0.18 [78]. Given the small reflection coefficient of the screen and the cover ($\rho_{cov} = 1 - \varepsilon_{cov}$ =0.16), the denominator of Equation (A.12) is assumed equal to one, leading to:

$$\dot{q}^{rad}_{scr,cov} = \varepsilon_{scr}\, \varepsilon_{cov}\, u_{scr}\, \sigma\, (T^4_{scr} - T^4_{cov}) \tag{A.15}$$

When the screen is open, the inner side of the cover exchanges long wave radiation with the canopy, the heating pipes and the floor. However, when the screen is in a position in between extremes, the computation of the view factors is of high complexity. Due to the fact that the screen is in that position for very reduced periods of time, it is fair to assume a linear correlation between the view factors from the cover and the screen closure. Therefore, the radiative heat flows between the cover and those elements will be factorized by the opening of the screen (i.e. $1 - u_{scr}$). The radiative flow between the canopy and the cover is defined by:

$$\dot{q}^{rad}_{can,cov} = (1 - u_{scr}) \frac{\varepsilon_{can}\, \varepsilon_{cov}\, A_{can}\, F_{can,cov}\, \sigma}{1 - \rho_{can}\, \rho_{cov}\, F_{can,cov}\, F_{cov,can}} (T^4_{can} - T^4_{cov}) \tag{A.16}$$

Because the canopy leaves are considered as black bodies [27], their emission coefficient is assumed to be one ($\varepsilon_{can} = 1$). Therefore, both reflection coefficients are close to zero, which allows disregarding the nominator. The radiative surface of the canopy is defined as the integral of the long-wave extinction function [27]:

$$A_{can} = A_{flr}\, (1 - e^{-k\, LAI}) \tag{A.17}$$

with k being the long-wave extinction coefficient, which is assumed to be 0.94 [22].

The view factor of the canopy to the cover can be retrieved from the reciprocity law (Equation (A.8)). The hemisphere from the cover occupied by the canopy is related to the LAI, with the long-wave extinction coefficient in an exponential function (as done for short-wave radiation, see Equation (2.25)). Thus, the view of the canopy to the cover is:

$$F_{can,cov} = F_{cov,can} \frac{A_{cov}}{A_{can}} = (1 - e^{-k\, LAI})\, cos(\varphi) \frac{\frac{1}{cos(\varphi)}}{(1 - e^{-k\, LAI})} = 1 \tag{A.18}$$

Consequently, the radiative heat flow from the canopy to the cover is reduced to:

$$\dot{q}^{rad}_{can,cov} = (1 - u_{scr})\, \varepsilon_{can}\, \varepsilon_{cov}\, (1 - e^{-k\, LAI})\, \sigma(T^4_{can} - T^4_{cov}) \tag{A.19}$$

The next surface is the heating pipes. The computation of the view factor from the cover to the heating pipes is quite complex. The heating pipes "see" the floor, the neighboring pipes, the canopy, the screen and the cover. By definition, the sum of all those view factors is equal to one. To ease the computation, the view factor from the pipes to the cover is computed indirectly by determining the rest of view factors from the pipes.

If there was no canopy, the view factor of an infinite long pipe to an infinite long cover would be 0.5, as only half the hemisphere of the pipe is located above the pipe. However, a small fraction of that hemisphere is interacted by the neighbouring pipes. According to [96], the view factor of a pipe with a diameter of 0.051 m to a neighbouring pipe on the left and on the right side at a distance of 1.6 m is 0.02. Therefore, a fraction of 0.01 of the upper hemisphere is occupied by the neighboring pipes, leading to a pipe to cover view factor of 0.49. Analogously, the pipe to floor view factor $F_{pip,flr}$ is 0.49. Nonetheless, the canopy does occupy the space between the pipe an the cover, decreasing the pipe to cover view factor to:

$$F_{pip,cov} = 0.49\, e^{-k\, LAI} \tag{A.20}$$

The emission coefficient of heating pipes covered in white paint is approximated at 0.88 [22]. Thus, the denominator of the general radiative flow equation can be omitted, leading to the radiative heat flow between the pipe and the cover:

$$\dot{q}^{rad}_{pip,cov} = (1 - u_{scr})\, \varepsilon_{pip}\, \varepsilon_{cov}\, F_{pip,cov}\, \pi\, d_{pip}\, l_{pip}\, \sigma(T^4_{pip} - T^4_{cov}) \tag{A.21}$$

where d_{pip} and l_{pip} are the pipe's diameter and length, respectively.

The view factor of the floor to the cover is hindered by all the aforementioned elements. If there was no canopy, the full hemisphere of the floor is interacted by the heating pipes, by $0.49\, \pi\, d_{pip}\, l_{pip}$. The reminder of the hemisphere is obstructed by the canopy. Therefore, the view factor from the floor to the cover is:

$$F_{flr,cov} = (1 - 0.49\, \pi\, d_{pip}\, l_{pip})\, e^{-k\, LAI} \tag{A.22}$$

The denominator of the radiative flow equation is once more disregarded, as the view factor from the floor to the cover is very small due to the canopy volume, and a low reflective coefficient from the cover. Therefore, the radiative heating flow from

the floor to the cover is:

$$\dot{q}^{rad}_{flr,cov} = (1 - u_{scr})\, \varepsilon_{flr}\, \varepsilon_{cov}\, F_{flr,cov}\, \sigma(T^4_{flr} - T^4_{cov}) \tag{A.23}$$

The next opaque surface in the greenhouse is the thermal screen. On the upper hemisphere, the screen exchanges with the cover, the radiative flow of which has already been described. On the lower hemisphere, the screen exchanges with the canopy, the pipes and the floor. As the screen is a horizontal surface, the radiative flow between the screen and these surfaces is similar to the one these have with the cover. Therefore, the radiative heat flows may be described as:

$$\dot{q}^{rad}_{can,scr} = u_{scr}\, \varepsilon_{can}\, \varepsilon_{scr}\, F_{can,scr}\, (1 - e^{-k\,LAI})\, \sigma\, \frac{1}{2}\, (T_{can} + T_{scr})^3 (T_{can} - T_{scr}) \tag{A.24}$$

$$\dot{q}^{rad}_{pip,scr} = u_{scr}\, \varepsilon_{pip}\, \varepsilon_{scr}\, F_{pip,scr}\, \pi\, d_{pip}\, l_{pip})\, \sigma\, \frac{1}{2}\, (T_{pip} + T_{scr})^3 (T_{pip} - T_{scr}) \tag{A.25}$$

$$\dot{q}^{rad}_{flr,scr} = u_{scr}\, \varepsilon_{flr}\, \varepsilon_{scr}\, F_{flr,scr}\, \sigma\, \frac{1}{2}\, (T_{flr} + T_{scr})^3 (T_{flr} - T_{scr}) \tag{A.26}$$

where $F_{can,scr}$, $F_{pip,scr}$ and $F_{flr,scr}$ are equal to the view factors the each opaque surface with the cover (Equations A.18, A.20 and A.22, respectively).

As previously elaborated, a fraction of 0.49 of the hemisphere of the heating pipes is considered to face upwards. The part occupied by the canopy leaves yields to the following view factor:

$$F_{pip,can} = 0.49\, (1 - e^{-k\,LAI}) \tag{A.27}$$

Since the canopy is considered to be practially a black body and consequenly multiple reflections are omitted, the radiative heat flow between the canopy and the pipes can be described by:

$$\dot{q}^{rad}_{pip,can} = \varepsilon_{pip}\, \varepsilon_{can}\, F_{pip,can}\, \pi\, d_{pip}\, l_{pip})\, \sigma(T^4_{pip} - T^4_{can}) \tag{A.28}$$

The radiative heat flow between the canopy and the floor is derived in a similar manner than the one between canopy and cover:

$$\dot{q}^{rad}_{can,flr} = \varepsilon_{can}\, \varepsilon_{flr}\, F_{can,flr}\, (1 - e^{-k\,LAI})\, \sigma(T^4_{can} - T^4_{flr}) \tag{A.29}$$

with the view factor from the canopy to the floor being:

$$F_{can,flr} = 1 - \pi\, d_{pip}\, l_{pip} \tag{A.30}$$

Finally, the radiative heat flow between the pipes and the floor, which can be computed analogous to the one between pipes and cover, is described by:

$$\dot{q}^{rad}_{pip,flr} = \varepsilon_{pip}\,\varepsilon_{flr}\,F_{pip,flr}\,\pi\,d_{pip}\,l_{pip}\,\sigma(T^4_{pip} - T^4_{flr}) \tag{A.31}$$

with $F_{pip,flr} = 0.49$.

The typical values of the aforementioned parameters for classic Dutch Venlo-type greenhouses are summarized in Table A.1.

TABLE A.1: Main parameters of the model.

Greenhouse Body	**Parameters**	**Value**	**Reference**
Sky	ε_{sky}	1	By definition
Cover	ε_{cov}	0.84	[22]
	φ_{cov}	25°	Classic Venlo-type design
Thermal screen	ε_{scr}	0.67	Classic thermal screen in Dutch greenhouses [78]
Floor	ε_{flr}	1	[78]
Canopy	ε_{can}	1	Leaves considered as black bodies [27]
	k	0.94	Extinction coefficient [22]
Heating pipes	ε_{pip}	0.88	White paint coated pipes [22]

Bibliography

[1] J. A. Aznar-Sánchez, J. F. Velasco-Muñoz, B. López-Felices, and I. M. Román-Sánchez, "An Analysis of Global Research Trends on Greenhouse Technology: Towards a Sustainable Agriculture," en, *International Journal of Environmental Research and Public Health*, vol. 17, no. 2, p. 664, Jan. 2020, Number: 2 Publisher: Multidisciplinary Digital Publishing Institute, ISSN: 1660-4601. DOI: 10.3390/ijerph17020664.

[2] FAO, *Good Agricultural Practices for greenhouse vegetable production in South Eastern European Countries* (FAO Plant Production and Protection Paper Series), en. Rome, Italy: FAO, 2017, ISBN: 978-92-5-109622-2.

[3] *Statistics | Eurostat - Under glass by NUTS 2 regions*. [Online]. Available: https://ec.europa.eu/eurostat/databrowser/view/EF_LUS_UNGLASS__custom_7245461/default/table?lang=en&page=time:2013 (visited on 08/25/2023).

[4] Glastuinbouw Nederland, *Let's get circular*, nl-NL. Jun. 2022.

[5] P. Smit and R. v. d. Meer, "Energiemonitor van de Nederlandse glastuinbouw 2021," dut, Wageningen Economic Research, Wageningen, Tech. Rep. 2022-124, 2022, ISBN: 9789464474947, pp. –.

[6] EGTOP (Expert Group for Technical Advice on Organic Production, "Final Report On Greenhouse Production (Protected Cropping)," fr, Tech. Rep.

[7] *StatLine - Energy consumption of agriculture and horticulture 1990-2013*, en. [Online]. Available: https://opendata.cbs.nl/statline/#/CBS/nl/dataset/80382ned/table?ts=1692790794605 (visited on 08/24/2023).

[8] B. Paris, F. Vandorou, A. T. Balafoutis, *et al.*, "Energy Use in Greenhouses in the EU: A Review Recommending Energy Efficiency Measures and Renewable Energy Sources Adoption," en, *Applied Sciences*, vol. 12, no. 10, p. 5150, Jan. 2022, Number: 10 Publisher: Multidisciplinary Digital Publishing Institute, ISSN: 2076-3417. DOI: 10.3390/app12105150.

[9] *Statistics | Eurostat - Simplified energy balances*. [Online]. Available: https://ec.europa.eu/eurostat/databrowser/view/NRG_BAL_S__custom_7242008/default/table?lang=en (visited on 08/24/2023).

[10] *Statistics | Eurostat - Final energy consumption by agriculture/forestry per hectare of utilised agricultural area*. [Online]. Available: https://ec.europa.eu/eurostat/databrowser/view/tai04/default/table?lang=en (visited on 08/24/2023).

[11] R. Lund and B. V. Mathiesen, "Large combined heat and power plants in sustainable energy systems," *Applied Energy*, vol. 142, pp. 389–395, Mar. 2015, ISSN: 0306-2619. DOI: 10.1016/j.apenergy.2015.01.013.

[12] H. Lund, P. A. Østergaard, M. Chang, *et al.*, "The status of 4th generation district heating: Research and results," *Energy*, vol. 164, pp. 147–159, Dec. 2018, ISSN: 0360-5442. DOI: 10.1016/j.energy.2018.08.206.

[13] S. Paardekooper, H. Lund, J. Z. Thellufsen, N. Bertelsen, and B. V. Mathiesen, "Heat Roadmap Europe - Strategic heating transition typology as a basis for policy recommendations," *Energy Efficiency*, vol. 15, no. 5, Jun. 2022, ISSN: 1570-646X. DOI: 10.1007/s12053-022-10030-3.

[14] "Climate Agreement," en-GB, Government of the Netherlands, The Hague, Tech. Rep., Jun. 2019. [Online]. Available: https://www.government.nl/documents/reports/2019/06/28/climate-agreement.

[15] *Warmtealliantie Zuid-Holland aan de slag met warmtenet*, nl, Publication Title: Port of Rotterdam, Mar. 2017. [Online]. Available: https://www.portofrotterdam.com/nl/nieuws-en-persberichten/warmtealliantie-zuid-holland-aan-de-slag-met-warmtenet.

[16] Panhellenic Confederation of Unions of Agricultural Cooperatives, "GREENERGY (Energy Optimisation in European Greenhouses)," en, Tech. Rep.

[17] D. Katzin, E. J. van Henten, and S. van Mourik, "Process-based greenhouse climate models: Genealogy, current status, and future directions," *Agricultural Systems*, vol. 198, p. 103 388, Apr. 2022, ISSN: 0308-521X. DOI: 10.1016/j.agsy.2022.103388.

[18] D. Katzin, S. van Mourik, F. Kempkes, and E. J. van Henten, "GreenLight – An open source model for greenhouses with supplemental lighting: Evaluation of heat requirements under LED and HPS lamps," en, *Biosystems Engineering*, vol. 194, pp. 61–81, Jun. 2020, ISSN: 1537-5110. DOI: 10.1016/j.biosystemseng.2020.03.010.

[19] O. Körner and N. Holst, "An open-source greenhouse modelling platform," *Acta Horticulturae*, no. 1154, pp. 241–248, Mar. 2017, ISSN: 0567-7572, 2406-6168. DOI: 10.17660/ActaHortic.2017.1154.32.

[20] S. Quoilin, K. Kavvadias, A. Mercier, I. Pappone, and A. Zucker, "Quantifying self-consumption linked to solar home battery systems: Statistical analysis and economic assessment," *Applied Energy*, vol. 182, pp. 58–67, Nov. 2016, ISSN: 0306-2619. DOI: 10.1016/j.apenergy.2016.08.077.

[21] B. H. E. Vanthoor, C. Stanghellini, E. J. van Henten, and P. H. B. de Visser, "A methodology for model-based greenhouse design: Part 1, a greenhouse climate model for a broad range of designs and climates," *Biosystems Engineering*, vol. 110, no. 4, pp. 363–377, Dec. 2011, ISSN: 1537-5110. DOI: 10.1016/j.biosystemseng.2011.06.001.

[22] H. De Zwart, "Analyzing energy-saving options in greenhouse cultivation using a simulation model," PhD Thesis, Wageningen University, 1996.

[23] G. Bot, "Greenhouse climate : From physical processes to a dynamic model," PhD Thesis, Wageningen University, 1983.

[24] L. Balemans, "Assessment of criteria for energetic effectiveness of greenhouse screens," PhD Thesis, Agricultural University, Ghent, 1989.

[25] A. A. F. Miguel, "Transport phenomena through porous screens and openings : From theory to greenhouse practice," PhD Thesis, Wageningen University, Jan. 1998.

[26] T. Boulard and A. Baille, "A simple greenhouse climate control model incorporating effects of ventilation and evaporative cooling," *Agricultural and Forest Meteorology*, vol. 65, no. 3, pp. 145–157, Aug. 1993, ISSN: 0168-1923. DOI: 10.1016/0168-1923(93)90001-X.

[27] C. Stanghellini, "Transpiration of greenhouse crops : An aid to climate management," PhD Thesis, Wageningen University, 1987.

[28] B. H. E. Vanthoor, P. H. B. de Visser, C. Stanghellini, and E. J. van Henten, "A methodology for model-based greenhouse design: Part 2, description and validation of a tomato yield model," *Biosystems Engineering*, vol. 110, no. 4, pp. 378–395, Dec. 2011, ISSN: 1537-5110. DOI: 10.1016/j.biosystemseng.2011.08.005.

[29] S. Quoilin, A. Desideri, J. Wronski, I. Bell, and V. Lemort, "ThermoCycle: A Modelica library for the simulation of thermodynamic systems," en, in *Proceedings of the 10th International Modelica Conference*, 2014.

[30] J. Lebrun, X. Ding, J.-P. Eppe, and M. Wasac, "Cooling Coil Models to be used in Transient and/or Wet Regimes," in *Proceedings of the International Conference on System Simulation in Buildings 1990*, 1990, pp. 405–411.

[31] Q. Altes-Buch, S. Quoilin, and V. Lemort, "Modeling and control of CHP generation for greenhouse cultivation including thermal energy storage," en, in *Proceedings of the 31st international conference on efficiency, cost, optimization, simulation and environmental impact of energy systems*, Guimaraes, Portugal, Jun. 2018.

[32] Q. Altes-Buch, T. Robert, S. Quoilin, and V. Lemort, "Assessment of short-term aquifer thermal energy storage for energy management in greenhouse horticulture: Modeling and optimization," English, 2022.

[33] *Eurostat (online data code: Nrg_bal_s)*, en. [Online]. Available: https://ec.europa.eu/eurostat/statistics-explained/index.php?title=Agri-environmental_indicator_-_energy_use (visited on 08/20/2021).

[34] *CBS StatLine: Energieverbruik; land- en tuinbouw*. [Online]. Available: http://statline.cbs.nl/StatWeb/selection/?DM=SLNL&PA=80382NED&VW=T.

[35] *SOLHO: Solar thermal energy systems to power greenhouse farms*. [Online]. Available: https://www.solho.eu/.

[36] M. Esen and T. Yuksel, "Experimental evaluation of using various renewable energy sources for heating a greenhouse," en, *Energy and Buildings*, vol. 65,

pp. 340–351, Oct. 2013, ISSN: 0378-7788. DOI: 10.1016/j.enbuild.2013.06.018. (visited on 08/20/2021).

[37] A. Buck, S. Hers, M. Afman, *et al.*, "The Future of Cogeneration and Heat Supply to Industry and Greenhouse Horticulture," CE Delft, Delft, Tech. Rep. 14.3D38.67, Oct. 2014, p. 113.

[38] J. P. Jiménez-Navarro, K. C. Kavvadias, S. Quoilin, and A. Zucker, "The joint effect of centralised cogeneration plants and thermal storage on the efficiency and cost of the power system," *Energy*, vol. 149, pp. 535–549, Apr. 2018, ISSN: 0360-5442. DOI: 10.1016/j.energy.2018.02.025.

[39] CODE2, "D5.1 - Final Cogeneration Roadmap Member State: The Netherlands," en-US, Cogeneration Observatory and Dissemination Europe, Tech. Rep., Jul. 2014.

[40] *CBS StatLine. Electricity; production and means of production*, 2018. [Online]. Available: https://opendata.cbs.nl/statline.

[41] I. Lopez-Cruz, E. Fitz-Rodríguez, S. Raquel, A. Rojano-Aguilar, and M. Kacira, "Development and analysis of dynamical mathematical models of greenhouse climate: A review," *European Journal of Horticultural Science*, vol. 83, pp. 269–279, Nov. 2018. DOI: 10.17660/eJHS.2018/83.5.1.

[42] H. F. De Zwart, "A simulation model to estimate prospectives of energy saving measures in horticulture," und, in *Proceedings of the International Conference and British-Israeli Workshop on Greenhouse Technologies*, 1997, pp. 119–127. [Online]. Available: http://library.wur.nl/WebQuery/wurpubs/305930.

[43] A. Costantino, L. Comba, G. Sicardi, M. Bariani, and E. Fabrizio, "Energy performance and climate control in mechanically ventilated greenhouses: A dynamic modelling-based assessment and investigation," en, *Applied Energy*, vol. 288, p. 116 583, Apr. 2021, ISSN: 0306-2619. DOI: 10.1016/j.apenergy.2021.116583.

[44] F. Casella, J. G. van Putten, and P. Colonna, "Dynamic Simulation of a Biomass-Fired Steam Power Plant: A Comparison Between Causal and A-Causal Modular Modeling," *ASME 2007 International Mechanical Engineering Congress and Exposition*, pp. 205–216, Jan. 2007. DOI: 10.1115/IMECE2007-41091.

[45] M. Wetter, W. Zuo, T. S. Nouidui, and X. Pang, "Modelica Buildings library," *Journal of Building Performance Simulation*, vol. 7, no. 4, pp. 253–270, Jul. 2014, ISSN: 1940-1493. DOI: 10.1080/19401493.2013.765506.

[46] F. Jorissen, G. Reynders, R. Baetens, D. Picard, D. Saelens, and L. Helsen, "Implementation and verification of the IDEAS building energy simulation library," *Journal of Building Performance Simulation*, vol. 11, no. 6, pp. 669–688, Nov. 2018, ISSN: 1940-1493. DOI: 10.1080/19401493.2018.1428361.

[47] F. Casella and A. Leva, "Modelling of thermo-hydraulic power generation processes using Modelica," *Mathematical and Computer Modelling of Dynamical Systems*, vol. 12, no. 1, pp. 19–33, Feb. 2006, ISSN: 1387-3954. DOI: 10.1080/13873950500071082.

[48] T. Resimont, Q. Altes-Buch, K. Sartor, and P. Dewallef, "Economic and environmental comparison of a centralized and a decentralized heating production for a district heating network implementation," en, *Proceedings of the 10th International Conference on System Simulation in Buildings*, Dec. 2018.

[49] *Tencent and WUR Autonomous Greenhouses International Challenge 2019*, 2019. [Online]. Available: http://www.autonomousgreenhouses.com.

[50] I. Impron, S. Hemming, and G. P. A. Bot, "Simple greenhouse climate model as a design tool for greenhouses in tropical lowland," *Biosystems Engineering*, vol. 98, no. 1, pp. 79–89, Sep. 2007, ISSN: 1537-5110. DOI: 10.1016/j.biosystemseng.2007.03.028.

[51] W. Luo, H. de Zwart, J. DaiI, X. Wang, C. Stanghellini, and C. Bu, "Simulation of Greenhouse Management in the Subtropics, Part I: Model Validation and Scenario Study for the Winter Season," *Biosystems Engineering*, vol. 90, no. 3, pp. 307–318, Mar. 2005, ISSN: 1537-5110. DOI: 10.1016/j.biosystemseng.2004.11.008.

[52] R. J. C. van Ooteghem, "Optimal Control Design for a Solar Greenhouse," *IFAC Proceedings Volumes*, 3rd IFAC Conference in Modelling and Control in Agriculture, Horticulture and Post-Harvest Processing - Agricontrol, vol. 43, no. 26, pp. 304–309, Jan. 2010, ISSN: 1474-6670. DOI: 10.3182/20101206-3-JP-3009.00054.

[53] K. L. Coulson, *Solar and Terrestrial Radiation*, en. Elsevier, 1975, ISBN: 978-0-12-192950-3. DOI: 10.1016/B978-0-12-192950-3.X5001-3.

[54] J. Ross, "Radiative transfer in plant communities," in *Vegetation and Atmosphere (Ed. J. L. Monteith)*, London, UK: Academic Press, 1975, pp. 13–55.

[55] L. Urban and I. Urban, *La production sous serre: La gestion du climat*, French, 2nd. Lavoisier, 2010, vol. 1.

[56] E. Dayan, H. van Keulen, J. W. Jones, I. Zipori, D. Shmuel, and H. Challa, "Development, calibration and validation of a greenhouse tomato growth model: I. Description of the model," *Agricultural Systems*, vol. 43, no. 2, pp. 145–163, Jan. 1993, ISSN: 0308-521X. DOI: 10.1016/0308-521X(93)90024-V.

[57] E. Heuvelink, "Tomato growth and yield : Quantitative analysis and synthesis," eng, PhD Thesis, Wageningen University, 1996.

[58] R. Linker, I. Seginer, and F. Buwalda, "Description and calibration of a dynamic model for lettuce grown in a nitrate-limiting environment," *Mathematical and Computer Modelling*, vol. 40, no. 9, pp. 1009–1024, Nov. 2004, ISSN: 0895-7177. DOI: 10.1016/j.mcm.2004.12.001.

[59] L. F. M Marcelis, E Heuvelink, and J Goudriaan, "Modelling biomass production and yield of horticultural crops: A review," *Scientia Horticulturae*, vol. 74, no. 1, pp. 83–111, Apr. 1998, ISSN: 0304-4238. DOI: 10.1016/S0304-4238(98)00083-1.

[60] I. Seginer, C. Gary, and M. Tchamitchian, "Optimal temperature regimes for a greenhouse crop with a carbohydrate pool: A modelling study," *Scientia Horticulturae*, vol. 60, no. 1, pp. 55–80, Dec. 1994, ISSN: 0304-4238. DOI: 10.1016/0304-4238(94)90062-0.

[61] P. A. Leffelaar and T. J. Ferrari, "Some elements of dynamic simulation.," eng, in *Simulation and systems management in crop protection*, Wageningen: Pudoc, 1989, pp. 19–45, ISBN: 978-90-220-0899-7.

[62] S. Nilsen, K. Hovland, C. Dons, and S. P. Sletten, "Effect of CO2 enrichment on photosynthesis, growth and yield of tomato," *Scientia Horticulturae*, vol. 20, no. 1, pp. 1–14, May 1983, ISSN: 0304-4238. DOI: 10.1016/0304-4238(83)90106-1.

[63] A. Elings, H. F. d. Zwart, J. Janse, L. F. M. Marcelis, and F. Buwalda, "Multiple-day temperature settings on the basis of the assimilate balance: A simulation study," English, *Acta Horticulturae*, 2006, ISSN: 0567-7572.

[64] J. M. Aaslyng, J. B. Lund, N. Ehler, and E. Rosenqvist, "IntelliGrow: A greenhouse component-based climate control system," *Environmental Modelling & Software*, vol. 18, no. 7, pp. 657–666, Sep. 2003, ISSN: 1364-8152. DOI: 10.1016/S1364-8152(03)00052-5.

[65] J. Dieleman, L. Marcelis, A. Elings, T. Dueck, and E. Meinen, "Energy Saving in Greenhouses: Optimal Use of Climate Conditions and Crop Management," *Acta Horticulturae*, no. 718, pp. 203–210, Oct. 2006, ISSN: 0567-7572, 2406-6168. DOI: 10.17660/ActaHortic.2006.718.22.

[66] J Dieleman, E Meinen, L. Marcelis, Z., and E. Van Henten, "Optimisation of CO2 and Temperature in Terms of Crop Growth and Energy Use," *Acta Horticulturae*, vol. 691, Oct. 2005. DOI: 10.17660/ActaHortic.2005.691.16.

[67] R. I. Grange and D. W. Hand, "A review of the effects of atmospheric humidity on the growth of horticultural crops," *Journal of Horticultural Science*, vol. 62, no. 2, pp. 125–134, Jan. 1987, ISSN: 0022-1589. DOI: 10.1080/14620316.1987.11515760.

[68] B. J. Bailey, "Control strategies to enhance the performance of greenhouse thermal screens," *Journal of Agricultural Engineering Research*, vol. 40, no. 3, pp. 187–198, Jul. 1988, ISSN: 0021-8634. DOI: 10.1016/0021-8634(88)90206-5.

[69] A. Grisey and E. Brajeul, *Serres chauffées: réduire ses dépenses énergétiques*, 1st. Editions Centre technique interprofessionnel des fruits et légumes (CTIFL), 2007.

[70] F. Casella, "Simulation of Large-Scale Models in Modelica: State of the Art and Future Perspectives," Sep. 2015, pp. 459–468. DOI: 10.3384/ecp15118459.

[71] J. Dieleman and F. Kempkes, "Energy screens in tomato: Determining the optimal opening strategy," *Acta Horticulturae*, no. 718, pp. 599–606, Oct. 2006, ISSN: 0567-7572, 2406-6168. DOI: 10.17660/ActaHortic.2006.718.70.

[72] S. Pfenninger, J. DeCarolis, L. Hirth, S. Quoilin, and I. Staffell, "The importance of open data and software: Is energy research lagging behind?" *Energy Policy*,

vol. 101, pp. 211–215, Feb. 2017, ISSN: 0301-4215. DOI: 10.1016/j.enpol.2016.11.046.

[73] Q. Altes-Buch and V. Lemort, "Modeling framework for the simulation and control of greenhouse climate," in *Proceedings of the 10th International Conference on System Simulation in Buildings*, Liege, Dec. 2018.

[74] A. Bolther, C. R, F. E, D. Marchio, and J. Millet, "Méthode de calcul des consommations d'énergie des bâtiments climatisés ConsoClim," Ecole des Mines, Paris, Tech. Rep. CSTB ENEA/CVA-99.176R, 1999.

[75] F. Jorissen, M. Wetter, and L. Helsen, "Simulation Speed Analysis and Improvements of Modelica Models for Building Energy Simulation," English, in *Proceedings of the 11th International Modelica Conference*, Versailles, France: Lawrence Berkeley National Lab. (LBNL), Berkeley, CA (United States), Sep. 2015.

[76] *Eurostat (online data code: Nrg_100a)*, Publication Title: Eurostat. [Online]. Available: http://appsso.eurostat.ec.europa.eu/nui/show.do?dataset=nrg_100a&lang=en.

[77] *Eurostat (online data code: Apro_acs_a)*, Publication Title: Eurostat. [Online]. Available: http://appsso.eurostat.ec.europa.eu/nui/show.do?dataset=apro_cpnh1&lang=en.

[78] B. H. E. Vanthoor, "A model-based greenhouse design method," dut, PhD Thesis, Wageningen University, 2011.

[79] Q. Altes-Buch, S. Quoilin, and V. Lemort, "Greenhouses: A Modelica Library for the Simulation of Greenhouse Climate and Energy Systems," English, Mar. 2019. DOI: 10.3384/ecp19157533.

[80] *GE Power \textbar General Electric*. [Online]. Available: https://www.ge.com/power.

[81] E. Commission, "The tomato market in the EU: Vol. 3a: Trade for fresh products," Tech. Rep. AGRI.G2 - F&V - 2021, 2021, p. 29.

[82] C. Stanghellini, B. Van 't Ooster, and E. Heuvelink, *Greenhouse horticulture*. Wageningen Academic Publishers, Sep. 2018, ISBN: 978-90-8686-329-7. DOI: 10.3920/978-90-8686-879-7.

[83] G. De Schepper, C. Paulus, P.-Y. Bolly, T. Hermans, N. Lesparre, and T. Robert, "Assessment of short-term aquifer thermal energy storage for demand-side management perspectives: Experimental and numerical developments," en, *Applied Energy*, vol. 242, pp. 534–546, May 2019, ISSN: 0306-2619. DOI: 10.1016/j.apenergy.2019.03.103.

[84] Q. Altes-Buch, S. Quoilin, and V. Lemort, "A modeling framework for the integration of electrical and thermal energy systems in greenhouses," en, *Building Simulation*, vol. 15, no. 5, pp. 779–797, May 2022, ISSN: 1996-8744. DOI: 10.1007/s12273-021-0851-2.

[85] O. Morisot, D. Marchio, and P. Stabat, "Simplified Model for the Operation of Chilled Water Cooling Coils Under Nonnominal Conditions," *HVAC&R Research*, vol. 8, no. 2, pp. 135–158, Apr. 2002, Publisher: Taylor & Francis, ISSN: 1078-9669. DOI: 10.1080/10789669.2002.10391433.

[86] M. J. Brandemuehl, *HVAC 2 Toolkit: A Toolkit for Secondary HVAC System Energy Calculations*, en. ASHRAE, 1993, Google-Books-ID: Bq7fAAAACAAJ, ISBN: 978-0-910110-98-3.

[87] W. Gang, L. Mingsheng, and D. E. Claridge, "Decoupled modeling of chilled-water cooling coils," English (US), in *ASHRAE Transactions*, ISSN: 0001-2505 Journal Abbreviation: 2018 ASHRAE Annual Conference, vol. 113 PART 1, ASHRAE, Aug. 2007, pp. 484–493.

[88] S. Gendebien, S. Bertagnolio, and V. Lemort, "Comparative and empirical validation of three water cooling coil models," en, p. 8, 2010.

[89] A. Harbaugh, E. Banta, M. Hill, and M. McDonald, "MODFLOW-2000, the U.S. geological survey modular ground-water flow model-User guide to modularization concepts and the ground-water flow process," *U.S. Geological Survey Open-File Report 00-92*, Jan. 2000.

[90] C. Zheng and P. Wang, "MT3DMS: A Modular Three-Dimensional Multispecies Transport Model for Simulation of Advection, Dispersion, and Chemical Reactions of Contaminants in Groundwater Systems; Documentation and User's Guide," Jan. 1999.

[91] J. Hecht-Méndez, N. Molina-Giraldo, P. Blum, and P. Bayer, "Evaluating MT3DMS for Heat Transport Simulation of Closed Geothermal Systems," en, *Groundwater*, vol. 48, no. 5, pp. 741–756, 2010, ISSN: 1745-6584. DOI: 10.1111/j.1745-6584.2010.00678.x.

[92] M. Bloemendal, T. Olsthoorn, and F. Boons, "How to achieve optimal and sustainable use of the subsurface for Aquifer Thermal Energy Storage," en, *Energy Policy*, vol. 66, pp. 104–114, Mar. 2014, ISSN: 0301-4215. DOI: 10.1016/j.enpol.2013.11.034.

[93] M. Bloemendal, M. Jaxa-Rozen, and T. Olsthoorn, "Methods for planning of ATES systems," en, *Applied Energy*, vol. 216, pp. 534–557, Apr. 2018, ISSN: 0306-2619. DOI: 10.1016/j.apenergy.2018.02.068.

[94] T. Takakura, *Climate under Cover*, en. Dordrecht: Springer Netherlands, 1993, ISBN: 978-0-7923-2105-7 978-94-011-1658-9. DOI: 10.1007/978-94-011-1658-9.

[95] D. Pitts and L. Sissom, *Heat transfer*, en. McGraw-Hill Education, 1986.

[96] E. M. Sparrow and R. D. Cess, *Radiation Heat Transfer*, en. Hemisphere Publishing Corporation, 1978, ISBN: 978-0-07-059910-9.